Durham University

Durham E-Theses

New Roads to String Theory: From a New On-shell Formalism to Applications of Quantum Computing

LUCA ARMANDO NUTRICATI

How to cite:

NUTRICATI, LUCA ARMANDO (2023) New Roads to String Theory: From a New On-shell Formalism to Applications of Quantum Computing. Doctoral thesis, Durham University.

Use policy

The full-text may be used and/or reproduced, and given to third parties in any format or medium, without prior permission or charge, for personal research or study, educational, or not-for-profit purposes provided that:

- a full bibliographic reference is made to the original source
- a https://etheses.durham.ac.uk/id/eprint/15271/ is made to the metadata record in Durham E-Theses
- the full-text is not changed in any way

The full-text must not be sold in any format or medium without the formal permission of the copyright holders.

Please consult the full Durham E-Theses policy for further details.

Academic Support Office, The Palatine Centre, Durham University, Stockton Road, Durham, DH1 3LE
e-mail: e-theses.admin@durham.ac.uk Tel: +44 0191 334 6107
https://etheses.durham.ac.uk

New Roads to String Theory

From a New On-shell Formalism
to Applications of Quantum Computing

Luca Armando Nutricati

This Thesis is submitted to the University of Durham, in
Fulfilment of the Requirements for the Degree of

Doctor of Philosophy

Centre for Particle Theory
Department of Mathematical Sciences
Durham University
England

September 2023

New Roads to String Theory

From a New On-shell Formalism
to Applications of Quantum Computing

Luca Armando Nutricati

Submitted for the degree of Doctor of Philosophy

Abstract

This thesis discusses new approaches to string theory, aiming to open novel perspectives to connect string models with low energy phenomena. We approach this problem from two complementary perspectives. Firstly, we take a formal approach, seeking to uncover universal properties inherent in all closed string theories. Secondly, we head towards a more computational direction, leveraging the power of quantum computing to develop innovative techniques. These techniques serve as powerful tools for exploring and identifying viable string theory vacua, significantly enhancing our search capabilities in this complex domain.

In particular, in the first part we conduct a general, model-independent analysis of the running of gauge couplings within closed string theories. In doing so, we develop a new framework which is completely general and can be in principle used to compute one-loop corrections to all physical quantities

in a given string model.

The second part of this study is dedicated to pioneering the development of novel search methodologies, marking the groundbreaking integration of quantum computing as a powerful and previously unexploited resource in our quest to explore the landscape of string vacua. We investigate its efficiency and effectiveness in the model discovery process. Through a thorough comparison with traditional methods such as simulated annealing, random scans, and genetic algorithms, we highlight the potential advantages offered by quantum annealers, which promised to be roughly fifty times faster than random scans and genetic algorithm and approximately four times faster than simulated annealing.

In this context, we also propose an enhanced version of a class of meta-heuristic algorithms called Genetic Algorithms (GAs). This enhanced version integrates GAs with quantum annealing techniques, promising a significant boost in performance and problem-solving capabilities. We have employed both genetic and genetic quantum annealing algorithms as tools to search for particular string models which go under the name of heterotic line bundle models. We shall discuss in which extent this new tool promises to outperform search scans based on classical GAs.

Declaration

I declare that no part of this thesis has been submitted elsewhere for any other degree or qualification. The work in this thesis is based on research carried out at the Centre for Particle Theory, Department of Mathematical Sciences, Durham University, England, and is the result of collaboration between the author and collaborators Steven A. Abel, Andrei Constantin, Keith R. Dienes, Thomas Harvey, Andre Lukas, John Rizos and Michael Spannowsky published in

[1] S. Abel and L. A. Nutricati, "Ising Machines for Diophantine Problems in Physics", Fortsch. Phys., Jun. 2022. doi: 10.1002/prop.202200114.

[2] S. Abel, L. A. Nutricati, and M. Spannowsky, "A Genetic Quantum Annealing Algorithm", Sep. 2022. arXiv: 2209.07455.

[3] S. Abel, K. R. Dienes, and L. A. Nutricati, "Running of gauge couplings in string theory", Phys. Rev. D, vol. 107, no. 12, p. 126 019, 2023. doi: 10.1103/PhysRevD.107.126019. arXiv: 2303.08534.

[4] S. Abel, A. Constantin, T. R. Harvey, A. Lukas, and L. A. Nutricati,

"Decoding Nature with Nature's Tools: Heterotic Line Bundle Models of Particle Physics with Genetic Algorithms and Quantum Annealing", Jun. 2023. arXiv: 2306.03147.

[5] S. A. Abel, L. A. Nutricati, and J. Rizos, "String Model Building on Quantum Annealers", Fortsch. Phys., Jun. 2023. doi:10.1002/prop.202300167.

The results of other works which are still in preparation [6, 7] have not been included in this thesis but only referred in the main text.

Copyright© 2023 by Luca Armando Nutricati.

"The copyright of this thesis rests with the author. No quotations from it should be published without the author's prior written consent and information derived from it should be acknowledged".

Acknowledgements

I would like to express my gratitude to a number of individuals who have played pivotal roles in the completion of this PhD thesis.

First and foremost, I extend my deepest appreciation to my supervisor, Professor Steven A. Abel. His effective advises and unwavering support to my academic and personal development have been instrumental in shaping this thesis.

I would like to acknowledge and thank all my collaborators. Your diverse perspectives and expertise have enriched the quality of this work, and your willingness to share your insights and ideas has been invaluable. A special thanks goes to Professor Keith R. Dienes for enlightening and fruitful physics discussions in our long Zoom sessions.

Finally, to my family and my partner, for their incessant support.

Contents

Chapter 1

Introduction

String theory is commonly considered as the ultimate framework for "UV completion" of theories that effectively explain experimental observations at lower energy levels. These include theories like the Standard Model and its various extensions. The Standard Model of particle physics is perhaps the greatest success of modern physics, consistently describing three of the four known fundamental forces with a remarkable precision. However, gravitational interactions fails to be incorporated in such a theory, leading to infinities which cannot be reabsorbed using renormalisation, in contrast with one can normally do with all the other known forces. On the other hand, string theory itself provides a quantum description of gravity, *i.e.*, the graviton and all its interactions are built-in components of any string model.

In order to be considered a viable candidate for a unified theory, string theory must inherently incorporate the Standard Model as a fundamental

component within its framework, particularly in a low-energy limit. For decades, a considerable amount of effort of the scientific community has been directed towards the attempt to recover the Standard Model as a low energy description of string theory. However, establishing a direct connection between string theory and observable phenomena at lower energy scales is still an unsolved problem. The reason is twofold: firstly, the lack of any experimental sign which deviates from the predictions dictated by the Standard Model; secondly, the enormous number of SM-like candidate models generated by string theory practically prevents any possibility to perform a comprehensive scan. Depending on the set-up, the various estimates of the number of available models in the parameter space vary from the original 10^{500} estimate in type IIB flux compactifications [8, 9] to significantly larger numbers, for example $10^{272,000}$ F-theory flux compactifications on a single elliptically fibered four-fold [10]. In fact the number of Standard Model (SM)-like compactifications could itself be as large as 10^{700} [11]. This number is nevertheless minute in comparison to the size of the entire string landscape. Random sampling is guaranteed to fail at identifying such standard-like models from string theory, as is systematic searching which given the scales involved is simply beyond any present computational capabilities.

Apart from the practical obstacles primarily stemming from the constraints of current technology, it is crucial to acknowledge that any approach aiming to yield phenomenological predictions within the realm of string theory cannot circumvent the intricate details associated with the specific model

under investigation. This encompasses factors such as the geometric properties of the compactification, the existence of supersymmetry, the presence of fluxes, the precise nature of the underlying string model, *etc*. Low energy predictions, such as Higgs mass or gauge coupling corrections often involve one-loop string computations and usually results in very complicated mathematical expressions whereby universal properties are hidden by the details of the model.

Limited computational resources combined with model-dependent approaches make extremely difficult to recover the Standard Model as a low energy approximation of some string model. The purpose of this thesis is to develop new techniques in both directions: from one side we shall present a new model-independent framework to extract universal features of certain classes of string models; from the other more computational-oriented side we shall employ, for the first time, quantum annealers as promising powerful tools to search for SM-like string vacua.

Let us now give an overview on the novel approaches we shall introduce in the first part. Traditionally, one attempts to extract low-energy phenomenological predictions from string theory by focusing on the effects associated with only the lightest of the string modes for two fundamental reasons: the string scale is normally considered to be unreachably remote; the particle spectrum of the string is generally quantised in units of this scale.

Unfortunately, this approach towards string phenomenology robs us of the full power of string theory to provide new insights into low-energy phe-

nomena. String theory, as a theory of extended objects, does not merely produce light states — it also gives rise to infinite towers of massive states which are also an intrinsic part of the string spectrum. Indeed, the "stringiness" of string theory — *i.e.*, the fundamental features of string theory that transcend our field-theoretic expectations and therefore have the power to suggest new solutions to old puzzles — lies within these states. By disregarding these states and their accumulated contributions to low-energy physics, we are severing the link between the UV-complete theory and its low-energy phenomenology. This reduces us to working within an effective field theory (EFT) whose relevant operators are very hard to explain.

For this reason, it may be argued that a proper approach to understanding many of the low-energy phenomenological implications of string theory is one in which these infinite towers of states are retained and their effects are incorporated in a natural way throughout our calculations. Indeed, the effects of such states are likely to be the most relevant for fundamental phenomenological questions — such as *hierarchy* problems — which focus on the difficulties of maintaining a peaceful coexistence of both light and heavy scales within a quantum-mechanical universe.

One clue as to the power of these infinite towers of states is that string theories generally have finiteness properties that transcend what can be expected in field theory. One normally attributes these finiteness properties to the extended nature of the string — a feature lacking in theories based on point particles — but this extended nature of the string is precisely what gives

rise to these infinite towers of states. For perturbative closed strings (which will be our main focus), worldsheet modular invariance is the exact fundamental symmetry which governs these states and their interactions. Thus, modular invariance holds the key to much of the stringiness of string theory and the finiteness (or softened divergences) associated with its low-energy phenomenological predictions. However, modular invariance also leads to much more, including a unique and surprising form of UV/IR mixing that can severely distort the validity of effective field theories, even at low energies where one might have assumed EFT-based approaches to hold.

For this reason, it is important to develop fully modular-invariant methods of extracting low-energy phenomenological predictions from string theory. The first part of this thesis is devoted to the developing of such a framework in the perspective to extract universal properties of string theories which may be used as additional constraints in performing computer-based search scan for SM-like string vacua.

This latter aspect forms the core of the second part, where our primary emphasis lies in developing innovative computational methodologies and employing them within the realm of string theory. In particular, we shall discuss an implementation of adiabatic computing known as Quantum Annealing (QA), we shall bench-mark the methods on several problems in pure number theory and finally we shall apply them to string theory set-ups.

Quantum annealing is a cutting-edge computational technique which uses the principles of quantum mechanics to solve complex optimisation problems.

Born out of the broader field of quantum computing, quantum annealing offers a unique approach to tackling problems that involve finding the optimal configuration among a vast number of possibilities. This technique holds the promise of revolutionising the various state-of-the art methods by significantly speeding up the solution of optimisation challenges that are currently computationally expensive or infeasible for classical computers. String theory is therefore one of the most natural set-ups in which quantum annealing could lead to a major progress. Indeed, there is continued interest in the problem of model selection in string theory which, due to the vast number of models available, presents a fascinating "big-data" challenge.

At its core, quantum annealing is based on quantum superposition and quantum entanglement – two fundamental properties of quantum systems. These properties enable quantum annealers to explore multiple solutions simultaneously and efficiently navigate through complex solution landscapes. While traditional computers process information using bits as either 0 or 1, quantum annealers use qubits, which can exist in a superposition of states, enabling them to explore a broader range of potential solutions in parallel.

The concept of annealing in quantum annealing draws inspiration from the annealing process in metallurgy, where a material is gradually cooled to reach a state of minimum energy. Similarly, in the quantum realm, annealing involves guiding a quantum system from a highly entangled state to a low-energy state that corresponds to a valid solution of the optimisation problem. By controlling the parameters of the quantum system, such as the strength

of interactions between qubits, one can manipulate the annealing process to find the optimal solution with higher probability.

However, due to technology limitations, current available quantum annealers cannot directly embed problems which contain trilinear or higher order couplings. Indeed, only quadratic Ising model Hamiltonians can be encoded in such machines. To encode higher order problem one has to find a procedure to reduce the original problem to an Ising model, preserving the degeneracy and the position of the minima. Using a multi-layer automatised reduction, we shall demonstrate how quantum annealers can be utilised to solve higher order Diophantine equations despite current hardware limitations. Although we are unable to prove the advantage of using quantum annealer against other classical techniques, the methods we have developed give valuable insights on the future applicability of quantum annealers to solve this kind of problems.

Diophantine equations are ubiquitous in physics, from anomaly cancellation conditions in particle physics to consistency conditions in strings theory. Being undecidable problems, they are notoriously hard to solve. Sometimes they can be significantly simplified using for example Gröbner basis methods, but typically such a problem is computationally hard.

This is certainly the case for the typical anomaly cancellation problem, which entails the solving of a coupled set of cubic equations with an independent rational variable appearing for every charge of every particle. In a system whose size is comparable to that of say the Standard Model of parti-

cle physics, an exhaustive scan becomes infeasible even when the domain of allowed charges is restricted. Indeed determining precisely which complexity class a problem falls into is itself an important question.

For such problems, scaleable Ising hardware solvers, which form the basis of both simulated and quantum annealers, could have huge impact, particularly as NP problems can be formulated as Ising problems with only polynomial overhead.

Anomaly cancellation and related physics problems do not constitute the sole physics applications of the technique we will present in this thesis. Indeed, we shall also discuss how to use annealers to search for a particular class of string theory vacua. This breaks new ground by for the first time implementing string models directly on a quantum annealer, using the annealer to search for string theories with SM-like properties. Indeed, quantum annealing has to date been utilised in other settings, notably for solving network problems, but its application in high energy theory has up to now been somewhat limited.

Besides their direct use in string theory, we shall discuss how these machines can be employed to enhance meta-heuristic algorithms. Our focus will be on a hybrid technique which combines genetic algorithms (GAs) and quantum annealing. Genetic algorithms are a class of optimisation algorithms inspired by the principles of biological evolution and natural selection. They are used to find approximate solutions to complex problems, especially in cases where the search space is vast and traditional optimisation methods

are less effective.

Although they represent a valuable computational resource for many problems, their effectiveness could be considerably reduced for larger search spaces, which is typical in string contexts. This constitutes the main reason why we have investigated on the possibility to enhance such algorithms using quantum annealers. We shall call this hybrid approach GQAA (*Genetic Quantum Annealing Algorithm*), which demonstrates to be superior to vanilla GA. We shall test the methods on various grounds, from pure number theory to heterotic line bundle models in string theory.

To recap, this thesis is structured as follows. After a review on the basic formulation of string theory in chapter 2, we shall introduce in chapter 3 a completely new model-independent framework for closed string theory. We shall see how these methods can be employed to compute one-loop physical quantities, with a closer focus on the running of gauge couplings at one-loop. Having developed a set of new formal tools, we then move on to new computational approaches with the aim to use them in string contexts. Chapter 4 illustrates one of these new methods which employs quantum annealers. We shall bench-mark it with a certain classes of problems in number theory which are also common in physics. We shall also introduce GQA and show how it performs in comparison with normal GA. We shall again road-test the method solving various number theory problems. Finally, in chapter 5 we will apply these techniques in string theory, directly constructing $SO(10)$ heterotic model on quantum annealers and using GQAA to search for SM-

like line bundle heterotic models. We then conclude summarising our results in chapter 6.

Chapter 2

String Theory: Basics Aspects

2.1 Action and symmetries

To study string theory, our starting point is the action in the path-integral formulation of field theory. In this formulation, the basic entities are fields representing point-particles, which can assume any value at any given point in spacetime. The transition amplitude between different points in space (or momentum space) is determined by integrating over all possible paths. Each path or worldline is assigned a weight based on its corresponding action. In the case of string theory, the fundamental entities are one-dimensional strings that sweep across a two-dimensional surface known as a worldsheet. As a result, the path integral comes from an action that depends on two variables. In bosonic string theory, the fields in the theory correspond to the spacetime coordinates. However, in superstring theory, we also introduce

fermionic coordinates for each dimension of spacetime.

To put it simply, for a free point-particle, the physical path taken between two points in spacetime is the world line of minimum length connecting those points. In analogy with that, the path of a free one-dimensional object will be the surface of minimum area that the object sweeps during its propagation. Thus, the action is a functional of this area and the true trajectory is described by the functions that extremise this action.

Let X^μ be the coordinates of the surface spanned by the string in the D-dimensional Minkowsky space-time, with $\mu = 0, ..., D-1$ and metric $\eta^{\mu\nu} = \text{diag}(-1, 1, ..., 1)$. This surface is parametrised by two variables: σ and τ, the so-called world-sheet parameters. By convention $\sigma \in [0, \pi]$ parametrises the points along the string, whereas $\tau \in (-\infty, +\infty)$ denotes its proper time. In this form the action is called the Nambu-Goto action and corresponds to the following expression

$$S_{\text{NG}} = -\frac{1}{4\pi\alpha'} \int d\sigma d\tau \sqrt{-\text{det}(\partial_\alpha X^\mu \partial_\beta X^\nu \eta_{\mu\nu})}\,, \tag{2.1}$$

where α' is a constant with $[\alpha'] = M^{-2}$. It can be shown that this action is classically equivalent to the following linear action [12–15]

$$S_{\text{P}} = -\frac{1}{4\pi\alpha'} \int d^2\sigma \sqrt{g} g^{\alpha\beta} \partial_\alpha X^\mu \partial_\beta X^\nu \eta_{\mu\nu} \tag{2.2}$$

where $g_{\alpha\beta}$ is the metric on the world-sheet, and $g \equiv -\text{det} g_{\alpha\beta}$. The action (2.2) is called the Polyakov–Brink–Di Vecchia–Howe action. This form of the

action manifests all its symmetries, which are

- Global Poincaré in the D-dimensional target space;
- Reparameterisation of the surface spanned by the string, namely two-dimensional diffeomorphism on the worldsheet coordinates: $(\sigma, \tau) \to (\sigma', \tau')$;
- Local Weyl rescaling of the worldsheet metric: $g_{\alpha\beta} \to \Omega(\sigma, \tau) g_{\alpha\beta}$, where Ω is an arbitrary function of σ and τ.

We can use the last two properties to fix the metric on the world-sheet $g_{\alpha\beta}$ to be flat, that is $g_{\alpha\beta} = \text{diag}(-1, 1)$. The action then simplifies to

$$S \;=\; -\frac{1}{4\pi\alpha'} \int d^2\sigma \partial_\alpha X^\mu \partial^\alpha X_\mu \,. \tag{2.3}$$

The analysis conducted thus far has been confined to examining the theory exclusively at a classical level. Indeed, we could now proceed one step further quantising this theory and analysing its property from a purely quantum point of view. However, it turns out that bosonic string theory is not a phenomenological useful theory as it contains a few critical issues which are ultimately the reasons why it cannot be used to describe the real world. Thus, we defer the discussion about quantisation until we shall treat the fermionic string. As far as bosonic string theory is concerned, we shall just highlight its main attributes:

- The consistency of the theory imposes that $D = 26$, *i.e.*, $25 + 1$ space-time dimensions;
- The mass spectrum contains only space-time bosons, which is the reason why the theory is called *bosonic*;
- The mass spectrum includes the graviton, gauge fields, but also tachyons (superluminal particles of negative squared mass) .

As already mentioned, this theory is not phenomenologically appealing for two main reasons: the presence of tachyons is a signal of vacuum instability and therefore inconsistency of the theory; from the spacetime point of view, the matter content of the theory involves only bosons which is clearly in contrast with what we observe in the real world.

To construct a much more interesting string theory we introduce fermionic degrees of freedom $\psi^\mu(\sigma, \tau)$ on the world-sheet along with the familiar bosonic coordinates $X^\mu(\sigma, \tau)$ such that the system enjoys supersymmetry in two dimensions. It is worth stressing that the two-dimensional fields $\psi^\mu(\sigma, \tau)$ are fermions on the world-sheet but they transform as vectors under the D-dimensional space-time Poincaré group, behaving as space-time bosons. The action is now

$$S = -\frac{1}{4\pi\alpha'} \int d^2\sigma \left\{ \partial_\alpha X^\mu \partial^\alpha X_\mu - i\bar{\psi}^\mu \rho^\alpha \partial_\alpha \psi_\mu \right\}, \tag{2.4}$$

where $\alpha = 0, 1$, $\mu = 0, ..., D-1$ and ρ^α are two dimensional Dirac matrices,

which obey the usual anticommutation relation: $\{\rho^\alpha, \rho^\beta\} = -2\eta^{\alpha\beta}$, with $\eta^{\alpha\beta} = \text{diag}(-1, 1)$. We adopted the following basis for the Dirac gamma matrices

$$\rho^0 = \begin{pmatrix} 0 & -i \\ i & 0 \end{pmatrix}, \qquad \rho^1 = \begin{pmatrix} 0 & i \\ i & 0 \end{pmatrix}. \tag{2.5}$$

We also set $\bar{\psi} \equiv \psi^\dagger \rho^0 = \psi^T \rho^0$, where ψ is a real Majorana spinor.

The action (2.4) is the gauge-fixed version of a more generical action which involves additional fields that promote the global supersymmetry to its local version. The two-dimensional supergravity involves now a two-dimensional world-sheet metric (as in the case of the bosonic string) and its fermionic super-partner, namely the gravitino. It turns out that these fields are not dynamical in two dimensions. Therefore, taking advantage of the large symmetry of the supergravity Lagrangian (local supersymmetry, diffeomorphisms on the world-sheet, Weyl and super-Weyl transformation) we can gauge away these non-dynamical degrees of freedom leaving with the action in Eq. (2.4). The inclusion of these symmetries within the complete Lagrangian yields several implications that are not immediately evident in Eq. (2.4). These implications assume paramount significance upon quantisation, as they ensure the appropriate probabilistic interpretation of the theory. We postpone this discussion and for now we just observe that the gauge fixed action in Eq. (2.4) is still invariant under the following global supersymmetry trans-

formations

$$\begin{cases} \delta X^{\mu} &= \bar{\epsilon}\psi^{\mu} \\ \delta\psi^{\mu} &= -i\rho^{\alpha}\partial_{\alpha}X^{\mu}\epsilon\,, \end{cases} \tag{2.6}$$

where ϵ is a constant (*i.e.*, independent of σ and τ) infinitesimal Majorana spinor.

To this symmetry is associated the following super-current

$$J_{\alpha} \;=\; \rho^{\beta}\rho_{\alpha}\partial_{\beta}X_{\mu}\psi^{\mu}\,, \tag{2.7}$$

with the property that $\rho^{\alpha}J_{\alpha} = 0$, which is a consequence of the super-conformal symmetry of the supergravity Lagrangian.

2.2 Quantisation

To initiate the quantisation of the theory described by the action in Eq. (2.4), we impose the canonical commutation and anti-commutation relations for both the bosonic and fermionic fields. These relations define the fundamental rules for quantising a system with dynamical variables and their conjugate momenta. Therefore we proceed by imposing

$$\begin{aligned} [X^{\mu}(\sigma,\tau), P_{X}^{\nu}(\sigma',\tau)] &= i\eta^{\mu\nu}\delta(\sigma-\sigma')\,, \\ \left\{\psi^{\mu}(\sigma,\tau), P_{\psi}^{\nu}(\sigma',\tau)\right\} &= i\eta^{\mu\nu}\delta(\sigma-\sigma')\,, \end{aligned} \tag{2.8}$$

where $P_X^\nu = \frac{1}{2\pi\alpha'}\dot{X}^\nu$ and $P_\psi^\nu = \frac{i}{4\pi\alpha'}\bar{\psi}^\mu\rho^0$ are the conjugate momenta to X^ν and ψ^ν, respectively. To proceed with the quantisation process, we must first derive the equations of motion for all the fields involved. To achieve this, we introduce a set of convenient coordinates on the world-sheet, known as the light-cone coordinates. These coordinates are defined as

$$\sigma^\pm \;=\; \tau \pm \sigma\,, \tag{2.9}$$

and lead to the following expression of the action

$$S \;=\; \frac{1}{2\pi\alpha'}\int d^2\sigma\left\{2\partial_+X^\mu\partial_-X_\mu \;+\; i(\psi_+^\mu\partial_-\psi_{\mu,+} + \psi_-^\mu\partial_+\psi_{\mu,-})\right\}, \tag{2.10}$$

where we have defined

$$\psi^\mu \;\equiv\; \begin{pmatrix}\psi_-^\mu\\ \\ \psi_+^\mu\end{pmatrix}\,, \tag{2.11}$$

with $\psi_\pm$ Majorana-Weyl spinors of opposite chirality. It is straightforward to deduce the equations of motion, which read

$$\partial_+\partial_-X^\mu \;=\; 0\,, \tag{2.12}$$

$$\partial_+\psi_-^\mu \;=\; 0\,, \tag{2.13}$$

$$\partial_-\psi_+^\mu \;=\; 0\,, \tag{2.14}$$

with the following boundary conditions

$$\begin{aligned} \partial_\sigma X^\mu \delta X_\mu \Big|_{\sigma=0}^{\sigma=\pi} &= 0\,, \\ (\psi_+^\mu \delta\psi_{\mu,+} - \psi_-^\mu \delta\psi_{\mu,-})\Big|_{\sigma=0}^{\sigma=\pi} &= 0\,. \end{aligned} \tag{2.15}$$

The solutions to the equations can be expressed as Fourier series

$$\begin{aligned} X^\mu(\sigma,\tau) &= X_R^\mu(\sigma^+) + X_L^\mu(\sigma^-) \\ &= x^\mu + \alpha' p_R^\mu \sigma^+ + \alpha' p_L^\mu \sigma^- + i\sqrt{\frac{\alpha'}{2}} \sum_{n\neq 0} \left\{ \frac{\alpha_n^\mu}{n} e^{-in\sigma^-} + \frac{\tilde{\alpha}_n^\mu}{n} e^{-in\sigma^+} \right\}, \\ \psi_+^\mu(\sigma^+) &= \sqrt{2\alpha'} \sum_\nu c_\nu^\mu e^{-i\nu\sigma^+}\,, \\ \psi_-^\mu(\sigma^-) &= \sqrt{2\alpha'} \sum_\nu c_\nu'^\mu e^{-i\nu\sigma^-}\,. \end{aligned} \tag{2.16}$$

The bosonic coordinate is written as a sum of two contributions which depend on σ^+ (left movers) and σ^- (right movers), respectively. At this stage, the frequencies n and ν remain still undetermined, their values will be fixed upon enforcing the boundary conditions. Furthermore, it is worth noting that α_n^μ, $\tilde{\alpha}_n^\mu$, c_ν, and c'_ν are currently classical numbers (c-numbers). However, during the quantisation process, we will identify them as creation and annihilation operators.

2.2.1 Closed string

Closed strings arise from the following boundary conditions

$$X^\mu(\sigma+\pi,\tau) \;=\; X^\mu(\sigma,\tau)\,, \tag{2.17}$$

$$\psi^\mu_\pm(\tau,\pi) \;=\; \psi^\mu_\pm(\tau,0) \quad \text{or} \quad \psi^\mu_\pm(\tau,\pi) = -\psi^\mu_\pm(\tau,0)\,. \tag{2.18}$$

It should be noted that nothing in Eqs. (2.15) prevents to impose anti-periodic conditions instead of periodic ones. Indeed, Eqs. (2.15) are satisfied in both cases leading to two different types of strings, or rather two sectors: the Ramond and Neveu-Schwarz sectors, respectively. Imposing the conditions in Eqs. (2.17), (2.18) the solutions in Eq. (2.16) become

$$\begin{aligned} X^\mu(\sigma,\tau) \;&=\; x^\mu + 2\alpha' p^\mu \tau + i\sqrt{\frac{\alpha'}{2}} \sum_{n\in\mathbb{Z},n\neq 0} \left\{ \frac{\alpha^\mu_n}{n} e^{-2in\sigma^-} + \frac{\tilde\alpha^\mu_n}{n} e^{-2in\sigma^+} \right\}, \\ \psi^\mu_+(\sigma^+) \;&=\; \sqrt{2\alpha'} \sum_{\nu\in\mathbb{Z}+\Phi} c^\mu_\nu e^{-2i\nu\sigma^+}, \end{aligned} \tag{2.19}$$

and analogous for ψ_-. For the Ramond sector $\Phi = 0$, $c^\mu_\nu \equiv d^\mu_\nu$ whereas for the Neveu-Schwarz sector $\Phi = 1/2$ and $c^\mu_\nu \equiv b^\mu_\nu$.

2.2.2 Open string

Open strings arise from the following boundary conditions

$$\begin{cases} \partial_\sigma X^\mu\big|_{\sigma=0} \;=\; 0 \quad \text{or} \quad \partial_\tau X^\mu\big|_{\sigma=0} \;=\; 0\,, \\ \partial_\sigma X^\mu\big|_{\sigma=\pi} \;=\; 0 \quad \text{or} \quad \partial_\tau X^\mu\big|_{\sigma=\pi} \;=\; 0\,, \\ \psi_+^\mu(\tau,0) \;=\; \psi_-^\mu(\tau,0)\,, \\ \psi_+^\mu(\tau,\pi) \;=\; \psi_-^\mu(\tau,\pi) \quad \text{or} \quad \psi_+^\mu(\tau,\pi) \;=\; -\psi_-^\mu(\tau,\pi)\,. \end{cases} \tag{2.20}$$

Focusing exclusively on bosonic coordinates, we note that four combinations of boundary conditions are possible. We shall refer to the conditions on the left and on the right as Neumann and Dirichlet conditions, respectively. Consequently, combing the two sectors, we have a total of four combinations: Neumann-Neumann (NN), Dirichlet-Dirichlet (DD), Neumann-Dirichlet (ND) and Dirichlet-Neumann (DN). These combinations correspond to the conditions at $\sigma = 0$ and $\sigma = \pi$, respectively.

In a similar fashion, Ramond and Neveu-Schwarz sectors appear also along the fermionic coordinates: the third line corresponds to the former, whereas the second one to the latter. We now impose Neumann-Neumann boundary conditions on all the bosonic coordinates, which results to the following expression

$$X^\mu(\sigma,\tau) \;=\; x^\mu + 2\alpha' p^\mu \tau + i\sqrt{2\alpha'} \sum_{n\neq 0} \frac{\alpha_n^\mu}{n}\, e^{-in\tau}\, \cos(n\sigma)\,. \tag{2.21}$$

On the other hand, imposing Dirichlet-Dirichlet (DD) conditions leads to

$$X^\mu(\sigma,\tau) \;=\; x^\mu + 2\alpha' p^\mu \sigma + i\sqrt{2\alpha'}\sum_{n\neq 0}\frac{\alpha_n^\mu}{n}\, e^{-in\tau}\,\sin(n\sigma)\,. \tag{2.22}$$

The crucial distinction between imposing NN and DD conditions lies in the behavior of the zero mode, which depends on the parameter τ in the NN case and σ in the DD case. When we impose DD conditions along a specific coordinate, let us call it X^ν, the momentum of the center of mass of the string will have no contribution along the ν direction. Consequently, if $D = 10$ as we shall set later, the endpoints of the string are constrained to reside in a 9-dimensional space, unable to move freely along the X^ν coordinate. These 9-dimensional entities are commonly known as D_p-branes, where p corresponds to the number of dimensions the branes span. In this particular case, we have a D_8-brane. On the other hand, if we impose NN conditions on all coordinates, the string retains the freedom to move throughout the entire 10-dimensional space-time, effectively representing a D_9-brane.

Applying both boundary conditions in Eq. (2.20) to the fermionic mode expansion leads to

$$\psi_+^\mu(\sigma^+) \;=\; \sqrt{2\alpha'}\sum_{\nu\in\mathbb{Z}+\Phi} c_\nu^\mu\, e^{-i\nu\sigma^+}\,, \tag{2.23}$$

and analogous for ψ_-. $\Phi = 0, 1/2$ corresponds to Ramond and Neveu-Schwarz sectors, respectively. We shall also denote c_ν^μ as d_ν^μ or b_ν^μ depending

on the sector, Ramond and Neveu-Schwarz, respectively.

After deriving the mode expansion for both open and closed strings in their respective sectors, our next step is to impose the canonical commutation relations as given in Eq. (2.8). For convenience we shall focus on closed strings only in the rest of this section, the quantisation procedure for open strings is completely analogous. By applying Neumann-Neumann conditions to all the coordinates we get the following relations

$$\begin{aligned} [\alpha_n^\mu, \alpha_m^\nu] &= [\tilde{\alpha}_n^\mu, \tilde{\alpha}_m^\nu] = n\,\delta_{n+m}\eta^{\mu\nu}\,, \\ \{d_p^\mu, d_q^\nu\} &= \{\tilde{d}_p^\mu, \tilde{d}_q^\nu\} = \delta_{p+q}\,\eta^{\mu\nu}\,, \\ \{b_r^\mu, b_s^\nu\} &= \{\tilde{b}_r^\mu, \tilde{b}_s^\nu\} = \delta_{r+s}\,\eta^{\mu\nu}\,, \end{aligned} \tag{2.24}$$

where the tilde distinguishes the left from the right sector in the closed string case and $m, n \in \mathbb{Z} \setminus \{0\}$, $p, q \in \mathbb{Z}$, $r, s \in \mathbb{Z} + 1/2$. It should be noted that these relations are the same as the ones between creation and annihilation operators for the bosonic and fermionic harmonic oscillators. Indeed, we can identify α_m^ν and $\tilde{\alpha}_m^\nu$ with $m < 0$ and $m > 0$ as creation and annihilation operators respectively. Upon imposing reality conditions for X^μ and the Majorana-Weyl spinors ψ^μ, we arrive at fundamental relations: $(\alpha_n^\mu)^\dagger = \alpha_{-n}^\mu$, $(b_r^\mu)^\dagger = b_{-r}^\mu$, and $(d_p^\mu)^\dagger = d_{-p}^\mu$. As a consequence of these relations, states like $b_r^0\,|0\rangle$, $d_\nu^0\,|0\rangle$, and $\alpha_n^0\,|0\rangle$ (where $n < 0$) have negative norms. This issue raises concerns in both the open and closed string sectors, leading to apparent inconsistencies at the quantum level. The presence of states with negative

norms undermines the fundamental probabilistic interpretation that is crucial for any viable quantum theory. This apparent contradiction is solved by considering the full set of symmetries of the action in Eq. (2.4). We note that this gauge fixed action has an additional symmetry, it is invariant under the following reparametrisation: $\sigma^{\pm} \to \tilde{\sigma}^{\pm}(\sigma^{\pm})$. Introducing the target-space coordinates

$$X^{\pm} = \frac{1}{\sqrt{2}} \left(X^0 \pm X^{D-1} \right), \tag{2.25}$$

$$\psi^{\pm} = \frac{1}{\sqrt{2}} \left(\psi^0 \pm \psi^{D-1} \right), \tag{2.26}$$

we can use this symmetry to set

$$\begin{cases} X^+ = x^+ + 2\alpha' p^+ \tau \,, \\ \psi^+ = 0 \,, \end{cases} \tag{2.27}$$

which in turn set α_n^+, b_r^+ and d_ν^+ to zero (and similar for the right sector). Being two symmetries of the theory, translational symmetry and supersymmetry have their own conserved currents: the stress-energy tensor $T_{\alpha\beta}$ and the super-current written in Eq. (2.7), respectively. Following the discussion in Ref. [12] we arrive at the following constraints

$$\begin{cases} T_{\alpha\beta} = 0 \,, \\ J_\alpha = 0 \,. \end{cases} \tag{2.28}$$

In the light-cone coordinates this translates into

$$\begin{cases} T_{++} \;=\; -2\partial_+ X^+ \partial_+ X^- + \partial_+ X^i \partial_+ X_i + \frac{i}{2}(-2\psi_+^+ \partial_+ \psi_+^- + \psi_+^i \partial_+ \psi_{+,i}) \;=\; 0\,, \\ J_+ \;=\; -\partial_+ X^+ \psi_+^- - \partial_+ X^- \psi_+^+ + \partial_+ X^i \psi_{+,i} \;=\; 0\,, \end{cases} \tag{2.29}$$

where $i = 1, ..., D-2$. By substituting Eq. (2.27) into Eq. (2.29), we can express the remaining longitudinal oscillators (α_n^-, b_r^-, and d_ν^-) in terms of the remaining transverse oscillators. Consequently, the transverse oscillators become the only independent degrees of freedom to construct the Fock space. This approach ensures that no states with negative norms will appear in the spectrum, resulting in a perfectly consistent ghost-free theory. The first line in Eq. (2.29) leads directly to the mass-shell condition for the string, which reads

$$\begin{cases} M^2 \;=\; \frac{2}{\alpha'}(N_X + N_\psi + \widetilde{N}_X + \widetilde{N}_\psi + \Delta + \widetilde{\Delta})\,, \\ N_X + N_\psi - \widetilde{N}_X - \widetilde{N}_\psi + \Delta - \widetilde{\Delta} \;=\; 0\,, \end{cases} \tag{2.30}$$

where we have defined the number operators

$$\begin{aligned} N_X \;&\equiv\; \sum_{n=1}^{+\infty} \alpha_{-n}^i \alpha_n^i\,, \\ N_\psi \;&\equiv\; \sum_{\nu=1}^{+\infty} d_{-\nu}^i d_\nu^i \qquad \text{for the Ramond sector}\,, \\ N_\psi \;&\equiv\; \sum_{s=1/2}^{+\infty} b_{-s}^i b_s^i \qquad \text{for the Neveu-Schwarz sector}\,, \end{aligned} \tag{2.31}$$

and where the sum over i is understood. The Δ and $\widetilde{\Delta}$ contributions in

Eq. (2.30) are the zero-point energies, corresponding to the sum of the bosonic and fermionic zero-point energies. They appear as a consequence of the normal ordering of the number operators and are regularised using the Riemann zeta function. Each fermionic coordinate contributes with $-\frac{1}{48}$ in the NS sector and with $\frac{1}{24}$ in the R sector, whereas each boson contributes with $-\frac{1}{24}$. As a result, for each set of modes the total energy shift in D dimensions is $-\frac{1}{16}(D-2)$ in the NS sector, but vanishes in the R sector.

The second line of Eq. (2.30) introduces the so-called level-matching condition. It states that not all states created by a random combination of bosonic and fermionic creation operators acting on the vacuum are physical states. Only those states that fulfill this condition are considered genuine states of the theory, contributing to meaningful physical quantities. However, we shall see that even unphysical states — referred to as non-level-matched states — play a crucial role in the theory. Despite being unphysical, they have noteworthy implications, particularly in determining certain physical quantities at the one-loop level.

Let us now move on to the analysis of the low-energy spectrum of the closed string. Without going into much details we briefly discuss the content of the mass spectrum. In the NS-NS sector the vacuum is tachyonic and the other massive excitations are space-time bosons; the right(left)-vacuum in the R-R sector carries spinorial representations of the $SO(8)$, which we denote as 8_s and 8_c (two irreducible representations of opposite chirality). Therefore, the R-R vacuum for the closed string is composed by the following massless

states: $|s,\tilde{s}\rangle$, $|s,\tilde{c}\rangle$, $|c,\tilde{s}\rangle$ and $|c,\tilde{c}\rangle$, corresponding to all possible combinations of the representations. Being objects with two spinorial indices, these states are space-time bosons. Finally, NS-R (or R-NS) sectors introduce the crucial difference between bosonic and superstring theory: these sectors introduce target-space fermions in the theory, which were missing in the bosonic theory. In a manner similar to the bosonic string, preserving Lorentz invariance requires us to enforce the vanishing mass of transverse vectors in the string's spectrum. This condition sets the spacetime dimension to $D = 10$.

2.3 One-loop vacuum amplitude and UV/IR mixing

Let us now proceed comparing quantum field theory and string theory, focusing on the structure of their one-loop amplitudes. In quantum field theory, the one-loop vacuum amplitude is a function of the masses of the finite number of fields of a given model, fully determined by the free spectrum that does not embody important structural information. On the other hand, strings describe infinitely many modes, a sort of quantum field theory with infinite fields. Computing the vacuum amplitude in string theory becomes is crucial for obtaining significant insights into both the massive and massless excitations of the string. This amplitude provides valuable information about the entire spectrum of the string's excitations. In quantum field theory, the one-loop vacuum amplitude is depicted using a circle Feynman diagram. How-

ever, for closed strings, this diagram takes on a distinct shape, forming torus due to the string's one-dimensional nature. Describing the propagation of a string, this torus is characterised by a complex variable called the Teichmüller parameter, or modulus of the torus, defined as τ and can be effectively represented by a periodic lattice in the complex plane, where the fundamental cell is identified by the modulus $\tau \equiv \tau_1 + i\tau_2$, as depicted in Fig. 2.1. This representation establishes a one-to-one correspondence between the points inside the cell and the points on the surface of the torus. The parallel segments that enclose the fundamental cell are matched pairwise, reflecting the torus's topological properties. One may now wonder whether two arbitrary

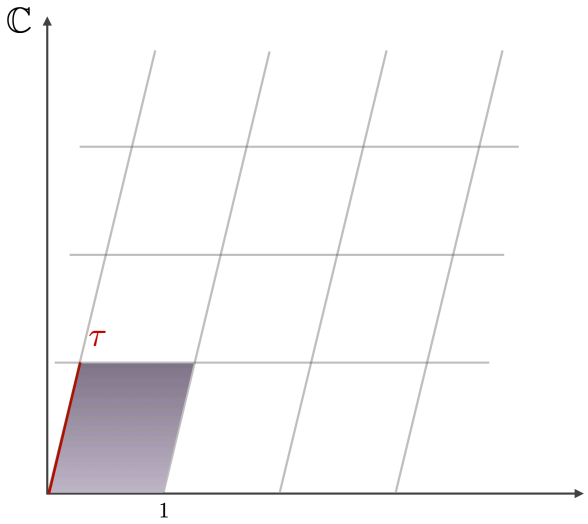

Figure 2.1: A torus represented as a fundamental cell in violet in the complex plane. The points in the cell are in one-to-one correspondence with the points of the surface of the torus.

choices of τ always correspond to two different tori. Indeed, one can eas-

ily prove that two τ's related by a $\mathrm{PSL}(2,\mathbb{Z}) = \mathrm{SL}(2,\mathbb{Z})/\mathbb{Z}_2$ transformation identify the same torus. This sort of redundancy buried in the theory is an unequivocal sign of the emerging of a fundamental symmetry of all closed string theories. This symmetry is commonly referred as modular invariance and corresponds to invariance under $\mathrm{PSL}(2,\mathbb{Z})$ transformations, which acts on τ according to

$$\tau \to \frac{a\tau + b}{c\tau + d} \qquad \text{with} \qquad ad - bc \;=\; 1\,, \quad a, b, c, d \in \mathbb{Z}\,. \tag{2.32}$$

One may now wonder which is the precise sub-region of the complex τ-plane that comprises exclusively inequivalent tori, which, in analogy with usual quantum field theory, has to be naturally identified with the integration domain. In other words, we are interested in identifying the τ values that are not connected by any $\mathrm{PSL}(2,\mathbb{Z})$ transformation. An essential property of this group, which will be relevant in our subsequent analysis, lies in the fact that all its elements can be expressed as words containing two generators, T and S, which are defined as

$$T = \begin{pmatrix} 1 & 1 \\ 0 & 1 \end{pmatrix}, \qquad S = \begin{pmatrix} 0 & -1 \\ 1 & 0 \end{pmatrix}, \tag{2.33}$$

and therefore every group element can be written as

$$g \in \mathrm{PSL}(2,\mathbb{Z}) \;\Leftrightarrow\; g = S^{n_1} T^{n_2} \cdot \ldots \cdot S^{n_k}\,, \tag{2.34}$$

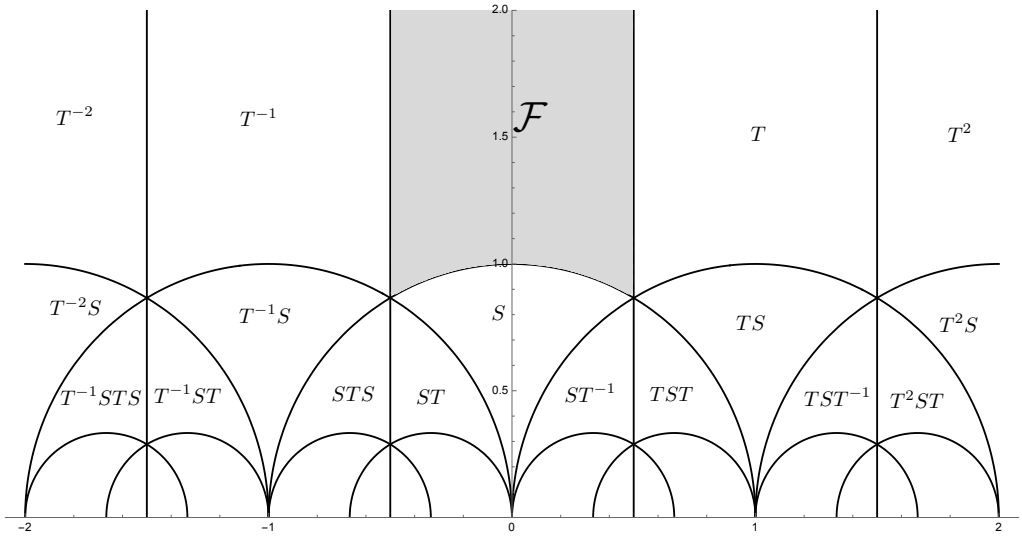

Figure 2.2: The complex τ-plane modded by T and S modular transformations. Each labelled region contains exclusively inequivalent tori, *i.e.*, the τ's inside the region are not related by any $\mathrm{PSL}(2,\mathbb{Z})$ transformation. The shaded region denoted by $\mathcal{F}$ is called fundamental domain and is the most common choice to express 1-loop integrals. All the other regions are labelled with the set of transformations (written in terms of T and S generators) one has to apply to $\mathcal{F}$ to retrieve the specific region and are perfectly well-defined alternative choices to $\mathcal{F}$.

where $n_1, ..., n_k$ are integers. The action of the two generators on τ can be expressed as follows

$$\tau \xrightarrow{\mathrm{T}} \tau + 1\,, \qquad \tau \xrightarrow{\mathrm{S}} -\frac{1}{\tau}\,. \tag{2.35}$$

Fig. 2.2 illustrates the complex τ-plane, partitioned by T and S transformations. Each distinct region in the figure consists solely of inequivalent

tori, represented by different values of τ that are not related through any $\mathrm{PSL}(2,\mathbb{Z})$ transformation. Therefore, to prevent over-counting, we need to select one of these regions as the domain of integration. The commonly preferred choice is the shaded area, often denoted as $\mathcal{F}$, which stands for fundamental domain. Inside the regions depicted in Fig. 2.2, the labels indicate the sequence of transformations needed to map the fundamental domain $\mathcal{F}$ onto the corresponding area. As we shall see, each of these regions represents a valid alternative choice to the fundamental domain $\mathcal{F}$, offering a distinct but well-defined approach to integrate over inequivalent tori.

Modular invariance has profound consequences on the distribution of strings states and will ultimately lead to an equivalence between the UV and IR, often referred as UV/IR mixing. In general, one-loop closed-string amplitudes are typically expressed in terms of modular-invariant integrands $F(\tau)$ which are integrated over the fundamental domain $\mathcal{F}$. If such an amplitude has a certain behaviour (even divergent) when $\tau_2 \to \infty$, it would be natural to interpret it as an IR limit involving low-energy physics. Indeed, we shall see that all the contributions from the heavy string states within the integrand are naturally suppressed as $\tau_2 \to \infty$.

However, such an interpretation would be inconsistent within a modular-invariant theory. In any modular-invariant theory with a modular-invariant integrand $F(\tau)$, we can always rewrite our amplitude through the identity

$$\int_{\mathcal{F}} \frac{d^2\tau}{\tau_2^2}\, F(\tau) \;=\; \int_{\mathcal{F}} \frac{d^2\tau}{\tau_2^2}\, F(\gamma\cdot\tau) \;=\; \int_{\gamma\cdot\mathcal{F}} \frac{d^2\tau}{\tau_2^2}\, F(\tau) \tag{2.36}$$

which holds for any $\gamma \in \mathrm{PSL}(2,\mathbb{Z})$. From the above equation we see that choosing $\mathcal{F}$ as our region of integration is mathematically equivalent to choosing any of its images $\gamma\cdot\mathcal{F}$ under any modular transformation γ. One of these equivalent choices is $\mathcal{F}' \equiv S\cdot\mathcal{F}$ where S is defined as in Eq. (2.35) and depicted in Fig. 2.2 as the "S" region, right below the fundamental domain $\mathcal{F}$. This region includes the $\tau_2 \to 0$ region but no longer includes the $\tau_2 \to \infty$ region. Indeed, via the identity in Eq. (2.36) we see that whatever behaviour the integrand has for large values of τ_2, the same behaviour is mapped onto the $\tau_2 \to 0$ within the "S" region. However, there is no suppression of the contributions from the heavy string states within the integrand as $\tau_2 \to 0$. Instead, the behaviour of the integrand as $\tau_2 \to 0$ depends on how the heavy string states accumulate in the limit and would therefore naturally be interpreted as a UV effect. Thus, by trading $\mathcal{F}$ for the "S" region we see that we can always mathematically recast what would naively appear to be an IR divergence as $\tau_2 \to \infty$ into what would naively appear to be a UV divergence as $\tau_2 \to 0$.

It is possible, and also very common, that the amplitude in question diverges. As we have seen, if we choose the fundamental domain $\mathcal{F}$ as defined in Fig. 2.2 then this divergence will manifest itself as an IR divergence. However, if we choose "S" as our fundamental domain, this same divergence of the amplitude will manifest itself as a UV divergence. Both interpretations are equally valid because the divergence of a one-loop modular-invariant string amplitude is neither intrinsically UV nor intrinsically IR. Indeed, such a di-

vergence is a property of the amplitude itself and is not intrinsically tied to any particular value of τ. Such a divergence is then merely represented as a UV or IR divergence depending on our choice of a region of integration. UV and IR are therefore folded upon each other. It is ultimately in this way that our modular-invariant string theory loses its ability to distinguish between UV and IR physics.

Let us not move on to the main ingredients of the following discussion. The one-loop vacuum amplitude of a closed oriented[1] string corresponds to a torus amplitude (which we shall denote by $\mathcal{T}$) and can be written as

$$\begin{aligned}\mathcal{T} &= \int_{\mathcal{F}} \frac{d^2\tau}{\tau_2^2}\,\tau_2^k\ \mathrm{tr}\Big\{q^{N_X+N_\psi+\Delta}\,\overline{q}^{\widetilde{N}_X+\widetilde{N}_\psi+\widetilde{\Delta}}\Big\} \\ &= \int_{\mathcal{F}} \frac{d^2\tau}{\tau_2^2}\,\tau_2^k \sum_{m,n} a_{mn}\ \overline{q}^m q^n\,, \end{aligned} \tag{2.37}$$

where a_{mn} is the net (bosonic minus fermionic) number of string states with right- and left-moving worldsheet energies (m,n) in the string spectrum, $k = 1 - D/2$ and D is the number of uncompactified dimensions, q is defined as $q \equiv e^{2i\pi\tau}$ ($\overline{q}$ is its complex conjugate), and

$$\mathcal{F} = \Big\{ -\frac{1}{2} < \tau_1 \leq \frac{1}{2},\ |\tau| \geq 1 \Big\} \tag{2.38}$$

[1]The term "oriented" refers to the surface spanned by the string in the spacetime during its propagation which is an orientable surface. Non-oriented strings may also appear in other string theories but they are not the object of this study.

is the fundamental domain. To recast the expression in the second form is sufficient to write explicitly the trace as a sum over the entire tower of discrete string states and define $m \equiv \widetilde{N}_X + \widetilde{N}_\psi + \widetilde{\Delta}$ and $n \equiv N_X + N_\psi + \Delta$ the right- and left-moving worldsheet energies of the string excitation. Thus, each term in the m, n sum corresponds to a string state, which is counted with its degeneracy $a_{m,n}$ and with a plus or minus sign depending whether the state is bosonic or fermionic, respectively. Using Eq. (2.30) and rewriting q in terms of τ_1 and τ_2, we can easily see that massive states are exponentially suppressed for large τ_2 as $e^{-\pi\tau_2 M^2}$. In a similar fashion, one can show that the opposite is valid when $\tau_2 \to 0$, *i.e.*, massless states are retained and massive ones are suppressed, according to the analysis above.

Computing the trace in Eq. (2.37) by combining all possible sectors — NS-NS, R-R, NS-R, and R-NS — would lead to a partition function that lacks modular invariance, and the spectrum would not be supersymmetric from a space-time perspective. Such a lack of modular invariance renders the theory inconsistent as we have developed it thus far. Thus, we must find a suitable way to combine the NS and R sectors between left and right movers. To accomplish this, we divide the NS and R sectors into two parts. Within the NS sector, we differentiate states with an odd number of fermionic oscillators (fermions from the world-sheet perspective) from those with an even number of oscillators (bosons from the world-sheet viewpoint). Whereas, in the Ramond sector, we distinguish the states based on their chirality. This separation will allow us to effectively combine the sectors and achieve

a modular-invariant and consistent theory. To keep track of chirality and world-sheet bosons and fermions, we introduce the following projectors

$$\frac{1 \pm (-1)^{F_{NS}}}{2} \qquad \text{and} \qquad \frac{1 \pm \Gamma_{11}(-1)^{F_R}}{2}\,, \tag{2.39}$$

where $F_{NS} \equiv \sum_{i,r} b^i_{-r} b^i_r$ is the world-sheet fermion number and F_R is defined as $F_R \equiv \sum_{i,\nu} d^i_{-\nu} d^i_\nu$, with Γ_{11} the 10-dimensional analogue of the 4-dimensional $\gamma^5 \equiv i\gamma^0 \cdot \ldots \cdot \gamma^3$, where γ^i are the Dirac matrices (four dimensional representation of the Clifford Algebra). Plus and minus signs refers to bosons and fermions respectively. We shall refer to NS bosons and fermions as NS_+ and NS_-, respectively. Similarly we call R_+ and R_- the two Ramond sub-sectors with opposite chirality. The next crucial question that arises is how we can combine the sectors NS$\pm$ and R$\pm$ (both in the left and right movers) to construct a modular-invariant partition function. However before addressing this question, let us start by computing the traces in Eq. (2.37) for the various sectors utilising the projectors in Eq. (2.39). It is worth noting that the trace in Eq. (2.37) factorises into two distinct parts — one for the left movers and one for the right movers — each carrying its own projector. For the sake of clarity and simplicity, we will now concentrate solely on the left sector. The calculations for the right sector is analogous. Moreover, it is crucial to consider an important property, namely, the commutation of the bosonic oscillators (α^i_n) with the fermionic ones (b^i_r and d^i_ν). Consequently, the trace can be further decomposed into two distinct parts: one pertaining

to the bosonic oscillators and the other to the fermionic oscillators. However, it is noteworthy that the projectors defined in Eq. (2.39) operate exclusively on the fermionic component, effectively reducing to identity operators for the bosonic oscillators. Therefore, our focus remains on applying the projectors solely to the fermionic part of the trace. Let us now focus on the NS sector. We have

$$\mathrm{tr}\Big\{\frac{1\pm(-1)^{F_{NS}}}{2}\,q^{N_X-\frac{D-2}{24}+N_\psi-\frac{D-2}{48}}\Big\}\;=\;\mathrm{tr}\Big\{q^{N_X-\frac{D-2}{24}}\Big\}\,\mathrm{tr}\Big\{\frac{1\pm(-1)^{F_{NS}}}{2}\,q^{N_\psi-\frac{D-2}{48}}\Big\}\,, \tag{2.40}$$

where we have not specified the number of uncompactified dimensions. Later on we shall set $D=10$ (no compactification). A straightforward computation gives

$$\mathrm{tr}\Big\{q^{N_X-\frac{D-2}{24}}\Big\}\;=\;\left(\frac{1}{\eta(\tau)}\right)^{D-2}\,, \tag{2.41}$$

where the Dedekind eta function is defined as

$$\eta(\tau)\;\equiv\;q^{\frac{1}{24}}\prod_{n=1}^{+\infty}(1-q^n)\,. \tag{2.42}$$

Similarly one can compute the traces involving world-sheet fermions. Bringing all the pieces together we get

$$\mathrm{tr}\Big\{\frac{1\pm(-1)^{F_{NS}}}{2}q^{N_X-\frac{D-2}{24}+N_\psi-\frac{D-2}{48}}\Big\}\;=\;\frac{1}{\eta^8(\tau)}\underbrace{\frac{1}{2}\left(\frac{\theta_3^4(0|\tau)}{\eta^4(\tau)}\pm\frac{\theta_4^4(0|\tau)}{\eta^4(\tau)}\right)}_{\equiv\mathrm{NS}_\pm}. \tag{2.43}$$

The computation in the right sector repeats identically with τ replaced by $\overline{\tau}$. In the Ramond sector the vacuum is degenerate, this has been taken into account introducing a factor of 16 by hand. Applying similar steps as in the previous computation we find

$$16\,\mathrm{tr}\left\{\frac{1\pm\Gamma_{11}(-1)^{F_R}}{2}q^{N_X-\frac{D-2}{24}+N_\psi-\frac{D-2}{48}}\right\} \;=\; \frac{1}{\eta^8(\tau)}\underbrace{\frac{1}{2}\left(\frac{\theta_2^4(0|\tau)}{\eta^4(\tau)}\pm\frac{\theta_1^4(0|\tau)}{\eta^4(\tau)}\right)}_{\equiv \mathrm{R}_\pm}, \tag{2.44}$$

where we have defined the Jacobi theta function as follows

$$\begin{aligned}
\theta_1(z|\tau) &= 2\sin(\pi z)q^{\frac{1}{8}}\prod_{n=1}^{+\infty}(1-q^n)(1-q^ne^{2i\pi z})(1-q^ne^{-2i\pi z})\,,\\
\theta_2(z|\tau) &= 2\cos(\pi z)q^{\frac{1}{8}}\prod_{n=1}^{+\infty}(1-q^n)(1+q^ne^{2i\pi z})(1+q^ne^{-2i\pi z})\,,\\
\theta_3(z|\tau) &= \prod_{n=1}^{+\infty}(1-q^n)(1+q^{n-1/2}e^{2i\pi z})(1+q^{n-1/2}e^{-2i\pi z})\,,\\
\theta_4(z|\tau) &= \prod_{n=1}^{+\infty}(1-q^n)(1-q^{n-1/2}e^{2i\pi z})(1-q^{n-1/2}e^{-2i\pi z})\,.
\end{aligned} \tag{2.45}$$

In order to build a consistent modular invariant theory it is useful to introduce

the SO($2n$) characters as follows

$$\mathrm{O}_{2n}(z|\tau) = \frac{\theta_3^n(z|\tau)+\theta_4^n(z|\tau)}{2\eta^n(\tau)}\,, \tag{2.46}$$

$$\mathrm{V}_{2n}(z|\tau) = \frac{\theta_3^n(z|\tau)-\theta_4^n(z|\tau)}{2\eta^n(\tau)}\,, \tag{2.47}$$

$$\mathrm{S}_{2n}(z|\tau) = \frac{\theta_2^n(z|\tau)+i^{-n}\theta_1^n(z|\tau)}{2\eta^n(\tau)}\,, \tag{2.48}$$

$$\mathrm{C}_{2n}(z|\tau) = \frac{\theta_2^n(z|\tau)-i^{-n}\theta_1^n(z|\tau)}{2\eta^n(\tau)}\,. \tag{2.49}$$

It is also useful to define χ as

$$\chi = \begin{pmatrix} \mathrm{O}_8 \\ \mathrm{V}_8 \\ \mathrm{S}_8 \\ \mathrm{C}_8 \end{pmatrix}, \tag{2.50}$$

where $z = 0$ is understood. Within the ten-dimensional superstring, the relevant group is SO(8), which allows us to set $n = 4$ for our analysis. As a result, several significant identifications follow

$$\mathrm{O}_8 = \mathrm{NS}_+\,, \quad \mathrm{V}_8 = \mathrm{NS}_-\,, \quad \mathrm{S}_8 = \mathrm{R}_+\,, \quad \mathrm{C}_8 = \mathrm{R}_-\,, \tag{2.51}$$

and $\overline{O}_8 = \widetilde{\mathrm{NS}}_+$ and similar for the right sectors. With these tools at hand, our aim is to combine the various sectors in Eq. (2.51) in such a way that the resulting torus amplitude is modular invariant. The problem can be therefore

rephrased in terms of finding a matrix $\mathcal{N}_{\alpha\beta}$ such that

$$\mathcal{T} \;=\; \int_{\mathcal{F}} \frac{d^2\tau}{\tau_2^6} \sum_{\alpha,\beta=1}^{4} \overline{\chi}_\alpha \mathcal{N}_{\alpha\beta}\chi_\beta \tag{2.52}$$

is modular invariant. The solutions correspond to four different types of closed string theories. Setting $\mathcal{T}_{\text{type}} \equiv \overline{\chi}_\alpha \mathcal{N}_{\alpha\beta}\chi_\beta$, they are

$$\begin{aligned}
\mathcal{T}_{\text{IIA}} &= (\mathrm{V}_8 - \mathrm{S}_8)(\overline{\mathrm{V}}_8 - \overline{\mathrm{C}}_8)\,, \\
\mathcal{T}_{\text{IIB}} &= (\mathrm{V}_8 - \mathrm{S}_8)(\overline{\mathrm{V}}_8 - \overline{\mathrm{S}}_8)\,, \\
\mathcal{T}_{\text{0A}} &= |\mathrm{O}_8|^2 + |\mathrm{V}_8|^2 + \mathrm{S}_8\overline{\mathrm{C}}_8 + \mathrm{C}_8\overline{\mathrm{S}}_8\,, \\
\mathcal{T}_{\text{0B}} &= |\mathrm{O}_8|^2 + |\mathrm{V}_8|^2 + |\mathrm{S}_8|^2 + |\mathrm{C}_8|^2\,.
\end{aligned}$$

This procedure is called GSO (Gliozzi, Sherk, Olive) projection, a consistent way to project the spectrum to obtain modular invariant partition functions [16]. Type 0A and 0B [17–19] are pathological theories: they contain tachyons (due to the presence of $|\mathrm{O}_8|^2$) and no space-time fermions due to the absence of NS-$\widetilde{\mathrm{R}}$ and R-$\widetilde{\mathrm{NS}}$ terms. They also lack space-time supersymmetry. Type IIA has $\mathcal{N} = (1,1)$ supersymmetry, whereas IIB has $\mathcal{N} = (2,0)$ supersymmetry in $D = 10$. Type IIB theory is also chiral and exhibits an extra symmetry; specifically, it remains invariant under the exchange of left and right sectors.

Having discussed the basic construction and quantisation of closed string theories, we now move on to a comprehensive examination of 1-loop inte-

grals, with a primary emphasis on gauge couplings. However, it is important to acknowledge that our analysis so far overlooked significant string constructions that have played a crucial role in developing and comprehending SM-like string theories. These constructions are known as heterotic strings [20], which are combinations of the left-moving sector of the 26-dimensional bosonic string with the right-moving sector of the 10-dimensional superstring. However, the details on how these theories are constructed are not of much importance for the scope of the following chapter, which develops a model-independent framework to compute 1-loop amplitude in all closed string theories, revealing universal properties and interesting insights on the structure of the theory beyond tree-level.

Chapter 3

Running of Gauge Couplings in String Theory

The traditional approach in string phenomenology focuses on extracting low-energy predictions from string theory by considering only the effects associated with the lightest string modes. However, this approach overlooks a significant aspect of string theory: the existence of infinite towers of massive states that are integral to the string spectrum. Disregarding these states and their contributions to low-energy physics severs the link between the UV-complete theory and its low-energy phenomenology, limiting the analysis to an effective field theory (EFT) approach. To understand the low-energy implications of string theory better, it may be more appropriate to retain these infinite towers of states and incorporate their effects naturally in calculations. These effects are likely to be most relevant for fundamental phenomenolog-

ical questions, such as the hierarchy problem, which focuses on reconciling light and heavy scales in a quantum-mechanical universe.

The finiteness properties of string theories, which transcend field theory expectations, are attributed to the extended nature of the string and the resulting infinite towers of states. Perturbative closed strings are governed by worldsheet modular invariance, a fundamental symmetry that governs these states and their interactions, which leads to unique UV/IR mixing effects that can significantly impact the validity of EFT-based approaches even at low energies.

To develop a more comprehensive understanding of low-energy phenomenological predictions from string theory, it is crucial to utilise fully modular-invariant methods that consider the full towers of string states and their preservation of the underlying modular symmetry. This approach may offer new insights into long-standing phenomenological puzzles and alternative ways to address hierarchy problems.

In Ref. [21], a framework was developed for performing calculations of the Higgs mass in a fully modular-invariant way. As discussed there, this framework is completely general and can be applied to any string model (vacuum state). Moreover, although the focus within Ref. [21] centered around calculations of the Higgs mass, this framework can be applied to numerous quantities of phenomenological interest, including the running of the gauge couplings. Explicitly performing such a calculation is thus the primary goal of this chapter. The analysis which follows focuses on calculating the running

of one-loop gauge couplings within closed string theories. While this topic has been explored before, the formalism we shall apply is model-independent and fully respects modular invariance, encompassing all the unique aspects of string theory.

3.1 Towards a modular invariant expression for gauge couplings at 1-loop

Let us now establish the groundwork for our analysis by introducing the notations and conventions we will be using. From now on we suppose that our closed string theory is compactified on an arbitrary 6-dimensional space, leaving four uncompactified flat dimensions ($D = 4$), *i.e.*, we imagine that the string target space can be written as a tensor product of a 4-dimensional Minkowski space-time and a 6-dimensional arbitrary compact space as follows

$$\mathcal{M}^{(1,9)} \;=\; \mathcal{M}^{(1,3)} \times \mathbb{K}^6 \,. \tag{3.1}$$

The primary objective of the following analysis is to study the behaviour of the one-loop contribution to the gauge coupling g_G associated with any spacetime gauge group G in closed string theories. Gauge coupling corrections have been extensively studied in the past, since Kaplunosky's seminal paper in Ref. [22], and have played a central role in many subsequent studies (see for example Refs. [23–26]). To derive the 1-loop integral expression for

gauge couplings corrections in closed strings, we shall pursue a slightly different route, starting from the analogous expression in quantum field theory and perform a so-called *modular completion* to obtain the corresponding expression in string theory. To achieve this, we will normalise these couplings such that the corresponding gauge-kinetic terms take the following form

$$\mathcal{L} \;=\; -\frac{1}{4g_G^2}F^{(G)}_{\mu\nu}F^{(G)\mu\nu}\;, \tag{3.2}$$

and we shall isolate the one-loop contributions to g_G by evaluating these couplings g_G to one-loop order and then separating out the tree-level contributions. In general, these quantities are related through

$$\left.\frac{16\pi^2}{g_G^2}\right|_{\substack{R\text{one-loop}\\ \text{order}}} \;=\; \left.\frac{16\pi^2}{g_G^2}\right|_{\text{tree}} \;+\; \Delta_G \tag{3.3}$$

where Δ_G denotes the one-loop contribution to $16\pi^2/g_G^2$. Indeed, in string theory we know that $g_G|_{\text{tree}} \sim e^{-\langle\phi\rangle}$ where $\langle\phi\rangle$ denotes the VEV of the dilaton ϕ. Our goal in this section is thus to study the properties of Δ_G.

In field theory, we know that Δ_G receives contributions from all of the states in our theory which transform in non-trivial representations R of G. Indeed, for each such state in the theory, the corresponding one-loop contribution to Δ_G is given by $b\cdot \text{tr}_R(Q_G^2)$, where

- Q_G^2 is the sum of the squares of the charges in the Cartan subalgebra of G;

- the trace tallies the values of Q_G^2 over all the states within the representation R (following the convention that each CPT-conjugate particle/anti-particle pair of states is counted only once); and

- the numerical coefficient b encapsulates the Lorentz helicity properties of the state, with $b = \{1/3, 2/3, -11/3\}$ for Lorentz scalars, spinors, and vectors respectively.

Indeed, we note that these b-coefficients are nothing but $b = -4(-1)^F(S^2 - 1/12)$ where $S = \{0, 1/2, 1\}$ is the Lorentz spin of the corresponding state and where F is the spacetime fermion number.

Given these observations, it is straightforward to generate an analogous expression in string theory. Of course, in string theory, our traces count *all* states in the theory independently and thus tally each member of a CPT-conjugate particle/anti-particle pair separately. With this effective doubling of the conventions for our traces, our field-theoretic b-coefficients are effectively rescaled to become $b = \{1/6, 1/3, -11/6\}$ for Lorentz scalars, spinors, and vectors respectively, or equivalently $b = -2(-1)^F(S^2 - 1/12)$. At this stage, then, our QFT-motivated expression for Δ_G in string theory can be expected to take the form

$$\Delta_G \;=\; -2\Big\langle \big(S^2 - 1/12\big)\; Q_G^2 \Big\rangle \tag{3.4}$$

where we have define the standard four-dimensional one-loop string ampli-

tude for any operator insertion A as

$$\langle A\rangle \;\equiv\; \int_{\mathcal{F}} \frac{d^2\tau}{\tau_2^2}\,\tau_2^{-1}\,\sum_{m,n}(-1)^F\,A_{mn}\,\overline{q}^m q^n\;, \tag{3.5}$$

where A_{mn} are the eigenvalues of the operator A when acting on each (m,n) string state multiplied by the degeneracy of that state, *i.e.*, we have buried the state degeneracy a_{mn} into the eigenvalue A_{mn}.

We note from Eq. (3.5) that these brackets already include the factor of $(-1)^F$ as well as the double sum $\sum_{m,n}$ which effects the sum over gauge-group representations R and the traces over Q_G^2 within each R.

We see that this quantity is written in terms of the product of two insertions, Q_G^2 and $S^2-1/12$, and thus resembles as closely as possible the field-theory result, only expressed in terms of a full one-loop string amplitude. Note that if our theory is spacetime-supersymmetric, then we are free to drop the factor of $-1/12$, since the contributions from this term will be proportional to $\mathrm{Tr}\,(-1)^F$ for each representation of the gauge group and thus vanish. We shall nevertheless keep this factor for generality.

As already mentioned, our next step is to perform a *modular completion* of the expression in Eq. (3.4). This will generally require the introduction of additional terms which may be interpreted as coming from extra intrinsically stringy effects such as gravitational backreactions. In particular, the ultimate goal of these extra terms is to restore in Eq. (3.4) the required modular invariance symmetry of the 1-loop string amplitude. In such situations, the

tight constraints of modular invariance render these modular completions fairly unique. Thus, after this step, one has obtained a general, fully modular-invariant, string-theoretic expression for gauge coupling corrections at 1-loop. Clearly, there are two separate insertions in play: Q_G^2 and $S^2-1/12$. We shall discuss each of these in turn, since neither insertion preserves the modular invariance of the full string amplitude.

Let us first discuss the modular completion of Q_G^2. In general, it was shown in Ref. [21] that the product of any two charge bilinears can be modular completed by substituting

$$Q_\ell Q'_\ell \;\to\; Q_\ell Q'_\ell - \frac{1}{4\pi\tau_2}\delta_{\ell,\ell'} \;. \tag{3.6}$$

Therefore, we find the modular completion of Q_G^2 is given by

$$Q_G^2 \;\to\; Q_G^2 - \frac{\xi}{4\pi\tau_2} \tag{3.7}$$

where $\xi \equiv \sum_\ell c_{\ell\ell}^{(G)}$. Indeed, with this result, we see that ξ is ultimately related to the *affine level* k_G at which the gauge group G is realised.

We now turn to the modular completion of the helicity factor $S^2 - 1/12$ in Eq. (3.4). In general, a given string theory gives rise to infinite towers of states with higher and higher spins. However, in the heterotic string, these states can ultimately be organised in terms of the CFT sector from which they arise, where the CFT in question is that associated with the transverse right-moving Lorentz group $SO(D-2)$. In the heterotic string, there are only

three such sectors: the identity (or scalar) sector, the spinor sector, and the vector sector. The ground states of these sectors have spins $S = \{0, 1/2, 1\}$ respectively. Loosely speaking, every other string state can be viewed as a member of one of these sectors in the sense that it can be realised through tensor products of this vacuum state (or one of its CFT descendants) with additional vector representations arising from excitations of the left-moving coordinate bosons. In this way, states with arbitrarily high spins can be generated.

Disregarding the contributions from the purely internal degrees of freedom and the two transverse spacetime-coordinate bosons, the contribution to the total partition function from the states in each of these three sectors takes the form $\overline{\Theta}/\overline{\eta}$, where η is the Dedekind eta-function and where Θ is given by

$$\begin{aligned} \text{scalar}: \quad \Theta &= \tfrac{1}{2}\left(\theta_3 + \theta_4\right) , \\ \text{spinor}: \quad \Theta &= \tfrac{1}{2}\theta_2 , \\ \text{vector}: \quad \Theta &= \tfrac{1}{2}\left(\theta_3 - \theta_4\right) , \end{aligned} \tag{3.8}$$

where θ_i are the three Jacobi theta-functions and are defined in Eq. (2.45). Indeed, in each of these cases we find that

$$\Theta \sim e^{\pi i \tau S^2}(1 + ...) , \tag{3.9}$$

thereby already suggesting a relationship between S and a modular deriva-

tive.

Given this, we now seek to understand how to incorporate the helicity factor $S^2 - 1/12$ in a fully modular-invariant way into the sum over string states. A direct string calculation [22] tells us that the proper procedure to generate the helicity part is to modify the total partition function of the string theory in question, replacing

$$\frac{\overline{\Theta}}{\overline{\eta}} \;\to\; \frac{\partial}{\partial\overline{\tau}}\left(\frac{\overline{\Theta}}{\overline{\eta}}\right) \;. \tag{3.10}$$

This is the result of a full string calculation, and thus this replacement does not disturb the modular invariance of the total partition function. In particular, the τ-derivative $d/d\overline{\tau}$ is modular-covariant when acting on a modular-covariant function of modular weight $k = 0$ such as $\overline{\Theta}/\overline{\eta}$. Thus, no further modular completion is required after this replacement is implemented. Or, to phrase this another way, the simple insertion $S^2 - 1/12$ has been "modular completed" by instead implementing the replacement in Eq. (3.10).

The issue that remains for us, however, is to express the replacement in Eq. (3.10) as an *insertion* into the numerator of the partition-function trace. We wish to do this in order to eventually express our results in terms of (weighted) traces over our original string spectrum. To accomplish this, we

observe that

$$\begin{aligned}\frac{\partial}{\partial\overline{\tau}}\left(\frac{\overline{\Theta}}{\overline{\eta}}\right) &= \frac{1}{\overline{\eta}}\frac{\partial\overline{\Theta}}{\partial\overline{\tau}} + \overline{\Theta}\frac{\partial}{\partial\overline{\tau}}\frac{1}{\overline{\eta}} \\ &= \frac{1}{\overline{\eta}}\left[\frac{\partial\overline{\Theta}}{\partial\overline{\tau}} - \overline{\Theta}\frac{\partial}{\partial\overline{\tau}}\log\overline{\eta}\right] \\ &= \frac{1}{\overline{\eta}}\left[\frac{\partial}{\partial\overline{\tau}} + \frac{\pi i}{12}\,\overline{E}_2(\overline{\tau})\right]\overline{\Theta} \end{aligned} \tag{3.11}$$

where in passing to the final line we have utilised the identity

$$E_2(\tau) \;=\; \frac{1}{2\pi i}\frac{\partial}{\partial\tau}\log\eta^{24}(\tau) \tag{3.12}$$

where $E_2(\tau)$ is the normalised weight-two holomorphic Eisenstein function

$$\begin{aligned}E_2(\tau) &\equiv 1 - 24\sum_{n=1}^{\infty}\sigma(n)e^{2\pi i n\tau} \\ &= 1 - 24q - 72q^2 - 96q^3 - 168q^4 - ... \end{aligned} \tag{3.13}$$

with $\sigma(n) \equiv \sum_{d|n} d$. We can shall find it convenient to simplify this notation slightly by writing $E_2(\tau) = \sum_{n=0}^{\infty}\chi_n q^n$ where

$$\chi_n \;=\; \begin{cases} 1\,, & n = 0 \\ -24\sigma(n)\,, & n > 0\ . \end{cases} \tag{3.14}$$

We thus see that the replacement in Eq. (3.10) is tantamount to the insertion of the modular-covariant derivative $\overline{D}_{\overline{\tau}}$ into that portion of the total

partition-function trace corresponding to the spacetime Lorentz group, where

$$D_\tau \;\equiv\; \frac{\partial}{\partial\tau} - \frac{i\pi}{12}E_2(\tau)\ . \tag{3.15}$$

In this sense D_τ is the operator that represents $S^2 - 1/12$ in string theory.

As evident from this discussion, the operator $d/d\overline{\tau}$ acting purely on $\overline{\Theta}$ represents the spin S^2. Indeed, we can identify the spin S as the "helicity charge" $\overline{Q}_H$ of the state relative to the spacetime Lorentz symmetry, where the subscript H can be identified as that right-moving lattice direction ℓ whose trace yields $\overline{\Theta}$. We can therefore identify $\overline{Q}_H^2 = \frac{i}{\pi}\partial/\partial\overline{\tau}$, allowing us to express our modular completion in the form

$$\overline{Q}_H^2 - \frac{1}{12} \quad\to\quad \overline{Q}_H^2 - \frac{1}{12}\overline{E}_2(\overline{\tau})\ . \tag{3.16}$$

At first glance, it might have seemed from Eq. (3.6) that the modular completion of $\overline{Q}_H^2$ would simply be $\overline{Q}_H^2 \to \overline{Q}_H^2 - 1/(4\pi\tau_2)$, just as occurred for the gauge charges. However, the critical difference here is that we are not seeking the modular completion of Q_H^2; we are seeking the modular completion of $Q_H^2 - 1/12$. It is the presence of the extra term $-1/12$ which induces the subtlety and ultimately requires the Eisenstein function in Eq. (3.15). Although it might have seemed that the extra shift $-1/12$ is only a pure number and thus should be completely harmless, this neglects the fact that we must preserve modular invariance. While the insertion of S^2 raises the modular weight of the corresponding portion of the partition function by two, the

insertion of a pure number such as $-1/12$ does not affect the modular weight at all. *We thus cannot subtract* $1/12$ *directly from* S^2 *or* Q_H^2 *in a modular-invariant theory; rather, the* $-1/12$ *must first be "modular completed" into a modular function (or in this case, a quasi-modular function) of weight two.* As it turns out, a theorem in modular-function theory asserts that there is only one (quasi-)modular function of weight $k = 2$: this is the Eisenstein function $E_2(\tau)$. It is thus natural and expected that the modular completion in Eq. (3.16) would involve the Eisenstein function. Indeed, in this sense we may regard $E_2/12$ as the properly normalised modular completion of $1/12$, with $E_2/12 = 1/12 + \mathcal{O}(q)$.

As noted above, the Eisenstein series E_2 (unlike the Eisenstein series E_{2k} for $k > 1$) is not a strict modular function. Instead, E_2 is only *quasi*-modular, transforming under modular transformations as

$$E_2\left(\frac{a\tau+b}{c\tau+d}\right) \;=\; (c\tau+d)^2 E_2(\tau) - \frac{6}{\pi} ic(c\tau+d)\;. \tag{3.17}$$

It is the latter "anomaly" term in this result which spoils the true modular covariance for E_2. However, this is precisely what is needed because the derivative $\partial/\partial\tau$ in Eq. (3.15) also fails to be modular invariant in exactly the opposite way. Thus, it is precisely the combination in Eq. (3.15) that yields a fully modular-invariant result.

Given these results, we see that our modular-completed expression for

Δ_G now takes the form

$$\Delta_G \;=\; -2\left\langle \tau_2^2\,\left(\overline{Q}_H^2-\frac{1}{12}\overline{E}_2\right)\,\left(Q_G^2-\frac{\xi}{4\pi\tau_2}\right)\right\rangle\;. \tag{3.18}$$

Note that the extra factor of τ_2^2 that has been inserted into Eq. (3.18) is another element of our modular completion. This reflects the fact that the insertions of the helicity and gauge factors — although preserving modular invariance — also together raise the modular weight of the resulting integrand in Eq. (3.5) by two units (from $k=-1$ to $k=+1$) for any four-dimensional string theory. Modular invariance then dictates that such an increase in the modular weight of the integrand be accompanied by a corresponding increase in the number of leading τ_2 prefactors.

At this stage, it may be worthwhile to compare with the classic results of Kaplunovsky in Ref. [22]. First, we emphasise that we are simply calculating the one-loop contributions to the gauge coupling. In particular, despite the algebraic resemblance of Eq. (3.3) to a renormalisation-group equation (RGE) for a running gauge coupling, at this stage we have not introduced any notion of running or scale. Second, this conceptual difference notwithstanding, there is a further critical difference in that the contributions from the massless states were explicitly removed within the calculation of the Δ_G-term in Ref. [22]. This was done because a separate field-theoretic logarithmic running (assumed to be contributed from the massless states) was explicitly introduced into the renormalisation-group version of Eq. (3.3) in Ref. [22].

This rendered Δ_G in Ref. [22] a mere tally of the contributions from only the massive modes. Thus, in this sense, the version of Δ_G in Ref. [22] became a mere threshold correction, one which is devoid of its own running.

By contrast, Δ_G will always represent the full one-loop contribution to the gauge coupling, with the contributions from both massless and massive states included together in a unified way. Indeed, it is only in such a manner that we can ever hope to preserve modular invariance throughout our calculations. Moreover, once we proceed to introduce a scale dependence into our eventual results and consider how these quantities run, we shall even find that the contributions from the massless string states are not strictly logarithmic, but instead take a more complex form which is dictated by modular invariance and which only reduces to a logarithmic running in a certain EFT-like limit.

Given our expression in Eq. (3.18), we see that our total operator insertion for the gauge couplings is given by

$$\mathcal{X} \;\equiv\; -2\tau_2^2 \left(\overline{Q}_H^2 - \frac{1}{12}\overline{E}_2\right)\left(Q_G^2 - \frac{\xi}{4\pi\tau_2}\right) \;. \tag{3.19}$$

Expanding $\mathcal{X}$ in leading powers of τ_2 then yields

$$\mathcal{X} \;=\; \tau_2\mathbb{X}_1 + \tau_2^2\mathbb{X}_2 \tag{3.20}$$

where we now identify

$$\begin{aligned} \mathbb{X}_1 &\equiv \frac{\xi}{2\pi}\left(\overline{Q}_H^2 - \frac{\overline{E}_2}{12}\right) \\ \mathbb{X}_2 &\equiv -2\left(\overline{Q}_H^2 - \frac{\overline{E}_2}{12}\right) Q_G^2 \ . \end{aligned} \tag{3.21}$$

This division of the total insertion into two separate terms $\mathbb{X}_1$ and $\mathbb{X}_2$ is based on their leading powers of τ_2 and will be important when we discuss how our expressions diverge and what kinds of running these quantities ultimately experience. However, we stress that neither $\langle \tau_2 \mathbb{X}_1 \rangle$ nor $\langle \tau_2^2 \mathbb{X}_2 \rangle$ is modular invariant by itself.

3.2 Divergences and regulator function

Our next step is to study the potential divergence structure of Δ_G. For example, any level-matched massless state which carries a non-zero $\mathbb{X}_2$ charge will induce a divergence in Δ_G unless this state is balanced against another similar state of opposite statistics. Indeed, in a rough sense to be clarified shortly, the divergence in Δ_G will be proportional to $\underset{M=0}{\mathrm{Str}}\ \mathbb{X}_2$. Likewise, we see that this divergence is at most *logarithmic*.

The fact that Δ_G formally diverges means that we must introduce a regulator. It might seem natural to proceed by simply subtracting the contributions from the massless states (or more precisely the $\mathbb{X}_2$-charged massless states) from Δ_G. This is reminiscent of what was done in Ref. [22], but intro-

ducing this sort of artificial distinction between massless and massive states necessarily breaks the modular invariance of Δ_G.

Instead, following what was done in Ref. [21] for the Higgs mass, we shall regulate our theory by deforming the one-loop amplitude introducing a regulator function $\widehat{\mathcal{G}}(a_i, \tau 3)$ into the integrand:

$$\Delta_G \;\to\; \widehat{\Delta}_G \;\equiv\; \left\langle \tau_2 \mathbb{X}_1 + \tau_2^2 \mathbb{X}_2 \right\rangle_{\widehat{\mathcal{G}}} \;=\; \left\langle \left(\tau_2 \mathbb{X}_1 + \tau_2^2 \mathbb{X}_2\right) \widehat{\mathcal{G}} \right\rangle . \tag{3.22}$$

The issue at hand is thus to choose a suitable $\widehat{\mathcal{G}}(a_i, \tau)$ regulator function, with a_i denoting the internal regulator parameters. We then must demand that this function exhibit certain properties in order to ensure that we have a sensible regulator. In particular, for such a regulator, we demand that there exist a combination or function $f(a_i)$ of regulator parameters such that taking $f(a_i) \to 0$ effectively removes the regulator while taking any non-zero value of $f(a_i)$ allows the regulator to suppress the unwanted divergences but otherwise leave the theory intact as far as possible. Given that all such divergences must come from those portions of the integration region in which $\tau \to \tau_{\text{cusp}}$ (where τ_{cusp} are the so-called "cusp" points $\tau_{\text{cusp}} = i\infty$ or $\tau_{\text{cusp}} = p/q$, where $p, q \in \mathbb{Z}$), we thus have three requirements for suitable modular-invariant regulator functions $\widehat{\mathcal{G}}(a_i, \tau)$:

- For all $f(a_i) > 0$, we require that $\widehat{\mathcal{G}}(a_i, \tau) \to 0$ sufficiently rapidly as $\tau \to \tau_{\text{cusp}}$. This enables our regulator to suppress divergences and yield a finite one-loop string amplitude.

- For all $f(a_i) > 0$, we also require that $\widehat{\mathcal{G}}(a_i, \tau) \approx 1$ when τ is sufficiently far away from the cusp points. This ensures that our regulator, while suppressing divergences near the cusp points, leaves the remainder of the theory intact as much as possible.

- As $f(a_i) \to 0$, we require that $\widehat{\mathcal{G}}(a_i, \tau) \to 1$ for all τ. This ensures the existence of a limit in which our regulator is effectively removed and our original theory is obtained.

- Once introduced an energy scale

$$\mu^2 = f(a_i) M_s^2 \,, \tag{3.23}$$

  we require scale-duality invariance, which is amount to impose

$$\widehat{\mathcal{G}}(\mu/\mu_*, \tau) \;=\; \widehat{\mathcal{G}}(\mu_*/\mu, \tau) \,, \tag{3.24}$$

  where we have rewritten the parameters a_i in terms of μ using Eq. (3.23) and where μ_* is some arbitrary mass scale.

The first three points do not require further explanation, as they are standard requirements for any well-defined regulator, as in usual quantum field theory. However, the last one stem directly from the "stringiness" of the theory and precisely from UV/IR mixing, which is in turn a consequence of modular invariance, as already discussed previously. In particular, modular invariance tells us that any physical quantities which depends on τ must be invariant

under $\tau \to -1/\tau$. Along $\tau_1 = 0$ axis, this becomes an invariance under $\mu \to \mu_*^2/\mu$, where μ_* is an arbitrary self-dual mass scale. Of course, the choice of the dual point is a matter of convention, and for convenience we now choose our normalisation for μ such that $\mu_* = M_s$. We thus see that while the particular choice of self-dual scale μ^* is a matter of convention, the existence of a scale-inversion duality symmetry of the form $\mu \to \mu_*^2/\mu$ is inevitable, emerging directly from the underlying modular invariance of the theory.

A function satisfying all of these properties was given in Ref. [21], adapting prior results in Ref. [24], and we shall use this function here as well. This function $\widehat{\mathcal{G}}_\rho(a,\tau)$ has two free regulator parameters $a_i \equiv \{\rho, a\}$ with $\rho \in \mathbb{R}^+$ and $\rho \neq 1$, and is given by

$$\widehat{\mathcal{G}}_\rho(a,\tau) \equiv \frac{1}{1+\rho a^2}\,\frac{\rho}{\rho-1}\,a^2\frac{\partial}{\partial a}\Big[Z_{\rm circ}(\rho a,\tau) - Z_{\rm circ}(a,\tau)\Big] \tag{3.25}$$

where

$$Z_{\rm circ}(a,\tau) \equiv \sqrt{\tau_2}\sum_{k,\ell\in\mathbb{Z}} \overline{q}^{(ka-\ell/a)^2/4}\, q^{(ka+\ell/a)^2/4}\ . \tag{3.26}$$

Note that $Z_{\rm circ}(a,\tau)$ represents the sum over the Kaluza-Klein (KK) and winding modes that would be associated with a bosonic worldsheet field compactified on a circle of radius $(M_s a)^{-1}$, with k and ℓ respectively indexing the KK and winding modes, while the leading factor of $\sqrt{\tau_2}$ is inserted into Eq. (3.26) in order to ensure that $Z_{\rm circ}$ is modular invariant. We stress that for our purposes $Z_{\rm circ}$ is merely an ingredient in the definition of our

regulator and does not correspond to any actual physical compactification of our theory. It turns out that $\widehat{\mathcal{G}}_\rho(a,\tau) \to 1$ as $a \to 0$, indicating that taking $a \to 0$ removes the regulator. Indeed, for this function we have

$$f(a_i) \;=\; \rho a^2 \;. \tag{3.27}$$

It then turns out that all of the bulleted requirements above are satisfied, in addition to the requirement that $\widehat{\mathcal{G}}_\rho(a,\tau)$ exhibit an invariance under $f(a_i) \to 1/f(a_i)$, or equivalently under $a \to (\rho a)^{-1}$. Indeed, we will eventually identify our spacetime running scale μ according to Eq. (3.23) with $f(a_i)$ given in Eq. (3.27).

3.3 Generic picture of running gauge couplings in string theory

Let us move on to the main task of the chapter: to evaluate the following amplitude

$$\begin{aligned}\widehat{\Delta}_G \;&= \Big\langle \big(\tau_2 \mathbb{X}_1 + \tau_2^2 \mathbb{X}_2\big)\, \widehat{\mathcal{G}} \Big\rangle \\ &= \Big\langle \Big[\big(\tau_2 \mathbb{A}^{(1)} + \tau_2^2 \mathbb{A}^{(2)}\big) + \big(\tau_2 \mathbb{B}^{(1)} + \tau_2^2 \mathbb{B}^{(2)}\big)\, \overline{E}_2 \Big]\, \widehat{\mathcal{G}} \Big\rangle \,,\end{aligned} \tag{3.28}$$

where the $\mathbb{X}_\ell$ are given in Eq. (3.21) and $\mathbb{A}^{(\ell)}$, $\mathbb{B}^{(\ell)}$ are defined as follows

$$\begin{aligned} \mathbb{A}^{(1)} &= \frac{\xi}{2\pi}\,\overline{Q}_H^2\ , \qquad \mathbb{A}^{(2)} = -2\,\overline{Q}_H^2 Q_G^2\ , \\ \mathbb{B}^{(1)} &= -\frac{\xi}{24\pi}\ , \qquad \mathbb{B}^{(2)} = \frac{1}{6}\,Q_G^2\ . \end{aligned} \tag{3.29}$$

and where the regulator function $\widehat{\mathcal{G}}_\rho(a,\tau)$ is given in Eq. (3.25).

As explained in Appendix A, the form of the regulator allows us to split the computation in two steps. Thus, we firstly compute the reduced amplitude defined as

$$P(a) \;=\; \Big\langle \big(\tau_2\mathbb{X}_1 + \tau_2^2\mathbb{X}_2\big)\; Z_{\rm circ}(a,\tau)\Big\rangle \tag{3.30}$$

and get the full amplitude using

$$\widehat{\Delta}_G(\rho,a) \;=\; \frac{a^2}{1+\rho a^2}\frac{\rho}{\rho-1}\frac{\partial}{\partial a}\Big[P(\rho a)-P(a)\Big]\ . \tag{3.31}$$

Following the results and the prescriptions in Appendix A we obtain

$$\begin{aligned} P(a) \;=\;& \operatorname*{Str}_{M=0}\left\{\frac{\xi}{2\pi}\left(\overline{Q}_H^2-\frac{1}{12}\right)\big[f_1(a)+f_2(a)\big]\right\} \\ &- \operatorname*{Str}_{M=0}\left[2\left(\overline{Q}_H^2-\frac{1}{12}\right)Q_G^2\,f_3(a)\right] + \operatorname*{Str}_{M>0}\left[\frac{\xi}{2\pi}\left(\overline{Q}_H^2-\frac{1}{12}\right)f_2(a)\right] \\ &+ \operatorname*{Str}_{M>0}\left[\frac{\xi}{2\pi}\,\overline{Q}_H^2\,f_4(M,a)\right] - \operatorname*{Str}_{E\ M_L>0}\left[\frac{\xi}{24\pi}f_4(M_L,a)\right] \\ &- \operatorname*{Str}_{M>0}\left[2\,\overline{Q}_H^2 Q_G^2\,f_5(M,a)\right] + \operatorname*{Str}_{E\ M_L>0}\left[\frac{1}{6}\,Q_G^2\,f_5(M_L,a)\right]\ , \end{aligned} \tag{3.32}$$

where the functions f_i, with $i = 1, \ldots, 5$ are defined in Eq. (A.5) along with the 'Str' notations, defined in Eqs. (A.6), (A.9). We insert the supertrace definitions definitions also here for convenience. The standard supertrace is defined as

$$\mathrm{Str}\, A \;\equiv\; \lim_{y\to 0} \sum_{\text{states } i} (-1)^{F_i}\, A_i\, e^{-y\alpha' M_i^2} \tag{3.33}$$

whereas

$$\mathrm{Str}_E\, X \;\equiv\; \sum_{r=0}^{\infty} \chi_r\, \mathrm{Str}^{(r)} X \tag{3.34}$$

where

$$\chi_n \;=\; \begin{cases} 1 & n = 0 \\ -24\sigma(n) & n > 0\ , \end{cases} \tag{3.35}$$

and where

$$\mathrm{Str}^{(r)} X \;\equiv\; \lim_{\tau_2\to 0} \sum_{p} a_{p-r,p}\, X_{p-r,p}\, e^{-\pi\alpha' M_L^2 \tau_2} \tag{3.36}$$

with $\alpha' M_L^2 = 4p$ and where the p-sum is a sum on the states in the theory.

By examining the definitions of supertraces, we observe that these quantities represent statistical-weighted traces over the string states. Specifically, the supertrace without the subscript E contains contributions solely from physical (level-matched) states. On the other hand, Str_E originates from the $\overline{E}_2$ insertion and includes contributions from unphysical states as well. We shall refer to this interplay between physical and unphysical states as *entwinement*, induced by the modular completion of the helicity operator needed for calculating gauge coupling corrections. This introduces a "de-

formed" notion of physicality for the string states, allowing states which are not level-matched to nevertheless act as physical states which contribute to the physical supertraces describing the values of physical string amplitudes. Entwinement thereby widens the class of states which can ultimately contribute to the supertraces when calculating amplitudes in closed string theories.

Finally, to write Eq. (3.32) we have also used the following identity

$$\underset{M_L>0}{\mathrm{Str}_E}\,\mathbf{1} \;=\; \mathrm{Str}_E\mathbf{1} - \underset{M_L=0}{\mathrm{Str}_E}\,\mathbf{1} \;=\; -\underset{M=0}{\mathrm{Str}}\,\mathbf{1} \;=\; \underset{M>0}{\mathrm{Str}}\,\mathbf{1}\;, \tag{3.37}$$

where the first equality comes for two reasons: because our original theory is presumed tachyon-free and because right-moving worldsheet energies in string theory are never smaller than -1, even for the bosonic string. This implies $M_L^2 \geq 0$. The second equality comes from Eq. (A.15) and from the fundamental result

$$\mathrm{Str}_E\,\mathbf{1} \;=\; 0\,, \tag{3.38}$$

which is a generalisation of the following identity [27]:

$$\mathrm{Str}\,\mathbf{1} \;=\; 0\,, \tag{3.39}$$

valid in any closed-string theory which is free of physical (on-shell) tachyons, regardless of spacetime supersymmetry. In particular, just as $\mathrm{Str}\,\mathbf{1}$ vanishes when evaluated along the principal diagonal for any self-consistent tachyon-

free closed string theory, it can be shown [7] that $\mathrm{Str}^{(r)}\mathbf{1} = 0$ as well — *i.e.*, that this supertrace also necessarily vanishes along each of the shifted diagonals. This result is ultimately the result of an *off-shell* misaligned supersymmetry that exists within the *off-shell* structure of any tachyon-free string theory [7, 28]. We thus find the general result

$$\mathrm{Str}^{(r)}\mathbf{1} \;=\; 0 \;\;\text{for all } r \qquad \Longrightarrow \qquad \mathrm{Str}_E\,\mathbf{1} \;=\; 0\;. \tag{3.40}$$

Finally, last equality comes straightforwardly from the fundamental result in Eq. (3.39).

Additional manipulations can further simplify the expression in Eq. (3.32) and render it more compact while also simultaneously elucidating its algebraic structure. This rewriting will also be useful for understanding certain properties of the resulting running of the gauge couplings. In particular, we note that the $f_2(a)$ term on the first line of Eq. (3.32) can be joined with the third line of this equation in order to remove the $M > 0$ restriction on the latter. The removal of this restriction then further allows us to eliminate the $-1/12$ term as a result of the identity $\mathrm{Str}\,\mathbf{1} = 0$. Likewise, the $f_1(a)$ term on the first line can be combined with the second expression in the third line and with the first expression in the fourth line in order to remove their $M > 0$ and $M_L > 0$ restrictions as well; indeed, these latter observations follow as a

result of the fact that $K_1(z) \sim z^{-1}$ as $z \to 0$, whereupon we see that

$$\lim_{M\to 0} \sum_{r=1}^{\infty} \left(\frac{M}{r\mathcal{M}}\right) K_1\left(\frac{rM}{a\mathcal{M}}\right) \;=\; \sum_{r=1}^{\infty} \frac{a}{r^2} \;=\; \frac{\pi^2 a}{6} \;, \tag{3.41}$$

or equivalently

$$\lim_{M\to 0} f_4(M,a) \;=\; f_1(a) \;. \tag{3.42}$$

Interpreting the quantity in Eq. (3.42) as $f_4(0,a)$, we thus find that Eq. (3.32) simplifies to

$$\begin{aligned} P(a) \;=\; & -\mathop{\rm Str}_{M=0}\left[2\left(\overline{Q}_H^2 - \frac{1}{12}\right) Q_G^2\, f_3(a)\right] \;+\; \mathop{\rm Str}\left[\frac{\xi}{2\pi}\,\overline{Q}_H^2\, f_2(a)\right] \\ & +\; \mathop{\rm Str}\left[\frac{\xi}{2\pi}\,\overline{Q}_H^2\, f_4(M,a)\right] \;-\; \mathop{\rm Str}_E\left[\frac{\xi}{24\pi}\, f_4(M_L,a)\right] \\ & -\mathop{\rm Str}_{M>0}\left[2\,\overline{Q}_H^2 Q_G^2\, f_5(M,a)\right] \;+\; \mathop{\rm Str}_{E\atop M_L>0}\left[\frac{1}{6}\, Q_G^2\, f_5(M_L,a)\right] \;. \end{aligned} \tag{3.43}$$

At first glance it might seem that the first term in the first line of Eq. (3.43) could be rewritten in an analogous manner as the $M \to 0$ limit of the terms in the final two lines. This would require that $f_3(a)$ somehow emerge as the $M \to 0$ limit of $f_5(M,a)$. However, this is ultimately not the case: we instead find that

$$f_5(M,a) \;\sim\; f_3(a) + \frac{M_s}{M} + \frac{2}{a}\log\left(e^\gamma \frac{M}{2M_s}\right) \quad \text{as } M \to 0 \;. \tag{3.44}$$

While the extra a-independent constant M_s/M would ultimately prove ir-

relevant under the operation in Eq. (A.3), the logarithmic divergence in Eq. (3.44) spoils the uniform convergence of the Bessel-function sum.

There is also a third way of rewriting these expressions which can be useful for understanding the ramifications of the entwinement in these theories. From Eqs. (A.9), (A.12), and (A.10) we can write

$$\mathrm{Str}_E X \;=\; \mathrm{Str}\, X + \sum_{r=1}^{\infty} \chi_r\, \mathrm{Str}^{(r)} X \;. \tag{3.45}$$

However, as we discussed below Eq. (A.12), we must have $p - r \geq \Delta$ where Δ is the right-moving vacuum energy within the type of string theory under study. We thus find that $p \geq \Delta + r$, which implies that we cannot have $r \geq 1$ unless $p \geq \Delta + 1$. This last constraint is evident in Fig. A.1 for the heterotic case in which $\Delta = -1/2$. Given

$$\alpha' M_R^2 = 4(p-r) \;, \qquad \alpha' M_L^2 = 4p \;, \tag{3.46}$$

this last constraint corresponds to $\alpha' M_L^2 \geq 4(\Delta + 1)$. We can thus write

$$\mathrm{Str}_E X \;=\; \mathop{\mathrm{Str}}_{M<M_E} X \;+\; \mathop{\mathrm{Str}_E}_{M_L \geq M_E} X \tag{3.47}$$

where M_E denotes the *entwinement scale*

$$M_E \;\equiv\; 2\sqrt{\Delta+1}\, M_s \tag{3.48}$$

at which the entwinement first appears. For heterotic strings we have $M_E = \sqrt{2}M_s$. Note that Eq. (3.47) is a general result, valid for all strings. Despite the $M < M_E$ upper limit on the first of the sums in Eq. (3.47), this sum can nevertheless involve a large number of states; this is especially true for cases in which compactification radii are far from the string scale.

Using Eq. (3.47), we can finally rewrite Eq. (3.43) in the form

$$\begin{aligned} P(a) \;=\; & -\underset{M=0}{\mathrm{Str}} \left[2\left(\overline{Q}_H^2 - \frac{1}{12}\right) Q_G^2\, f_3(a)\right] \;+\; \mathrm{Str}\left[\frac{\xi}{2\pi}\,\overline{Q}_H^2\, f_2(a)\right] \\ & + \underset{M<M_E}{\mathrm{Str}} \left[\frac{\xi}{2\pi}\left(\overline{Q}_H^2 - \frac{1}{12}\right) f_4(M,a)\right] \;+\; \underset{M\geq M_E}{\mathrm{Str}} \left[\frac{\xi}{2\pi}\,\overline{Q}_H^2\, f_4(M,a)\right] \\ & - \underset{M_L\geq M_E}{\mathrm{Str}_E} \left[\frac{\xi}{24\pi}\, f_4(M_L,a)\right] \;-\; \underset{0<M<M_E}{\mathrm{Str}} \left[2\left(\overline{Q}_H^2 - \frac{1}{12}\right) Q_G^2\, f_5(M,a)\right] \\ & - \underset{M\geq M_E}{\mathrm{Str}} \left[2\,\overline{Q}_H^2 Q_G^2\, f_5(M,a)\right] \;+\; \underset{M_L\geq M_E}{\mathrm{Str}_E} \left[\frac{1}{6}\, Q_G^2\, f_5(M_L,a)\right] \;. \end{aligned} \tag{3.49}$$

Although this expression has more individual terms than its two predecessors, it explicitly shows that the entwinement is wholly restricted to string states with $M_L \geq M_E$. Indeed, all terms that receive contributions from states with masses $M < M_E$ depend not on $\overline{Q}_H^2$ but rather on the explicit un-entwined combination $\overline{Q}_H^2 - 1/12$. This statement includes the contribution on the second line of Eq. (3.49) once we realise that the $1/12$ term that would otherwise appear there has vanished as a result of the identity $\mathrm{Str}\,\mathbf{1} = 0$.

Eqs. (3.32), (3.43), and (3.49) represent fully modular-invariant evaluations of the reduced string amplitude $P(a)$ defined in Eq. (3.30), expressed

purely in terms of supertraces over our string states. Given that these supertraces are to be evaluated over the states within the spectrum of whatever the string model happens to be, these results are completely general and model-agnostic, applicable to any four-dimensional string model — with or without spacetime supersymmetry — so long as the model lacks physical tachyons. Although the modular invariance of $P(a)$ in each of these expressions is not manifest, it is hidden in supertrace identities that relate the various terms in these expressions to each other.

Using these expressions in conjunction with Eq. (A.3) we can then trivially evaluate our full desired amplitude $\widehat{\Delta}_G(\mu)$. Indeed, following the procedure outlined in Appendix A, we see from Eq. (A.3) that we can easily turn $P(a)$ into $\widehat{\Delta}_G(\mu)$ by replacing f_i with Φ_i, which are defined in Eq. (A.18). We can also introduce an energy scale as $\mu^2 \equiv \rho a^2 M_s^2$ with $\rho = 2$ chosen as a benchmark value.

These ϕ_i-functions are extremely important and have direct physical interpretations. While the specific charges that enter into the $\mathbb{X}_i$ expressions tell us which specific quantity is under study (such as the Higgs mass versus the gauge coupling), and while the particular numerical values of these charges tell us about the particular string model under study, the ϕ_i functions are essentially universal and tell us how these phenomenological quantities *run* as functions of the scale μ in the corresponding EFT. As we have seen, these running functions are universal for all quantities (such as the one-loop Higgs mass or gauge couplings) which have at most a logarithmic diver-

gence in string theory prior to regularisation. More specifically, substituting $P(a) \to \widehat{\Delta}(\mu)$ and $f_i(a) \to \phi_i(\mu)$ within our previous expression for $P(a)$ in Eq. (3.32), we find that

- $\phi_1(\mu)$ is the contribution to $\widehat{\Delta}_G(\mu)$ per unit $(\mathbb{A}^{(1)} + \mathbb{B}^{(1)})$ charge from each massless physical state;
- $\phi_2(\mu)$ is the additional contribution to $\widehat{\Delta}_G(\mu)$ per unit $(\mathbb{A}^{(1)} + \mathbb{B}^{(1)})$ charge from each physical state, *regardless* of mass;
- $\phi_3(\mu)$ is the additional contribution to $\widehat{\Delta}_G(\mu)$ per unit $(\mathbb{A}^{(2)} + \mathbb{B}^{(2)})$ charge from each massless physical state;
- $\phi_4(M,\mu)$ is the additional contribution to $\widehat{\Delta}_G(\mu)$ per unit $\mathbb{A}^{(1)}$ charge for each physical state of non-zero mass M, while $\phi_4(M_L,\mu)$ is χ_r^{-1} times the additional contribution to $\widehat{\Delta}_G(\mu)$ per unit $\mathbb{B}^{(1)}$ charge for each physical *or unphysical* string (m,n) state with left-moving mass M_L for which $n-m \equiv r$ with $r \geq 0$; and
- $\phi_5(M,\mu)$ is the additional contribution to $\widehat{\Delta}_G(\mu)$ per unit $\mathbb{A}^{(2)}$ charge for each physical state of non-zero mass M, while $\phi_5(M_L,\mu)$ is χ_r^{-1} times the additional contribution to $\widehat{\Delta}_G(\mu)$ per unit $\mathbb{B}^{(2)}$ charge for each physical *or unphysical* string (m,n) state with left-moving mass M_L for which $n-m \equiv r$ with $r \geq 0$.

Here the $\mathbb{A}^{(i)}$ and $\mathbb{B}^{(i)}$ charges are given in Eq. (3.29), and the above results are quoted for bosonic states; fermionic states of course contribute with op-

posite signs. Once again, we stress that these results are completely general for all phenomenological quantities which diverge at most logarithmically when unregulated; it is only when we substitute the particular forms of $\mathbb{A}^{(i)}$ and $\mathbb{B}^{(i)}$ in Eq. (3.29) that we limit our attention to $\widehat{\Delta}_G(\mu)$ of the gauge couplings. Indeed, in the case of the Higgs mass in Ref. [21], no entwinement occurs and $\mathbb{B}^{(1)} = \mathbb{B}^{(2)} = 0$.

As we have seen, the results quoted above for $P(a)$ in Eqs. (3.32), (3.43), and (3.49) come directly from the results in Eqs. (A.4), (A.16). This in turn is taken directly from Eq. (A15) of Ref. [21]. Although the derivation given in Ref. [21] is sufficient for the Higgs mass, it makes the implicit assumption that supertraces of the general form $\mathrm{Str}\,[\tau_2 \mathbb{X}_2 f(M)]$ are all vanishing as a result of the explicit factor of τ_2 within the supertrace. At this stage, the potential presence of a supertrace with a τ_2 factor inside might appear unfamiliar to the reader. Indeed, this potential extra piece comes from an additional step in evaluating integrals of the form in Eq. (A.1), which entails the application of the so-called Rankin-Selberg (RS) technique (see Refs. [29–31] for details). For the purpose of this computation, we shall not dwell on these details. Indeed, it is sufficient to bear in mind that the RS procedure involves the computation of the $\tau_2 \to 0$ limit of the supertrace above, where $\pi\tau_2$ plays the role of the regulating parameter y in Eq. (A.6). In particular, the potential missing term can be written as follows

$$\mathrm{Str}\,[\tau_2 \mathbb{X}_2 f(M)] \;=\; \lim_{\tau_2 \to 0} \sum_n a_{nn} A_{nn}\, e^{-\pi\alpha' M_n^2 \tau_2}\,, \tag{3.50}$$

where a_{nn} is the net (bosonic minus fermionic) number of string states at mass level n. Otherwise, such terms would also have appeared in Eq. (A.4). At first glance, the absence of such terms from *all* calculations might appear to be justified, given that our supertraces are defined in Eq. (A.6) in terms of a limiting procedure that involves taking the $\tau_2 \to 0$ limit. Indeed, in most circumstances (including those considered in Ref. [21], where the Higgs mass was calculated), the extra factor of τ_2 inside the supertrace would drive the overall supertrace to vanish, as assumed. However, as discussed earlier, it is possible (especially near the borders of moduli space) that our spectrum of string states can become extremely dense. In such cases, the accumulated "pile-up" of states can cause quantities such as $\mathrm{Str}\,\mathbb{X}_2 f(M)$ to diverge, thereby allowing supertraces such as $\mathrm{Str}\,[\tau_2 \mathbb{X}_2 f(M)]$ to have non-zero values.

In the present calculation of gauge couplings, we would like to maintain complete generality and allow our results to remain valid even as we approach the boundaries of moduli space. For this reason, we must amend our results for $P(a)$ quoted above. However, it turns out that this is relatively straightforward and amounts to introducing only one additional contribution

$$\mathop{\mathrm{Str}}_{M>0}\, \tau_2 \mathbb{X}_2\, [f_2(a)] \tag{3.51}$$

within Eq. (A.4) with $\ell = 2$. This extra term will then propagate into Eqs. (3.32), (3.43), and (3.49). In fact, given that the "pile-up" phenomenon that gives rise to this term involves the infinite towers of massive states, we

note that $\operatorname{Str}_{M=0} \tau_2 \mathbb{X}_2 [f_2(a)] = 0$. The contribution in Eq. (3.51) can thus be equivalently written as

$$\operatorname{Str} \tau_2 \mathbb{X}_2 [f_2(a)] \ , \tag{3.52}$$

with no restriction on the masses of the states in the supertrace.

At this stage, we are able to extract a considerable amount of information about the running of $\widehat{\Delta}_G(\mu)$. For example, let us consider the behavior of $\widehat{\Delta}_G(\mu)$ in the deep-IR limit, *i.e.*, as $\mu \to 0$. As $\mu \to 0$, we find that $\phi_1(\mu)$, $\phi_4(\mu)$, and $\phi_5(\mu)$ all vanish; in the latter two cases this happens because the Bessel functions $K_2(z)$ in Eq. (A.18) all vanish exponentially as $z \to \infty$. Thus, only $\phi_2(\mu)$ and $\phi_3(\mu)$ survive in the deep-IR limit. Of course, $\phi_3(\mu)$ actually diverges in this limit. This divergence is not a surprise, however, since the deep-IR limit corresponds to the limit $a \to 0$ in which our regulator is removed. *Thus this divergence corresponds to the logarithmic divergence of our original unregulated quantity.* As anticipated in Sect. 3.2, and as apparent from each of our above expressions for $P(a)$, this divergence is proportional to

$$\operatorname*{Str}_{M=0} \left(\mathbb{A}^{(2)} + \mathbb{B}^{(2)} \right) \ = \ -2 \operatorname*{Str}_{M=0} \left(\overline{Q}_H^2 - \frac{1}{12} \right) Q_G^2 \ . \tag{3.53}$$

However, in theories for which this quantity vanishes, we find that only $\phi_2(\mu)$ survives, with $\lim_{\mu \to 0} \phi_2(\mu) = \pi/3$. In such cases we find from Eqs. (3.32)

and (3.52) that

$$\begin{aligned}\lim_{\mu\to 0}\widehat{\Delta}_G(\mu) &= \frac{\pi}{3}\,\mathrm{Str}\,(\mathbb{X}_1+\tau_2\mathbb{X}_2)\\ &= \frac{\xi}{6}\,\mathrm{Str}\,\overline{Q}_H^2-\frac{2\pi}{3}\left(\mathrm{Str}\,\tau_2\overline{Q}_H^2Q_G^2-\frac{1}{12}\mathrm{Str}_E\,\tau_2Q_G^2\right).\end{aligned} \tag{3.54}$$

The fact that $\widehat{\Delta}_G(\mu)$ asymptotes to a constant as $\mu\to 0$ is not particularly surprising, given the assumed vanishing of the quantity in Eq. (3.53). However, what *is* surprising is that the asymptotic value in Eq. (3.54) receives contributions not only from the light or massless string states, but from the *entire tower of string states*, all the way up into the UV. Indeed, *all* of the string states contribute to the unrestricted supertraces in Eq. (3.54). This is an example of the UV/IR mixing inherent in a modular-invariant theory such as string theory.

Let us now consider the behavior of $\widehat{\Delta}_G(\mu)$ as we proceed upwards in energy scale μ away from the deep-IR limit. Let us first focus on energy scales for which $\mu\ll M_s$. In this regime, we find that ϕ_1 and ϕ_4 continue to remain vanishingly small. However, whether ϕ_5 remains small as well for a particular state of mass M depends on the value of $z\sim M/\mu$ — *i.e.*, on whether the state whose contribution we are assessing is heavier or lighter than μ. In this connection it is important to realise that our supertraces receive contributions from the entire string spectrum. This necessarily includes states with masses $M\gtrsim M_s$, but may also include potentially light states with non-zero

masses far below M_s. The existence of such light states depends on our string construction and on the specific string model in question. Thus, even though we are considering situations in which $\mu \ll M_s$, there need not be any fixed hierarchical relationship between μ and M.

In Fig. 3.1, we have plotted $\phi_5(M,\mu)$ as a function of μ/M. Recalling that this is the contribution to $\widehat{\Delta}_G(\mu)$ per unit $\mathbb{A}^{(2)}$ charge from a given physical bosonic string state of mass M, certain aspects of this behavior are easy to understand. For example, when $\mu \ll M$ the state is much heavier than the relevant energy scale μ and is effectively "integrated out" of our theory. Thus all running stops, and $\phi_5(M,\mu)$ becomes flat. Mathematically, this occurs because

$$\mathcal{K}_\nu^{(n,p)}(z) \;\sim\; \sqrt{\frac{\pi\rho}{2}}\, z^{n-1/2}\, e^{-z/\rho} \qquad \text{as } z\to\infty\ . \tag{3.55}$$

Thus all running is exponentially suppressed as $z \sim M/\mu \to \infty$, leaving behind only an exponential tail. By contrast, for energy scales $\mu \gg M$, our state is still dynamical. We then see from Fig. 3.1 that the effective contribution to the running from this state is effectively *logarithmic*. Indeed, as $z \to 0$, we find that [32]

$$\begin{aligned} \mathcal{K}_0^{(0,1)}(z) \;&\sim\; -\tfrac{1}{2}\log\, z + \tfrac{1}{2}\left[\log\left(2\pi\right) - \gamma\right]\ , \\ \mathcal{K}_1^{(1,2)}(z) \;&\sim\; 1 \end{aligned} \tag{3.56}$$

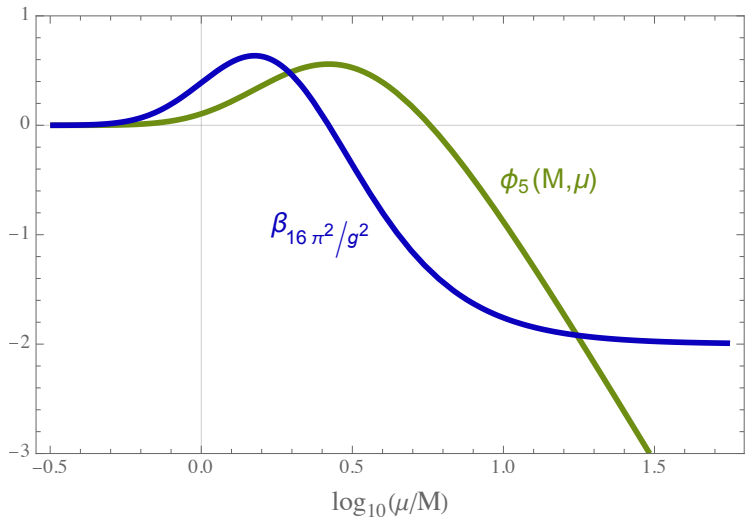

Figure 3.1: The function $\phi_5(M,\mu)$ in Eq. (A.18) and the corresponding contribution to the beta function β_Δ in Eq. (3.62), plotted as functions of $\log_{10}(\mu/M)$ [green and blue, respectively]. Note that $\phi_5(M,\mu)$ is the Bessel-function contribution to $\widehat{\Delta}_G(\mu)$ per unit $\mathbb{A}^{(2)}$ charge from a given physical bosonic string state of non-zero mass M. When $\mu \ll M$, the state is effectively integrated out of the theory, whereupon the running contribution $\phi_5(M,\mu)$ asymptotes to a constant. However, at larger energy scales $\mu \gg M$, the state is fully dynamical and produces a running which is effectively logarithmic. Finally, within the intermediate $\mu \sim M$ region, the Bessel-function expression for $\phi_5(M,\mu)$ in Eq. A.18) provides a smooth connection between these two asymptotic behaviors and even gives rise to a transient "hump" in the value of $\widehat{\Delta}_G(\mu)$, or equivalently a "dip" in the value of the running coupling $g_G(\mu)$.

where γ is the Euler-Mascheroni constant. For $\mu \gg M$, this leads to an asymptotic logarithmic running for $\phi_5(M,\mu)$ of the form

$$\phi_5(M,\mu) \;\approx\; -2\log\left[\frac{1}{\sqrt{2}}\,e^{-(\gamma+1)}\,\frac{\mu}{M}\right] \;. \tag{3.57}$$

Finally, between these two extremes, we see that $\phi_5(M,\mu)$ interpolates smoothly and even gives rise to a transient "hump" in $\widehat{\Delta}_G(\mu)$, or equivalently a "dip" in g_G. This behavior results from the specific combination of Bessel functions within $\phi_5(M,\mu)$. Of course, the statistics factor $(-1)^F$ within the supertrace flips the sign of this contribution for degrees of freedom which are fermionic.

Likewise, for any fixed scale μ, adjusting the mass M upwards or downwards simply corresponds to shifting this curve rigidly to the right or left, respectively. In this way one can imagine summing over all such contributions to the running (while also weighting each contribution by the appropriate net numbers of states at each mass level) as one takes the supertrace over the entire string string spectrum. Of course, for any energy scale μ, the contributions from states with $M \gg \mu$ are exponentially suppressed, as discussed above. Thus, at any energy scale μ, the only states which contribute meaningfully to $\widehat{\Delta}_G(\mu)$ are those with $M \lesssim \mu$.

Thus, combining these Bessel-function contributions with those from Eq. (3.54) and keeping only those (leading) terms which dominate when $M \lesssim \mu \ll M_s$,

we see that we can approximate the exact result in Eq. (3.49) as

$$\widehat{\Delta}_G(\mu) \;\approx\; \frac{\pi}{3}\,\mathrm{Str}\;(\mathbb{X}_1+\tau_2\mathbb{X}_2) \;+\; 2\sum_{M=0}^{\mathrm{Str}}\;\left(\mathbb{A}^{(2)}+\mathbb{B}^{(2)}\right)\,\log\left(\frac{2\sqrt{2}eM_s}{\mu}\right) \\ -\,2\sum_{0<M\lesssim\mu}^{\mathrm{Str}}\left(\mathbb{A}^{(2)}+\mathbb{B}^{(2)}\right)\log\left[\frac{1}{\sqrt{2}}e^{-(\gamma+1)}\,\frac{\mu}{M}\right] \tag{3.58}$$

or equivalently

$$\widehat{\Delta}_G(\mu) \;\approx\; \frac{\xi}{6}\,\mathrm{Str}\,\overline{Q}_H^2 \;-\; \frac{2\pi}{3}\left(\mathrm{Str}\,\tau_2\overline{Q}_H^2Q_G^2-\frac{1}{12}\mathrm{Str}_E\,\tau_2Q_G^2\right) \\ -\,4\sum_{M=0}^{\mathrm{Str}}\left(\overline{Q}_H^2-\frac{1}{12}\right)Q_G^2\,\log\left(\frac{2\sqrt{2}eM_s}{\mu}\right) \\ +\,4\sum_{0<M\lesssim\mu}^{\mathrm{Str}}\left(\overline{Q}_H^2-\frac{1}{12}\right)Q_G^2\,\log\left[\frac{1}{\sqrt{2}}e^{-(\gamma+1)}\,\frac{\mu}{M}\right]. \tag{3.59}$$

Given these results, our gauge couplings $g_G(\mu)$ can exhibit a variety of running behaviors. These will ultimately depend on the spectrum of states associated with the string model under study. Of course, the final terms in Eqs. (3.58) and (3.59) do not exhibit any running until we reach $\mu\sim M_{\rm lightest}$, where $M_{\rm lightest}$ is the mass of the lightest massive string state carrying a non-zero $(\mathbb{A}^{(2)}+\mathbb{B}^{(2)})$ charge. Therefore, if we first restrict our attention to energy scales $\mu\lesssim M_{\rm lightest}$, the only running that arises is due to the massless $(\mathbb{A}^{(2)}+\mathbb{B}^{(2)})$-charged states. These are the contributions that appear on

the first and second lines of Eqs. (3.58) and (3.59), respectively.

This running can be expressed in a manner which is more traditional for describing the running of gauge couplings in string theory, namely in terms of an RGE that relates the couplings $g_G(\mu)$ to their values *at the string scale* M_s (see, *e.g.*, Refs. [33–36]). From Eq. (3.3), we obtain the general running equation for the total gauge couplings $g_G(\mu)$:

$$\frac{16\pi^2}{g^2(\mu)} \;-\; \frac{16\pi^2}{g^2_{\rm tree}} \;=\; \widehat{\Delta}_G(\mu) \tag{3.60}$$

where from Eq. (3.59) can write

$$\begin{aligned}\widehat{\Delta}_G(\mu) \;&=\; \widehat{\Delta}_G(M_s) - 2\,\mathop{\rm Str}_{M=0}\,\left(\mathbb{A}^{(2)}+\mathbb{B}^{(2)}\right)\,\log\left(\frac{\mu}{M_s}\right)\\ &\equiv\; \widehat{\Delta}_G(M_s) + \beta_\Delta(0)\,\log\left(\frac{\mu}{M_s}\right)\;.\end{aligned} \tag{3.61}$$

Here the quantity $\beta_\Delta(0)$ may be regarded as the $\mu = 0$ value of the general beta function $\beta_\Delta(\mu)$ for $\widehat{\Delta}_G(\mu)$, which in turn is defined as

$$\beta_\Delta(\mu) \;\equiv\; \frac{\partial\widehat{\Delta}_G(\mu)}{\partial\log\,\mu} \;=\; -\frac{32\pi^2}{g^3_G}\,\beta_g(\mu) \tag{3.62}$$

where $\beta_g(\mu) \equiv \partial g_G/\partial\log\mu$ is the usual beta function for the gauge coupling g_G. Indeed, we see from Eq. (3.61) that $\beta_\Delta(0)$ is precisely -2 times the

quantity given in Eq. (3.53), *i.e.*,

$$\beta_\Delta(0) \;=\; -2 \sum_{M=0}^{\rm Str} \left(\mathbb{A}^{(2)} + \mathbb{B}^{(2)}\right) \;=\; 4 \sum_{M=0}^{\rm Str} \left(\overline{Q}_H^2 - \frac{1}{12}\right) Q_G^2 \; . \tag{3.63}$$

Likewise, using an asterisk '$*$' to indicate the couplings that would have arisen in our theory if $\beta_\Delta(0)$ had vanished, we can write

$$\widehat{\Delta}_G(M_s) \;=\; \widehat{\Delta}^*_G(0) + \kappa \tag{3.64}$$

where $\widehat{\Delta}^*_G(0)$ is given in Eq. (3.54) and where [within our regulator scheme defined by our regulator function $\widehat{\mathcal{G}}_\rho(\mu)$ with $\rho = 2$] we have

$$\kappa \;=\; -\beta_\Delta(0) \left[1 + \log\left(2\sqrt{2}\right)\right] \; . \tag{3.65}$$

Thus, putting the pieces together, we have the RGE

$$\frac{16\pi^2}{g^2(\mu)} \;-\; \frac{16\pi^2}{g^2_{\rm tree}} \;=\; \widehat{\Delta}_G(M_s) \;+\; \beta_\Delta(0)\, \log\left(\frac{\mu}{M_s}\right) \tag{3.66}$$

where $\widehat{\Delta}_G(M_s)$ is given in Eq. (3.64).

Thus far, Eq. (3.66) captures the effects of the massless $(\mathbb{A}^{(2)} + \mathbb{B}^{(2)})$-charged string states. However, as μ increases still further, additional $(\mathbb{A}^{(2)} + \mathbb{B}^{(2)})$-charged string states enter the EFT and contribute their own individual logarithmic contributions. Of course, if these additional states have masses $M \gg M_{\rm lightest}$, the logarithmic nature of the running shown in Fig. 3.1 from

the state with mass $M_{\rm lightest}$ will survive intact until $\mu \sim M$. However, if the spectrum of states is relatively dense beyond $M_{\rm lightest}$, the logarithmic contributions from each of these states must be added together, leading to a far richer behavior.

One interesting possibility arises in cases of string theories with large compactification radii $R \gg M_s^{-1}$. In such cases, our theory will have Kaluza-Klein (KK) modes with masses $m_n \sim n/R$ that appear well below M_s. Thus, as μ increases towards M_s, increasingly many KK states enter the EFT. Although each KK state contributes the same logarithmic running, our natural field-theoretic expectation is that the full supertrace over the string spectrum will begin to experience an accumulated effective *power-law* growth, with $\widehat{\Delta}_G(\mu) \sim \mu^\delta$ where δ is the number of spacetime dimensions whose inverse compactification radii R^{-1} lie below μ. Indeed, this is precisely the field-theoretic behavior discussed in Refs. [37,38], which can algebraically be interpreted as resulting from a beta function $\beta_\Delta(\mu)$ which itself is growing polynomially with μ. However, as we shall shortly see, in a string context we also have a scale-duality symmetry under $\mu \to M_s^2/\mu$. This means that even at energy scales $\mu \ll M_s$ the *winding* modes associated with such compactifications can also contribute. Remarkably, these have the generic effect of *cancelling* this power-law running (and even the original logarithmic running), thereby producing a situation in which there can be no running at all. We will refer to the region in which such running terminates as a "fixed-point region". This non-renormalisation phenomenon, surprising as it is, is

actually quite general and will be discussed in detail in Ref. [6].

Thus far our results are valid for energy scales below the string scale. However, as mentioned above, it turns out that we also have information about what happens in the opposite region, namely that with $\mu > M_s$: *we simply enter a "dual" infrared region in which this same behavior again emerges, but in reverse.* This is a direct consequence of the modular invariance which we have been careful to maintain throughout our calculations. Indeed, modular invariance ensures that the running is symmetric under the *scale-inversion* duality transformation

$$\mu \;\to\; \frac{M_s^2}{\mu}\;. \tag{3.67}$$

As a result, when plotted as a function of $\log(\mu/M_s)$, the behavior of $\widehat{\Delta}_G(\mu)$ for $\mu \ll M_s$ is reflected symmetrically through the self-dual point $\mu_* = M_s$ to yield the reverse behavior for $\mu \gg M_s$.

As discussed in Ref. [21], the origins of this scale-duality symmetry are easily understood. To see this, we note that in general the contribution of a string states of mass M to the one-loop partition function experiences a Boltzmann-like suppression factor $\sim e^{-\pi\alpha' M^2\tau_2}$. Thus, for any particular benchmark value $\tau_2 = t$, we can separate our string spectrum into two groups: "heavy" states whose Boltzmann suppressions at $\tau_2 = t$ are significant according to some convention, and whose contributions therefore do not require regularisation, and "light" states whose Boltzmann suppressions

are not significant, and whose contributions therefore require regularisation. On this basis, with an eye towards interpreting these results in terms of an EFT with a running scale μ, we are directly led to identify μ^2 inversely with t. However, modular invariance tells us that any physical quantities which depend on τ must be invariant under $\tau \to -1/\tau$. Upon integration over τ_1, this invariance is reflected by an invariance under $t \to 1/t$, or equivalently under $\mu \to \mu_*^2/\mu$ where μ_* is an arbitrary self-dual mass scale.

Of course, the choice of normalisation for μ in relation to t is purely a matter of convention, since the former is a dimensionful spacetime quantity while the latter is a dimensionless worldsheet quantity. In keeping with the traditional string-theoretic conventions relating worldsheet and spacetime physics, we take this conversion factor to be given by α'. This then tells us that $\mu_* = M_s$.

Although this scale-duality symmetry follows directly from modular invariance, its implications are profound. *Ultimately, the existence of such a symmetry implies the existence of a fundamental limit on the extent to which an EFT perspective can possibly remain valid in string theory.* For example, it is well known that string theory is rife with duality symmetries which defy EFT notions: an immediate example of this is T-duality, under which the physics associated with a closed string propagating on a spacetime with a compactified dimension of radius R is indistinguishable from the physics associated with a closed string propagating on a spacetime with a compactified dimension of radius $R' \equiv \alpha'/R$. This is true as an exact symmetry

not only for the string spectrum but also for all interactions. Thus such strings cannot distinguish between large and small compactification geometries, thereby preventing us from establishing a Wilsonian EFT-like ordering of length scales from large to small, or equivalently from IR to UV. Phrased somewhat differently, the existence of a T-duality symmetry tells us that there is a fundamental limit to which we may consider a spacetime compactification radius to be "small". However, what we are seeing now is that a somewhat different phenomenon — namely the scale-duality symmetry under $\mu \to M_s^2/\mu$ which is guaranteed by modular invariance — implies a fundamental limit on the extent to which our EFT can exhibit UV behavior. Indeed, pushing μ beyond M_s only serves to reintroduce the original IR behavior of our theory —a behavior which we may now associate with the *dual* energy scale $\mu' \equiv M_s^2/\mu$ associated with a "dual" EFT. In this sense, the energy scales near M_s exhibit the "most possible UV" behavior that can be realised.

At first glance, it may be tempting to associate this scale-duality symmetry with T-duality, since both tend to place limits on UV behavior and have similar algebraic forms. We stress, however, that T-duality is a *spacetime* symmetry, and as such comes with certain assumptions about the spacetime geometry. By contrast, modular invariance is a fundamental *worldsheet* symmetry which is required for the self-consistency of the theory itself. As such, modular invariance and T-duality are unrelated. Indeed, T-duality relates two *a priori* different string theories to each other, one with a large com-

pactification volume and the other with a small compactification volume, and maps a given state with KK and winding numbers (m,n) in the first theory to the *equally massive* (n,m) state in the other. By contrast, modular invariance is a symmetry that operates *within* a single string theory and involves Poisson resummations across the *entire* string spectrum simultaneously. As such, no two string states in the theory are directly related to each other under modular transformations. Indeed, only through such non-trivial resummations involving the *entire* string spectrum — including the oscillator states as well — could we ever hope to obtain features such as misaligned supersymmetry and supertrace constraints (such as $\mathrm{Str}\,\mathbf{1}=0$) that simultaneously balance all of our string states at all energy scales against each other within a single string theory, even without supersymmetry.

Taken together, all of these observations lead to a running for $\widehat{\Delta}_G(\mu)$ as sketched in Fig. 3.2. In the deep IR, the coupling approaches an asymptotic value which receives contributions from *all* of the states in the string spectrum which carry non-trivial helicity $\mathbb{A}^{(1)}\sim\overline{Q}_H^2$ charges. This assumes that our theory contains no net massless states charged under $\mathbb{A}^{(2)}+\mathbb{B}^{(2)}\sim(\overline{Q}_H^2-1/12)Q_G^2$ where Q_G^2 is the sum of the squares of the charges in the Cartan subalgebra of G; otherwise $\widehat{\Delta}_G(\mu)$ diverges in the IR limit. Moving towards higher values of μ, we see that a non-trivial scale-dependence does not emerge until $\mu\sim M_{\rm lightest}$, where $M_{\rm lightest}$ collectively represents the masses of the lightest massive states which are charged under $\mathbb{A}^{(2)}+\mathbb{B}^{(2)}$. The non-monotonic "dip" in g_G (or "hump" in $\widehat{\Delta}_G$) that is observed in this

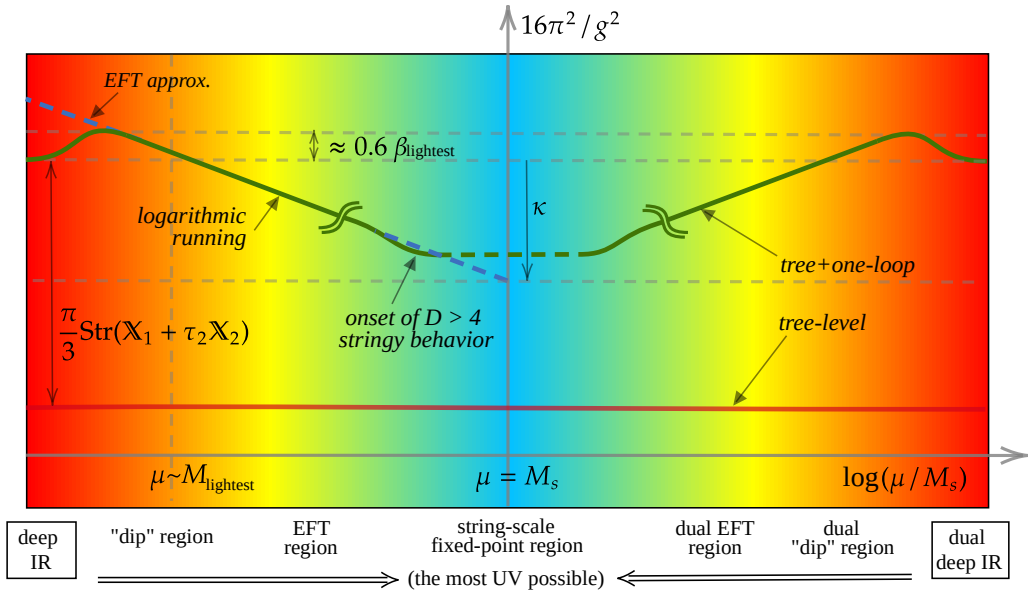

Figure 3.2: The one-loop running of the inverse gauge coupling $\widehat{\Delta}_G = 16\pi^2/g_G^2$ for any gauge group G, as calculated from first principles in a fully modular-invariant string framework. The tree-level contribution is sketched in red, and the total one-loop coupling is sketched in green.

region is a transient effect which smoothly connects the asymptotic deep-IR region $\mu \ll M_{\text{lightest}}$ to an EFT-like region $M_{\text{lightest}} \lesssim \mu \ll M_s$. Beyond the dip region, the theory then enters an EFT-like region in which the gauge coupling experiences a logarithmic running. As $\mu \to M_s$, it is possible that we might cross the energy threshold R^{-1} associated with large compactification radii. In such cases, this logarithmic running can be modified by the appearance of Kaluza-Klein and winding states which might appear at mass scales significantly below M_s and which might tend to *cancel* this logarithmic

running, leading to the existence of a higher-dimensional fixed-point regime, as shown. The subtleties involved in this behavior will be discussed further in Ref. [6]. However, as a general principle, modular invariance requires that the running of $\widehat{\Delta}_G$ exhibit an invariance under $\mu \to M_s^2/\mu$. Thus, as μ increases beyond M_s, the theory inevitably begins to re-enter an IR-like regime which we may associate with a "dual" EFT, followed by a dual dip region and then a dual deep-IR region. The background colors of this sketch indicate the transition from the deep IR (red) to the UV (blue) and then back to IR (red). As such, there is a maximum degree to which our theory can approach the UV: once the energy scale μ passes the self-dual point $\mu \sim M_s$, further increases in μ only push us towards increasingly IR behavior. The quantity κ is defined in Eq. (3.64).

We conclude this chapter with three comments. First, we observe that the running of the gauge coupling is essentially the same as the running of the Higgs mass in Ref. [21] — indeed for $\mu \lesssim M_E$ the only differences are the *coefficients* of the different running terms. These coefficients change because they tally the appropriate charges of our states across the string spectrum, and the charges that are appropriate or relevant change when we switch our attention from the Higgs mass to the gauge couplings.

Our second comment concerns the running of the gauge couplings themselves. Within our calculations we have implicitly assumed that these couplings remain perturbative throughout the running shown in Fig. 3.2; otherwise our one-loop calculation is no longer applicable and higher-loop (and

even non-perturbative) calculations would be needed. Depending on the relative signs and magnitudes of the various supertraces involved, these couplings could be in danger of becoming non-perturbative either as $\mu \to M_S$ (which represents one extremum of the gauge-function plotted in Fig. 3.2) or within the "dip" region.

Most importantly, however, there is a deep and fundamental difference between the running of the gauge couplings $\widehat{\Delta}_G$ and the running of the Higgs mass in Ref. [21]. As we see directly from Eqs. (3.32), (3.43), and (3.49), the gauge-coupling calculation now includes contributions from off-shell string states for which $M_L \neq M_R$. This is a strange but not entirely unexpected feature: states which are not *physical* in the underlying string theory, and which therefore can only contribute in string loop diagrams, also contribute to the running of the gauge couplings in the corresponding low-energy EFT. This feature did not appear in the running of the Higgs mass in Ref. [21]. However, as we have seen, this feature ultimately stems from the fact that the contributions to the Higgs mass are proportional not to the square of the helicity charge $\overline{Q}_H^2$, but rather to this quantity *minus* 1/12. In field theory, this extra $-1/12$ is not problematic. However, in string theory it has deep repercussions because a pure number such as $-1/12$ cannot be subtracted from a squared-charge operator such as $\overline{Q}_H^2$ because a pure number has modular weight $k = 0$ while the squared-charge operator has modular weight $k = 2$. Modular invariance thus requires that the $-1/12$ term be "completed" to the weight-two modular function $\overline{E}_2/12$, and this in turn has

reverberations throughout the string spectrum, shifting left-moving string masses M_L relative to right-moving string masses M_R.

That said, these states do not contribute to the low-energy running in a standard way. Normally, we would expect a string state to contribute in the low-energy theory according to its mass $M^2 = (M_L^2 + M_R^2)/2$. Indeed, this quantity in some sense tells us how much worldsheet energy has been "invested" in creating that state as an excitation in the underlying worldsheet theory. However, what we are now learning from Eqs. (3.32), (3.43), and (3.49) is that although a given entwined string state may have a string-theoretic mass given by M, it contributes to the low-energy EFT precisely as if it had a mass simply given by M_L. In other words, the combined *string-theoretic mass* M is irrelevant; what matters — and what we may therefore consider to be the effective *EFT mass* in such theories, at least as far as the gauge couplings are concerned — is determined by M_L alone. This, of course, is the effect of the shift in left-moving masses relative to right-moving masses induced by $\overline{E}_2$.

We also observe that the entwined resonances all have left-moving masses that exceed the string scale: $M_L \geq M_E = \sqrt{2}M_s$. Thus, one might be tempted to argue that these states have no effects at energy scales below M_s. However, this would not be correct. Thanks to scale-inversion duality, any state that affects the running of quantities *above* the string scale will also affect the running of these quantities *below* the string scale. This is not a new phenomenon unique to the entwined states. After all, we have already

seen that the behavior of our amplitudes in the deep IR is in part determined by the extremely heavy string states in the deep UV. In a similar way, the entwined states also have effects below the string scale and thereby also have an indirect role in affecting the low-energy EFT below the string scale.

Chapter 4

Quantum Annealing: From Basics to a New Quantum Metaheuristic Algorithm

4.1 Basic principles

Having introduced a framework in which universal properties of closed string theory naturally emerge and physical quantities are easily expressed as supertraces, let us now change perspective introducing novel computational techniques which we shall apply to string theory in the next chapter. This change of perspective is justified from the necessity to tackle the problem from different points of view: a more formal one which allows one to extract universal features of closed string theories; a second more computational one

where we develop new techniques to search for SM-like vacua.

These methods revolve around a particular implementation of adiabatic computing known as Quantum Annealing (QA). Quantum annealing is a fascinating computational technique that uses the principles of quantum mechanics to solve complex optimisation problems. It operates on the fundamental concept of quantum tunneling and the quantum adiabatic theorem to explore the vast solution space of a problem and find the optimal configuration or solution. Thus, string theory with its vast number of possible models represents one of the most natural set-ups to apply these techniques, as already discussed in chapter 1.

The quantum annealing device we shall utilise is developed by the D-Wave Systems, which employ specialised hardware designed to create and maintain the required quantum states. These devices use superconducting qubits and powerful magnetic fields to create controlled quantum environments where the annealing process takes place. In particular we shall perform our analysis on the `Advantage_system4.1` architecture [39]: this annealer contains 5627 qubits, connected in a *Pegasus* structure, but only has a total of 40279 couplings between them.

However, it is important to note that while quantum annealing has shown promise for certain optimisation problems, it is not a universal quantum computing approach like gate-based quantum computers. Indeed, gate-based quantum computers are versatile and capable of performing a wide range of computations, while quantum annealers are specialised devices tailored

for optimisation problems. In particular, quantum annealers can only solve problems which can be mapped into the minimisation of an Ising Hamiltonian. The full Hamiltonian in quantum annealing comprises an admixture of this Ising *problem-Hamiltonian* and a trivial Hamiltonian for which the ground state is known. The original idea behind quantum annealing (and quantum adiabatic algorithms more generally) is to begin in the ground state of the trivial system and adiabatically replace the trivial Hamiltonian with the problem Hamiltonian, while remaining in the ground state throughout. Provided we can remain in the ground state the final configuration will yield a solution to the problem. More modern approaches have extended this idea,

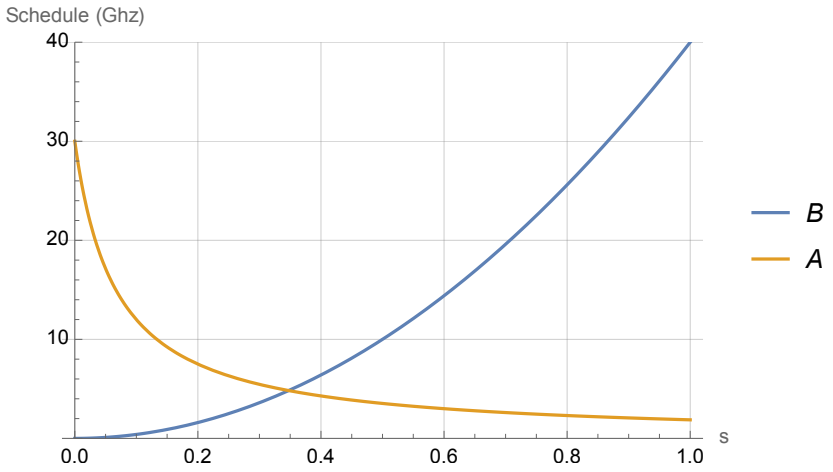

Figure 4.1: Anneal schedule parameters. A and B are the coefficients scaling the transverse field and classical Ising contributions respectively. These coefficients are functions of the parameter $s \in [0, 1]$ which in turn depends on the physical time t.

for example using *reverse annealing*, which consists in initialising the qubits into a specific classical states rather than in a superposition of states as in a usual *forward anneal* run. However the basic principle of arranging an interplay between a problem Hamiltonian and a trivial Hamiltonian is universal. In particular, the Hamiltonian takes the form of a generalised Ising model:

$$\mathcal{H} \;=\; B(s)\left(\sum_{ij} J_{ij}\sigma_i^z\sigma_j^z \;+\; \sum_i h_i\sigma_i^z\right) \;+\; A(s)\sum_i \sigma_i^x\,, \tag{4.1}$$

where i,j label the qubits, σ_i^z are the $z-$spin Pauli matrices, and σ_i^x are the transverse field components, while the couplings h_i and J_{ij} between the qubits are set and kept constant. The parameter $s(t)$ (with t being time) is a user-defined control-parameter that can be adjusted, while $A(s)$ and $B(s)$ describe the consequent change in the quantum characteristics of the annealer. As shown in Fig. 4.1, smaller $s \in [0,1]$ means larger transverse field parameter A compared to B, which induces more "hopping" of σ^z spins, which overall means a system that is more characteristically "quantum".

The main difference between forward and reverse annealing lies in the different anneal schedule, *i.e.*, in how the function $s(t)$ is defined. In the case of forward annealing, s increases linearly with time, with $s(0) = 0$ and $s(t_f) = 1$ (eventually with a pause in between), where t_f is the total annealing time. The network of qubits starts in a global superposition over all possible classical states and, as $s \to 1$, the system localises into a single classical state once a measurement of σ_i^z on all sites has been performed.

In this case, a typical anneal schedule is depicted in Fig. 4.2. By contrast, reverse annealing allows one to initialise the qubits into a specific classical state, begin the evolution at $s = 1$, anneal along a path towards $s = 0$, and then return back up to $s = 1$. Fig. 4.3 shows a typical reverse annealing process.

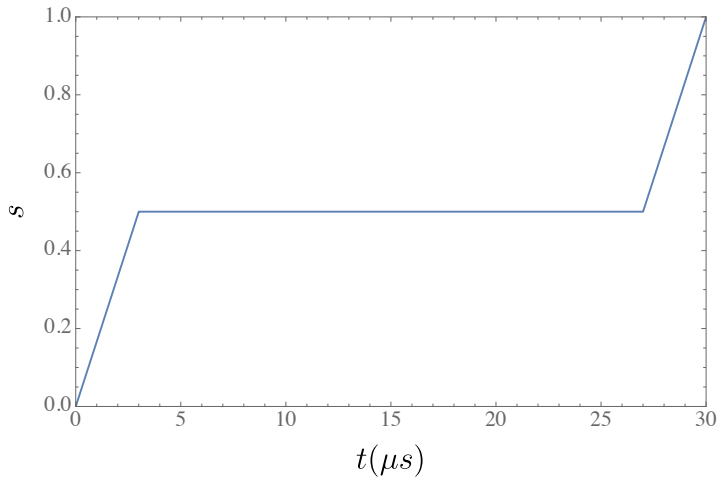

Figure 4.2: Typical forward anneal schedule with a $5\mu s$ ramp rate from $s = 0$ to $s = 0.5$ and from $s = 0.5$ to $s = 1$ with a pause at $s = 0.5$ for $25\mu s$.

To perform the task of finding a global optimisation, the first objective is to encode the problem to be solved into the "classical" Ising model Hamiltonian represented by the B-terms, such that the energetic minimum would correspond to the desired solution. One then adjusts s to alter the relative sizes of the parameters A, B to perform a so-called anneal, in the hope that the systems ends up in the global minimum.

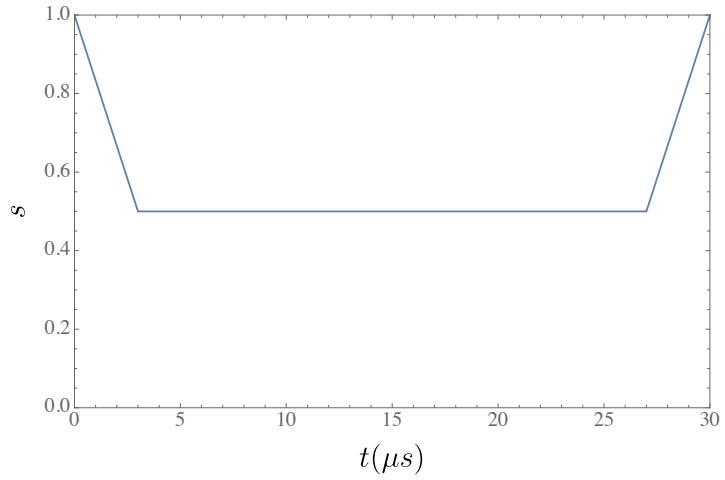

Figure 4.3: Typical reverse annealing protocol with a $5\mu s$ equivalent ramp rate from $s = 1$ to $s = 0.5$, followed by a pause at $s = 0.5$ for $25\mu s$, and then a ramp back to $s = 1$.

4.2 Solving Diophantine equations with quantum annealers

In the following sections we shall focus on a particular class of mathematical equations known as Diophantine equations, which typically consist of a polynomial equation in two or more unknowns with integer coefficients, such that the only solutions of interest are the integer ones. As well as being of intrinsic interest in number theory, Diophantine problems play an important role in fundamental physics. In Ref. [1] we developed methods for solving the kinds of Diophantine problems that frequently occur in physics, where for example they appear in anomaly cancellation conditions as systems of cu-

bic equations. They also appear in string model-building (which will be our main focus in chapter 5), in consistency conditions in string theory, in problems relevant for computing the effective potential in string theory and for finding vacua with small cosmological constant, as well as in powerful non-perturbative methods that are used in field theory, such as 't Hooft anomaly matching [40], and a multitude of other applications.

Specialising to the present case, we are interested in solving a set of polynomial Diophantine equations $f_A(t_i) = 0$, where $t_i \in \mathbb{Z}$ are the would-be integer solutions to the problem of interest. These integers will be encoded on the annealer in a binary format, namely we will use the following encoding:

$$t_i \;=\; \tau_{i,0} + 2\tau_{i,1} + \cdots + 2^{\beta-1}\tau_{i,\beta-1} + s_i \ . \tag{4.2}$$

We use τ to denote the binary variables corresponding to a given spin,

$$\tau_{i,k} \;=\; \frac{1}{2}(1 + \sigma^z_{i,k}) \ , \tag{4.3}$$

with $\sigma^z_{i,k} \in \{-1, 1\}$ classical c-numbers corresponding to measurement of the corresponding spin operator, $\tau_{i,k} \in \{0, 1\}$, and where we allow classical integer shifts, $s_i \in \mathbb{Z}$. These shifts can for example be negative to allow the domain to include negative integers or they can be adjusted iteratively to explore the search space, as we shall see in the following.

We would like to use such an encoding to solve the Diophantine equations, and this can *in principle* be done by finding the minimum of a loss-function

Hamiltonian,

$$H_{\mathrm{D}} \equiv \sum_{A} (f_A(t_i(\sigma_\ell)))^2 \ . \tag{4.4}$$

We shall see in the following that in some particular Diophantine problem one may wish to add several constraints. Such conditions can be included with a constraint Hamiltonian, H_C. Thus we begin with an idealised (*i.e.*, non-quadratic) system,

$$\widetilde{H}(\sigma_\ell) \ = \ H_D(t_i(\sigma_\ell)) + H_C(t_i(\sigma_\ell)) \ . \tag{4.5}$$

Note that solutions to the Diophantine equations all have $H_D = 0$, so that constraints imposed by H_C would independently select the preferred solution. However the converse is generally not true: that is one should avoid over-weighting the constraints H_C such that competing minima appear that have lower H_C but $H_D \neq 0$. Of course in many cases the desired solutions are very rare, so it is often much more efficient (or more precisely not an NP-hard problem) to simply apply any desired constraints by post-processing the solutions.

4.2.1 Reduction

Constructing suitably efficient encodings for these sorts of problems requires significant advancement. Firstly as we shall review we are interested in the kinds of set-ups found in quantum annealers, in which problems are encoded in the Hamiltonian of a quadratic Ising model, which must then be minimised

to solve the problem. Thus the crux of the matter in encoding a non-trivial system of cubic- and higher-order Diophantine equations is to implement a reduction procedure that can represent the complete system as a single loss-function represented by a spin-Hamiltonian that is at most quadratic. Of course Diophantine problems, in particular factorisation, have been considered on Ising model annealers before [41–46], along with quadratic systems of polynomial equations [47,48]. However, both these problems can be mapped into the optimisation of an order four Hamiltonian which can in turn be reduced to a quadratic Ising model suitable for a quantum annealer, with only two layers of reduction. By contrast, here we shall consider problems of order much higher than two. To accomplish this, we use a procedure to automate the reduction of an arbitrary order Hamiltonian to a quadratic one. This procedure, which iterates that first appearing in Ref. [49] and then more recently in Refs. [42, 50–52], is completely problem-independent and therefore potentially applicable to any set of Diophantine equations. It can perform the many layers of reduction required to reach a quadratic spin-Hamiltonian representation of the high order problems we will be considering.

For this task we shall use the reduction method described in the Appendix of Ref. [52]. This method works by introducing auxilliary spins[1] to represent pairs of spins in the original Hamiltonian of Eq. (4.5), and is one of the many methods in the comprehensive survey of Ref. [50]. (We should remark that

[1]We think it is more accurate to use 'auxilliary' to refer to both abstract spins and later to qubits, rather than the quantum computing term, 'ancillary'.

there exist "qubit-saving" reduction methods that do not require auxilliary spins, but these are more task specific and currently appear to be restricted to reduction of terms in the Hamiltonian with products of 3 or 4 spins [42].)

The method works as follows. We begin with the raw polynomial $\widetilde{H}(\sigma_\ell)$ written as a function of binary variables using Eq. (5.1). Suppose $\widetilde{H}$ has terms involving products of two binary variables τ_1 and τ_2. Now consider adding to the polynomial $\widetilde{H}$ a quadratic term that involves the binary variables together with a new auxiliary variable τ_{12}, which is of the form

$$Q(\tau_{12};\tau_1,\tau_2) \;=\; \Lambda(\tau_1\tau_2 - 2\tau_{12}(\tau_1+\tau_2) + 3\tau_{12}) \;. \tag{4.6}$$

Inspection shows that a sufficiently large and positive overall coupling Λ enforces $\tau_{12} \;=\; \tau_1\tau_2$. Importantly the minimum at this point has $Q = 0$. Therefore we may replace the product $\tau_1\tau_2$ with τ_{12} wherever it appears within $\widetilde{H}$, and the new Hamiltonian is guaranteed to have the same set of minima as the original $\widetilde{H}$. Therefore the process can be iterated until one arrives at the desired problem-Hamiltonian which is quadratic in spins, and which is schematically of the form

$$\begin{aligned} H_D + H_C \;=\; & \widetilde{H}(\tau_1,\tau_2,\ldots,\tau_{12},\tau_{13},\ldots,\tau_{12,34},\tau_{12,56}\ldots) \\ & + \sum_{i>j} Q(\tau_{ij};\tau_i,\tau_j) \;+\; \sum_{i<j,k<m} Q(\tau_{ij,km};\tau_{ij},\tau_{km}) \;+\; \ldots \end{aligned} \tag{4.7}$$

with the constraints imposed by the Q terms ensuring that this quadratic Hamiltonian has the same minima as the original order-$2d$ polynomial.

We can check that the reduction works correctly with the example order-3 Hamiltonian

$$\widetilde{H} \;=\; \sigma_1\sigma_2\sigma_3 \;\equiv\; 8\tau_1\tau_2\tau_3 - 4\tau_1\tau_2 - 4\tau_1\tau_3 - 4\tau_2\tau_3 + 2\tau_1 + 2\tau_2 + 2\tau_3 \;, \quad (4.8)$$

where we drop the constant -1 in translating to the binary variables. This Hamiltonian has 4 minima at $\sigma_1\sigma_2\sigma_3 \;=\; -1$ (which corresponds in binary language to any one of the τ_ℓ being zero, or all of them), as opposed to the seven solutions to $\tau_1\tau_2\tau_3 \;=\; 0$. As described above we can reduce the trilinear term by trading $\tau_1\tau_2$ for an auxiliary binary τ_{12} and adding the Hamiltonian $Q(\tau_{12};\tau_1,\tau_2)$. The quadratic problem-Hamiltonian is then

$$H \;=\; Q(\tau_{12};\tau_1,\tau_2) \;+\; 8\tau_{12}\tau_3 - 4\tau_{12} - 4\tau_1\tau_3 - 4\tau_2\tau_3 + 2\tau_1 + 2\tau_2 + 2\tau_3 \;. \quad (4.9)$$

It is easy to verify that provided $\Lambda > 2$ the original 4 degenerate solutions hold in the new combined Hamiltonian as required.

With the increasing complexity of the raw Hamiltonian $\tilde{H}$ and a limited number of physical qubits at our disposal, we of course aim to find a reduction procedure that minimises the number of auxiliary variables. Therefore, the central question is how can we choose the smallest set of spin pairs that correctly collapses all the higher order terms to quadratics? In the case of cubic to quadratic, finding a spin-optimised procedure is equivalent to the set

cover problem which can in turn be cast as 0-1 ILP [53]. Both set cover and 0-1 ILP are well known to be NP-complete by analogy with vertex cover [54]. Therefore, generalising this to arbitrary order Hamiltonians would recast our spin-optimised problem into a task which is at least equivalent to solving $k-2$ NP-complete problems, where k is the order of the Hamiltonian and therefore $k-2$ are the required layers of reduction. For this reason, we shall use a different approach based on a simple greedy algorithm which works as follows: at each reduction stage it finds the pair of binary variables $\tau_i\tau_j$ that appears most often in the Hamiltonian; wherever the pair appears, we replace $\tau_i\tau_j$ with the auxilliary logical spin τ_{ij}, and add the penalty term in Eq. (4.6). The quadratised Hamiltonian is constructed by repeating these three steps iteratively. In the language of set covering, this is equivalent to the greedy heuristic algorithm first proposed in Ref. [55]. In Figs. 4.4, 4.5, 4.6 we have collected three plots which show how the average number of required auxilliary variables grows as we increase the number of cubic interactions, the rate of this growth in the linear central region and the time required to perform the reduction as a function of the number of cubic couplings. These results are very similar to those obtained in Ref. [53] where the optimal reduction is found by solving exactly the equivalent 0-1 ILP. Two important remarks are in order. First, as we can see in Fig. 4.4, both methods saturate approximately when the Hamiltonian contains all possible cubic interactions with n qubits, namely when $N_{\text{3-couplings}} \approx \binom{n}{3}$. Second, we see that in either case the number of auxilliary spins increases linearly with the square root of the

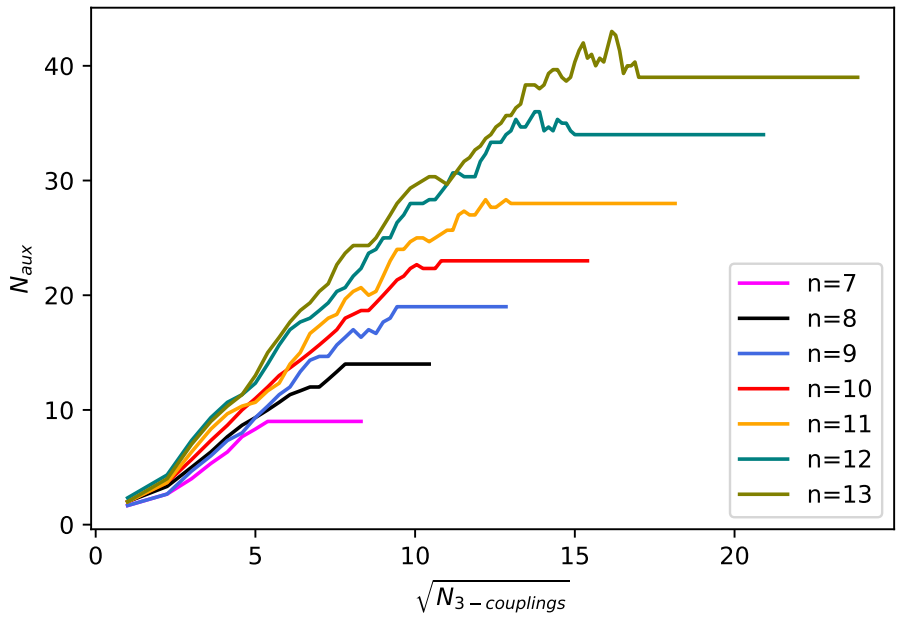

Figure 4.4: Plot of the average number of auxilliary spins required to quadratise the Hamiltonian, versus the square root of the number of cubic interactions for different numbers of total spins n. We note that these curves exhibit a linear behavior in the central region.

number of cubic interactions and the growth rate is given by the square root of the total number of spins, as shown in Fig. 4.5. Nevertheless, as we can see in Fig 4.4, in some regions our procedure uses a number of auxiliaries that is larger than the value at saturation, especially in the $n = 12$ and $n = 13$ cases. This is of course due to the fact that we are not seeking an exact solution of the spin-optimised reduction problem. Indeed, a local optimal choice of our reduction algorithm does not necessarily lead to a global minimum

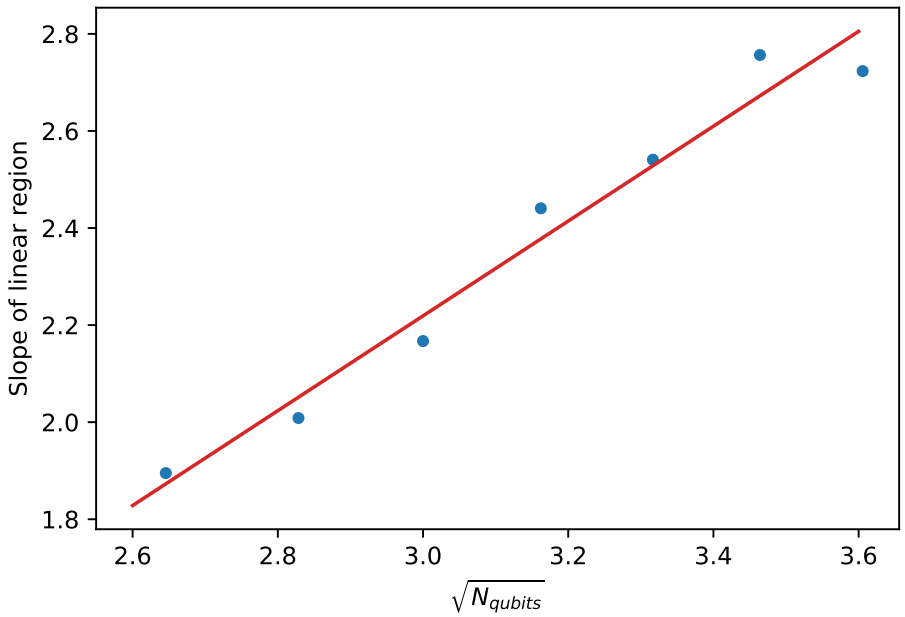

Figure 4.5: Slope of the linear region of the curves in Fig. 4.4 for various values of the total number of spins N_{qubit}. Fitting these data, we see that the slope is a linear function of $\sqrt{N_{\text{qubit}}}$.

in terms of the number of auxilliary spins. More precisely, in the language of the equivalent set covering problem, it has been shown in Ref. [55] that this greedy algorithm returns to an approximate solution which cannot be bigger than $H(n)$ times the minimum one, where $H(n)$ is the n-th harmonic number and n the size of the set to be covered (namely in our case the set of all higher order couplings). However, in the problems treated below, the greedy algorithm we adopt returns quadratised Hamiltonians with at most ~ 300 logical spins, far below the limit imposed by for example the number

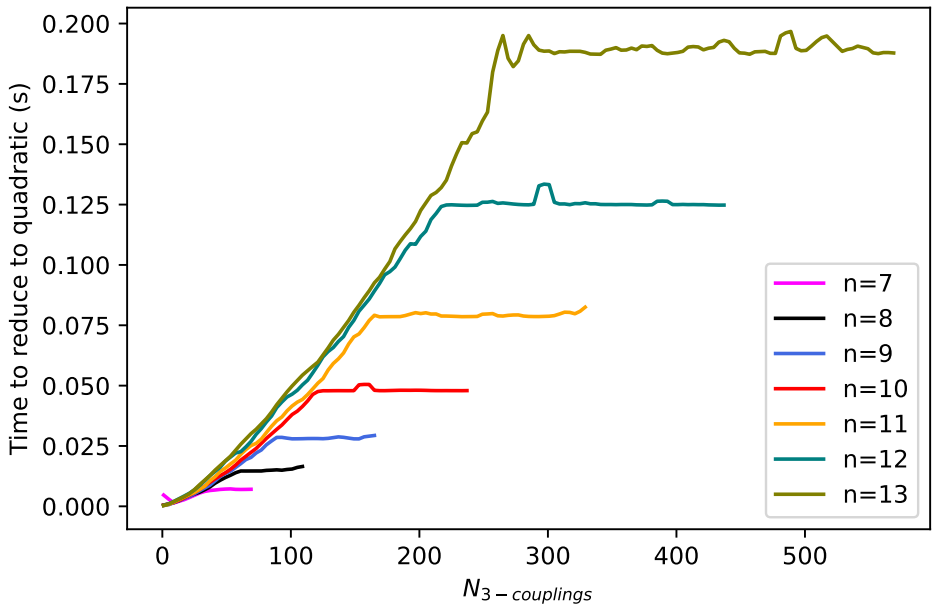

Figure 4.6: Plot of the time required to quadratise the Hamiltonian as a function of the number of cubic couplings. We clearly see the time increasing linearly with the size of the problem.

of available qubits in the currently accessible quantum annealers, making it unnecessary to solve the problem exactly. Finally, we should remark that this procedure is straightforwardly generalisable to Hamiltonians of arbitrary order, requiring a number of steps which grows roughly linearly with the size of the problem, as we can see in Fig. 4.6 and also in Ref. [55]. As expected, this is in contrast with the exact method discussed in Ref. [53] which shows an exponentially increasing amount of time with the increasing complexity of the Hamiltonian. Reduced Hamiltonians can be represented using connected

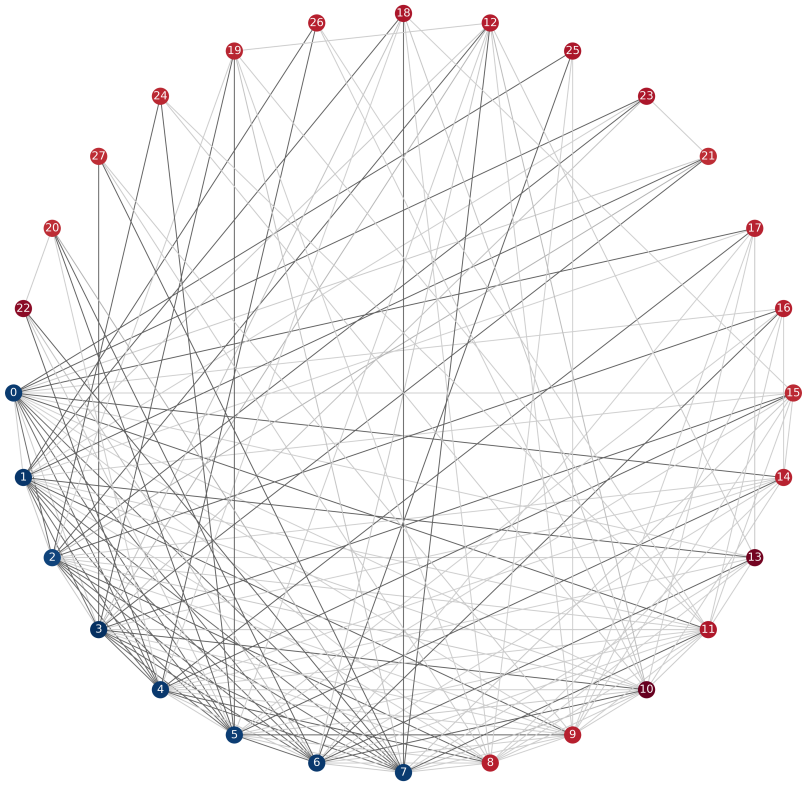

Figure 4.7: Representation of $H = (x_1^2 + x_2^2 - 149)^2$ as a quadratised Ising model. Nodes, corresponding to spins, can be arranged in a circle, and they are quadratically coupled by the links. (Diagrams for non-quadratised models would contain junctions in the couplings). Weaker couplings are represented in light grey, gradually getting darker for higher coupling strengths. Linear couplings are coloured from dark blue (large negative terms) to dark red (large positive terms).

.

graphs in which nodes correspond to spins and links to couplings. As an example, Fig. 4.7 is a representation of the quadratised Hamiltonian associated

to the first Diophantine equation $x^2 + y^2 = 149$, which has solution $(7, 10)$.

4.2.2 Taxicab Numbers

As warm-up problems, let us move on to a complicated class of Diophantine problems which consists in finding the so-called Taxicab numbers, namely those numbers that can be expressed in more than one way as sums of equal powers. The most famous example is the number of Hardy and Ramanujan's eponymous taxi, $\mathrm{Ta}(2) = 1729$. This is the smallest of the following list of numbers, all of which are expressible as the sum of two cubes in two different ways:

$$\begin{aligned} 1729 &= 1^3 + 12^3 = 9^3 + 10^3, \\ 4104 &= 9^3 + 15^3 = 16^3 + 2^3, \\ 20683 &= 24^3 + 19^3 = 10^3 + 27^3, \\ 32832 &= 32^3 + 4^3 = 18^3 + 30^3, \\ &... \end{aligned} \tag{4.10}$$

We shall use the notation (k, m, n), to refer to such numbers, where k is the power, while m and n are the number of terms on each side. Thus $\mathrm{Ta}(2) = 1729$ is defined to be the smallest $(3, 2, 2)$ number, while Fermat's theorem is the statement that $(k, 1, 2)$ numbers only exist for $k = 2$. Here we will develop annealing methods to determine the above list of $(3, 2, 2)$

numbers (where we consider all numbers in the list to be of interest not just the smallest). We also test our methods on several variations, namely $(4,3,3)$, $(3,1,5)$, $(3,1,7)$, $(3,6,6)$, $(3,7,7)$, $(3,8,8)$. Examples of most of these are known, and can be found in Refs. [56–60], although some were discovered only with the advent of high performance computing and appeared relatively recently. However some, such as $(3,7,7)$ and $(3,8,8)$ numbers, do not seem to have been known before. (Indeed as we shall see the latter represent solutions in a search space of size $\sim 10^{24}$.)

As one would expect, the higher the number of variables involved in the problem, the higher will be the average number of interactions per qubit. This often means that when the connectivity of the problem exceeds the native connections supported by the D-Wave Quantum Processor Unit (QPU), a single binary variable in the quadratic optimisation problem needs to be represented by two (or more) qubits (called a 'chain') instead of one. This procedure, known as embedding is carried out by an embedding algorithm, and should be carefully monitored as it can lead to so-called *broken-chains* that have two or more physical qubits in the same chain taking different values. This ultimately limits the size of problems that can be solved on quantum annealers, while performing classical annealing on the same Ising Hamiltonian turns out to be successful. This is exactly the case of Taxicab numbers: classical simulated annealing turns out to be superior currently for these problems, so we will use that annealing method in this and the next section.

In general, finding Taxicab numbers is not a trivial task and for higher Taxicabs, such as Ta(7), Ta(8) etc., only an upper bound is known [61]. Indeed (using the (k, m, n) notation for these numbers), it is interesting to note that no $(5, 2, 2)$ numbers have been found, despite searches up to 10^{26} (see Ref. [56]).

Let us show explicitly how we use the reduction technique of Subsection 4.2.1 to construct an Ising Model Hamiltonian whose ground states are precisely the Taxicab numbers we want to find. As a first example we focus on Ta(2), *i.e.*, we want to find four non-negative integer numbers such that

$$a^3 + b^3 \;=\; c^3 + d^3\,, \quad a \neq \{c, d\}\,. \tag{4.11}$$

We again use binary encoding (see Eq. (4.2)) with $\beta = 5$, $s_i = 1$ (numbers from 1 to 32) and $t_i \in \{a, b, c, d\}$. To impose the equality between the two sums of cubes we define the following Hamiltonian

$$H_D \;=\; (a^3 + b^3 - c^3 - d^3)^2\,. \tag{4.12}$$

However, this is not the end of the story as must also encode the constraint $a \neq \{c, d\}$ to avoid all the trivial minima of the above Hamiltonian, which occur when $a = c$ and $b = d$ or vice versa. In other words we want to construct the H_C Hamiltonian such that it has its global minimum when $a \neq c$ and $a \neq d$. It is more straightforward to write such a constraint Hamiltonian directly in terms of binary variables $\tau_{i,k}$, where $i \in \{a, b, c, d\}$

and $k = 0, ..., \beta - 1$. It is easy to see that the Hamiltonian

$$\begin{aligned} H_C &\equiv H_\delta(a, c) + H_\delta(a, d) \\ &\equiv \prod_{k=0}^{\beta-1} \left(1 - (\tau_{a,k} - \tau_{c,k})^2\right) + \prod_{k=0}^{\beta-1} \left(1 - (\tau_{a,k} - \tau_{d,k})^2\right) \end{aligned} \tag{4.13}$$

achieves this. Explicitly, one finds that

$$H_C = \begin{cases} 0, \text{ when } a \neq c \text{ and } a \neq d\,, \\ 1, \text{ when } a = c \text{ and } a \neq d\,, \\ 1, \text{ when } a = d \text{ and } a \neq c\,, \\ 2, \text{ when } a = c = d\,. \end{cases} \tag{4.14}$$

The Hamiltonian we shall use is then the sum

$$\widetilde{H} = H_D + H_C\,. \tag{4.15}$$

Written is terms of τ's, this Hamiltonian is a polynomial of order 2β for $\beta \geq 3$. Again, setting $\beta = 5$ and using the technique described in Sec. 4.2.1 we can reduce it to a quadratic Hamiltonian by adding 98 auxilliary spins.

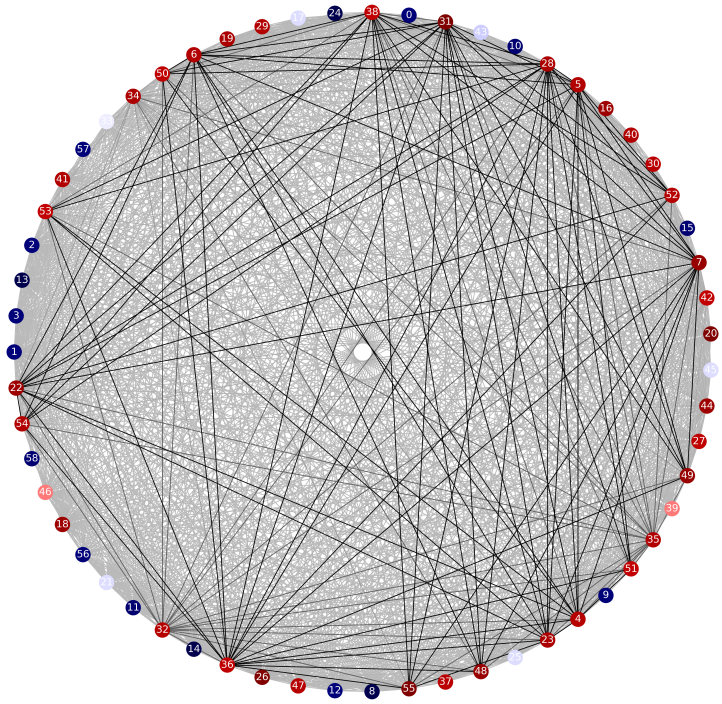

Figure 4.8: Representation of the Ising Hamiltonian corresponding to the Ta(2) problem.

In Fig. 4.8 we represent the reduced Hamiltonian for $\beta = 4$. We see that stronger couplings are rare among the interactions, which mostly form a very complex network of weaker couplings in the background. Classical annealing on the reduced Hamiltonian yields all the solutions written in Eq. (4.10), namely all the Taxicab numbers with $a, b, c, d \leq 32$.

Let us now push this further and attempt to solve more complicated generalisation of the Taxicab problem, (k, m, n) where

$$(k, m, n) \equiv a_1^k + ... + a_m^k = b_1^k + ... + b_n^k, \tag{4.16}$$

where $\{a_1, ..., a_m\} \neq \{b_1, ..., b_n\}$. Beginning with $(4, 3, 3)$ numbers,

$$(4, 3, 3) \;=\; a^4 \,+\, b^4 \,+\, c^4 \;=\; d^4 \,+\, e^4 \,+\, f^4\,, \tag{4.17}$$

we define the following Hamiltonians

$$H_D \;=\; (a^4 + b^4 + c^4 - d^4 - e^4 - f^4)^2\,, \tag{4.18}$$

and

$$H_C \;=\; H_\delta(a, d) + H_\delta(a, e) + H_\delta(a, f)\,, \tag{4.19}$$

to impose the equality in Eq. (4.17) and also to force $a \neq d, e, f$. The order of the complete Hamiltonian, which is the sum of Eq. 4.19 and Eq. 4.18, is 2β for $\beta \geq 4$. Again, it can be reduced to a quadratic one by adding 66 auxilliary variables in the case with $\beta = 4$ and 154 in the case with $\beta = 5$. Several anneal runs (each with 10000 reads) with $\beta = 4, 5$ yield the following results

$(4,3,3)$	a	b	c	d	e	f
2673	3	6	6	7	2	4
16562	9	1	10	11	6	5
28593	2	13	2	9	6	12
35378	13	4	9	11	12	1
43218	11	13	2	14	7	7
54977	4	8	15	9	14	10
195122	21	5	2	9	13	20
324818	14	9	23	21	2	19
619337	28	8	5	7	26	20
847602	1	25	26	29	19	10
1071713	12	32	7	28	26	3
1178898	29	11	26	1	32	19
1328498	29	9	28	23	32	3

Table 4.1: List of $(4,3,3)$ numbers found using $\beta = 3,4,5$ and 10000 reads per anneal run.

To comment on the efficacy of the method: the search space is of order $32^6 \sim 10^9$, and yet these solutions are found after order 10^5 reads.

For the remainder of this section we consider the $(3,n,m)$ numbers, where $n,m \in \mathbb{N}^+$. For this purpose we define the following Hamiltonian

$$\widetilde{H} = \left(\sum_{i=1}^{n} a_i^3 - \sum_{i=1}^{m} b_i^3\right)^2 , \tag{4.20}$$

where in this case we do not add any constraint Hamiltonian to enforce $\{a_i\} \neq \{b_i\}$ when $n = m$, because here it is sufficient to simply check at the end of each anneal run if the minimum is trivial or not.

Tables 4.2-4.3 list some of the solutions found for $n = 1$ and $m = 5,7$ with

$\beta = 5, 6$. Cases with $n = m \equiv N$, with $N = 6, 7, 8$ are listed in Tables 4.4-4.6.

(3,1,5)	a_1	b_1	b_2	b_3	b_4	b_5
729	9	1	3	4	5	8
1728	12	3	10	4	8	5
68921	41	3	17	21	28	32
125000	50	2	8	24	36	40
185193	57	16	17	30	40	44
216000	60	11	16	25	45	47
262144	64	9	18	31	44	52

Table 4.2: A list of $(3, 1, 5)$ numbers found using $\beta = 5, 6$. The reduction needs 120 and 216 auxilliary spins respectively.

(3,1,7)	a_1	b_1	b_2	b_3	b_4	b_5	b_6	b_7
2744	14	2	3	5	7	8	9	10
13824	24	3	5	8	9	13	15	19
32768	32	1	6	15	16	17	20	23
148877	53	3	21	24	28	29	32	36
205379	59	5	12	13	18	23	43	47
238328	62	17	20	22	31	32	38	46

Table 4.3: A list of $(3, 1, 7)$ numbers found using $\beta = 5, 6$. The reduction needs 160 and 288 auxilliary spins respectively.

$(3,6,6)$	a_1	a_2	a_3	a_4	a_5	a_6	b_1	b_2	b_3	b_4	b_5	b_6
5012	2	4	5	7	12	14	3	6	8	9	11	13
7975	1	7	8	10	14	15	3	4	9	11	12	16
8309	1	5	7	10	14	16	4	6	9	12	13	15
41873	3	8	11	14	26	27	1	6	13	19	22	28
48438	9	13	17	20	22	28	1	4	15	18	23	30
51318	1	10	15	17	21	32	3	5	9	16	28	29
52359	5	6	7	11	26	32	3	14	15	20	24	29
78730	2	3	23	26	28	30	11	14	16	20	31	32
86400	3	9	21	24	31	32	4	5	26	27	28	30

Table 4.4: $(3,6,6)$ solutions with $\beta = 4, 5$. The reduction needs 120 and 240 auxilliary spins respectively.

$(3,7,7)$	a_1	a_2	a_3	a_4	a_5	a_6	a_7	b_1	b_2	b_3	b_4	b_5	b_6	b_7
39256	3	8	9	14	17	22	27	2	5	11	16	19	21	26
45063	3	5	7	13	14	19	32	2	9	10	15	18	23	28
46411	7	9	14	17	18	23	27	3	5	8	10	11	22	32
52094	1	6	13	17	22	23	28	3	7	14	16	18	21	31
63224	7	9	12	18	20	24	32	2	3	13	14	19	29	30
73276	6	12	14	15	24	29	30	9	17	18	20	23	27	28
77687	2	9	17	21	24	28	30	4	5	15	16	26	27	32

Table 4.5: $(3,7,7)$ solutions with $\beta = 5$. The reduction needs 280 auxilliary spins.

$(3,8,8)$	a_1	a_2	a_3	a_4	a_5	a_6	a_7	a_8	b_1	b_2	b_3	b_4	b_5	b_6	b_7	b_8
50139	1	3	6	10	12	20	23	30	2	5	9	13	17	19	25	27
73206	1	3	4	17	20	25	26	30	5	8	9	10	19	21	28	32
78202	3	4	17	18	19	24	27	30	1	2	9	16	20	22	28	32
85418	2	3	9	16	18	23	31	32	6	10	14	15	24	26	27	30

Table 4.6: $(3,8,8)$ solutions with $\beta = 5$. The reduction needs 320 auxilliary spins. Note that even the smallest $(3,8,8)$ number represents a solution in a search space of size $32^{16} \sim 10^{24}$.

Note that all the above solutions are non-trivial $(3,n,m)$ numbers, in that they are not sums of smaller solutions. Indeed, it may happen that a $(3,n,m)$ number is actually the sum of $(3,p,q)$ and $(3,k,l)$ numbers with $p+k = n$ and $q+l = m$. In order to avoid such trivial solutions, we have simply removed them by hand at the end of each anneal run.

4.3 A physics-related problem: solving anomaly cancellation conditions

Having road-tested our reduction methods on Taxicab numbers, we now move on to an application of these methods in physics, solving the anomaly cancellation conditions in the Standard Model extended by an extra $U(1)$ gauge symmetry. This is one of the simplest and most studied extensions of the Standard Model (see Ref. [62] for a review of Z' physics), and it has been the target of numerous experimental searches [63].

The generalities of anomaly cancellation for such systems have been dis-

cussed in Refs. [64–77].

In this part we will for concreteness specialise to the models studied in Ref. [76]. Here, the main assumption is that the chiral fermions appear in the usual 3 families of quarks and leptons, together with 3 right-handed neutrinos. The charges under the additional $U(1)$ are labelled by $\{Q_i, U_i, D_i, L_i, E_i, N_i\}$, respectively, with $i \in \{1, 2, 3\}$ indicating the generation number. Under this assumption the anomaly cancellation condition yields the following set of Diophantine equations for the charges:

$$\sum_{i=1}^{3} (6Q_i + 3U_i + 3D_i + 2L_i + E_i + N_i) \;=\; 0\,, \tag{4.21}$$

$$\sum_{i=1}^{3} (3Q_i + L_i) \;=\; 0\,, \tag{4.22}$$

$$\sum_{i=1}^{3} (2Q_i + U_i + D_i) \;=\; 0\,, \tag{4.23}$$

$$\sum_{i=1}^{3} (Q_i + 8U_i + 2D_i + 3L_i + 6E_i) \;=\; 0\,, \tag{4.24}$$

$$\sum_{i=1}^{3} (Q_i^2 - 2U_i^2 + D_i^2 - L_i^2 + E_i^2) \;=\; 0\,, \tag{4.25}$$

$$\sum_{i=1}^{3} (6Q_i^3 + 3U_i^3 + 3D_i^3 + 2L_i^3 + E_i^3 + N_i^3) \;=\; 0\,. \tag{4.26}$$

A general solution to the above equations has already been found analytically in Ref. [76]. However, we shall demonstrate here that these problems can be also tackled using Ising model annealing (in practice here we use simulated annealing, but ultimately quantum annealers will be practicable).

As for the Taxicab problem, we begin constructing the Hamiltonian by simply squaring and summing the left hand side of all the above equations. We encode all the variables involved as in Eq. (4.2) with $t_i \in \{Q_i, U_i, D_i, L_i, E_i, N_i\}$ and take $s_i = -1$ for all the charges. We set $\beta = 2$, thus looking for solutions with entries from -1 to 2. Note that although the number of bits we use to represent each variable is relatively low, the number of possible configurations of these $3 \times 6 = 18$ charges with possible values in $[-1, 2]$ is already quite high: $4^{18} \sim 10^{10}$. It is worth mentioning that in this particular case a comprehensive scan can be completed with far fewer attempts due to generation permutation symmetry in the equations. Indeed, it is easy to see that the anomaly equations are invariant under arbitrary permutations of $\{A_1, A_2, A_3\}$, where $A \in \{Q, U, D, L, E, N\}$, giving an $(S_3)^6$ permutational symmetry that could be exploited if we were looking for solutions by exhaustive scanning over all the different configurations.

Of course our goal here is to avoid using such tricks, but to instead find solutions using annealing on the reduced Ising Hamiltonian. For $\beta = 2$ the reduction requires only 18 auxiliaries. We have performed several anneal runs with 10000 reads obtaining an average of 60 distinct solutions per anneal run. In the following table we present a sample of three of them.

Q_1	Q_2	Q_3	U_1	U_2	U_3	D_1	D_2	D_3	L_1	L_2	L_3	E_1	E_2	E_3	N_1	N_2	N_3
1	0	-1	-1	1	0	1	-1	0	-1	0	1	-1	0	1	0	1	-1
-1	1	0	0	-1	1	-1	1	0	-1	0	1	0	1	-1	1	0	-1
1	-1	0	-1	1	0	1	0	-1	1	0	-1	-1	1	0	-1	0	1

Table 4.7: A sample of three solutions found using $\beta = 2$ and 10000 reads in each anneal run.

One might expect higher values of β to lead to new solutions with bigger entries, along with those previously found. However, for this specific problem, classical annealing turns out to be unfruitful for $\beta > 2$. To explain why it is useful to inspect how the energy gap Δ between the ground state and the first excited state scales as a function of the size of the problem. It can be shown (see Ref. [48]) that

$$\Delta \sim \mathcal{O}\left(\frac{2^{-n\mu}}{m\alpha}\right) , \tag{4.27}$$

where α and μ are the number of additions and multiplications respectively in the Hamiltonian written in terms of binary variables, m is the number of equations we want to solve and n is the effective precision, which is the difference between the largest and smallest nonzero absolute values representable among all the variables in the system. Increasing β makes all these parameter bigger, including n and μ, causing an exponential shrinkage of the energy gap between the ground states and the first excited states, which in turn considerably affects the algorithm's performance.

To improve our results and find solutions with bigger entries we use a

technique we called "solution-mining". This method allows one to explore larger regions of parameter space (*i.e.*, larger integers) without increasing β, yielding in turn solutions with larger values. The method operates iteratively, by at each run constructing a brand new Hamiltonian from the previously found solutions. At say the k-th iteration, we minimise the Hamiltonian looking for solutions of the form

$$t_i^k \;=\; \tau_{i,0}^{(k)} + 2\tau_{i,1}^{(k)} + s_i^k \;, \tag{4.28}$$

where $k \;=\; 0, ..., N$ (with N being the total number of anneal runs), and where s_i^k is a classical shift that centres the new search, which is determined from a solution found in the $(k-1)$-th run: if we designate the previous solution $\hat{t}_i^{k-1}$, then the $\{s_i^k\}$ are chosen such that

$$t_i^k \;\in\; [\hat{t}_i^{k-1} - 1\,,\, \hat{t}_i^{k-1} + 2] \quad \text{or}$$

$$t_i^k \;\in\; [\hat{t}_i^{k-1} - 2\,,\, \hat{t}_i^{k-1} + 1] \;, \tag{4.29}$$

based on a random choice.

This procedure finds new solutions by performing a kind of "random tunnelling" from previously found solutions (hence the name "solution-mining"). It generally operates well when there are many variables in the system and many different equations, because in such systems the solutions can be rel-

atively close in each dimension of the search space (even though the total Hamming distance could be very large due to the large number of dimensions). For the two specific example problems we are discussing here, it is not a useful enhancement for finding Taxicab numbers because there one is seeking the smallest numbers, and (as we shall see) the solutions to the Diophantine system are very widely spaced. However for solving anomaly equations the method is a significant improvement. In such systems, new solutions to the anomaly equations tend to appear with consistent frequency when the allowed charge size is increased, and it is the sheer number of anomaly equations and charges that makes the problem difficult.

It should be noted that there is no additional cost for solution-mining because even though a brand new Hamiltonian must be constructed at each stage, the embedding graph remains the same if the values of β do not change. This means we construct an entirely new Hamiltonian $\widetilde{H}$, but do not need to perform a new reduction of the solution. On a quantum annealer we perform reverse annealing in order to collect the solution and construct the new Hamiltonian at each stage, which then simply has to be translated into new couplings via the updated $\{s_i^k\}$ values.

Applying solution-mining with 30 anneal runs yields to 153 solutions with entries between -13 and 13. Note that a complete scan on all possible such configurations, even exploiting the $(S_3)^6$ permutational symmetry, would involve $\binom{13\times 2+1}{3}^6 \sim 10^{20}$ trials, which is infeasible with conventional computing methods. It should be noted that we do not make use of the permutational

symmetry and the Ising machine is in principle succeeding within a search space of $26^{18} \sim 3 \times 10^{25}$, although it is not yet clear how exhaustive the method of small β plus solution mining can eventually be.

In Table 4.8 we present a sample of ten of the solutions found.

Q_1	Q_2	Q_3	U_1	U_2	U_3	D_1	D_2	D_3	L_1	L_2	L_3	E_1	E_2	E_3	N_1	N_2	N_3
-1	0	1	-1	0	1	1	-1	0	1	0	-1	0	-1	1	1	0	-1
0	-2	2	1	-1	2	-2	0	0	0	1	-1	0	-1	-1	0	1	1
3	-1	-2	-1	-2	3	-4	2	2	0	-3	3	2	-2	0	2	-3	1
3	-2	-1	1	-3	3	-4	3	0	-1	0	1	-1	0	0	3	-3	1
-1	1	0	-2	-1	4	-5	4	0	-2	-1	3	0	2	-3	1	-2	2
1	-1	0	0	-2	5	-6	4	-1	-1	0	1	0	-1	-2	0	-2	5
1	0	0	-1	-2	6	-7	4	-2	-3	0	0	2	1	-4	0	0	7
2	-1	-1	2	-3	4	-6	2	1	0	0	0	-3	1	-1	-3	-2	8
2	-2	-2	2	1	2	-2	-1	2	6	-1	1	-3	-1	-5	-10	-2	9
1	-3	0	1	5	2	-2	1	-3	2	1	3	-5	-3	-4	-13	0	13

Table 4.8: A sample of ten solutions found using the solution-mining method.

The first of these solutions is equivalent to one found previously in Table 4.7. This is because in the first anneal run the algorithm looks for solutions centered around zero, *i.e.*, with entries between $[-1, 2]$. Then it starts exploring the neighborhood of the solution found in the previous anneal run, gradually finding solutions with larger entries.

4.4 GQAA: Genetic Quantum Annealing Algorithm

Having used quantum annealers to directly address physics-related problems, we now turn to a slightly different use of these machines, *i.e.*, as a

tool to enhance meta-heuristic search algorithms, in particular evolutionary algorithms. As already outlined, from this perspective string theory represents a sort of "big-data" challenge, where meta-heuristic algorithms are the most promising approaches to scan over string models. Improving on these techniques using quantum annealer may therefore be crucial in developing effective strategies to search for string vacua.

The general idea of combining quantum computing and evolutionary algorithms is a relatively old one in the framework of traditional gate quantum computers, but the success that is claimed in this arena is on a fairly restricted set of problems (see [78–81] for reviews). The situation with quantum annealers is even less well developed [81–85]. However both GAs and quantum annealers have each individually been having increasing impact in similar domains, especially recently in the context of particle physics and string theory (see for example [86–102] and [103–105] respectively). This still strongly suggests that there is benefit to be gained by combining them.

Before going into the details of this novel combined approach, let us summarise how genetic algorithms work.

4.4.1 Introduction to genetic algorithms

Genetic Algorithms (GAs) are a type of optimisation algorithm inspired by the process of natural evolution. They are used to find solutions to complex problems by mimicking the principles of natural selection, crossover, and mutation. GAs are particularly useful for solving problems that involve a

large search space, such typical problems in string theory. The algorithm goes through several steps, which we summarise as follows:

- *Initialisation*: a population of potential solutions, often represented as strings of *genes* or *alleles*, is randomly generated. These series of genes constitutes the *genotype* of each individual, which yields its particular properties, the so-called *phenotype*, which is essentially the list of parameters that define the problem of interest. Each genotype represents a potential solution to the problem at hand.

- *Evaluation*: each potential solution in the population is evaluated based on a predefined fitness function that quantifies how well a solution solves the problem. The fitness function guides the algorithm by assigning higher values to better solutions. Fig. 4.9 illustrates a single individual with its own genotype, needed to compute the phenotype and ultimately the fitness.

- *Selection*: solutions with higher fitness values have a greater chance of being selected for the next generation. This simulates the principle of natural selection, where fitter individuals have a better chance of passing on their genes to the next generation. In particular, selection can proceed after having ranked the individuals according to their fitness. In Fig. 4.10 we refer to this part of the algorithm, in which the fitnesses of the phenotypes are compared with the problem of interest, as the *environment*. Individuals are then selected for breeding with a

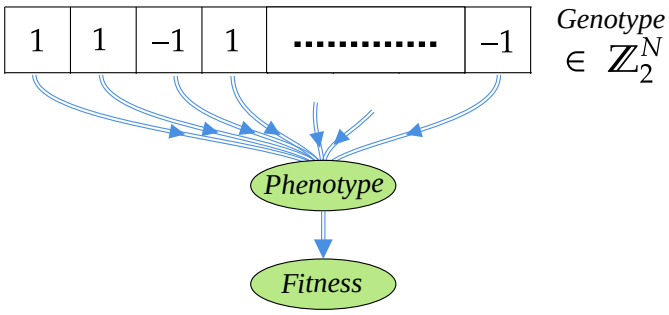

Figure 4.9: An individual member of the population in a classical GA, where here the genotype contains N discrete alleles (for pedagogical purposes we represent the genotype with $\sigma = \pm 1$ spin values, which are translated to binary digits τ in the obvious way, $\tau = (1+\sigma)/2$).

probability that increases with the ranking. A convenient choice is for the dependence to be linear, such that the probability p_k of the k^{th} individual being selected for breeding is

$$p_k \;=\; \frac{2}{(1+\alpha)P}\left(1+\frac{P-k}{P-1}(\alpha-1)\right)\;, \tag{4.30}$$

where P is the population size and where $\alpha > 1$ is a constant meta-parameter that can be thought of as the 'learning rate' of the GA. In particular, the probability p_1 for the fittest individual to be selected is a multiple α of the probability p_P for the least fit. Typically, α is chosen in the range $2 \leq \alpha \leq 5$.

- *Crossover*: selected solutions are paired up, and their genetic information is combined through a process called crossover. This involves exchanging segments of genetic material between the parents to create new offspring with a mix of their traits.

- *Mutation*: a small random change (mutation) is applied to the genetic information of offspring. This introduces diversity into the population, preventing the algorithm from converging prematurely to a sub-optimal solution. A typical value for the mutation rate is a few percent, but the optimum rate tends to be problem specific.

- *Replacement*: the new offspring, along with some of the parents, replace the old population. This forms the next generation of potential solutions.

- *Termination*: As indicated in Fig. 4.10, this process is then repeated for multiple generations, typically a few hundred. The algorithm iterates through the selection, crossover, mutation, and replacement steps for a certain number of generations until a stopping criterion is met (e.g., a satisfactory solution is found). Over successive generations, the population evolves towards better solutions as the algorithm exploits the information gained from previous generations and explores new areas of the solution space.

Genetic algorithms can be applied to a wide range of optimisation problems, in principle without any limitation on the nature of the problem. How-

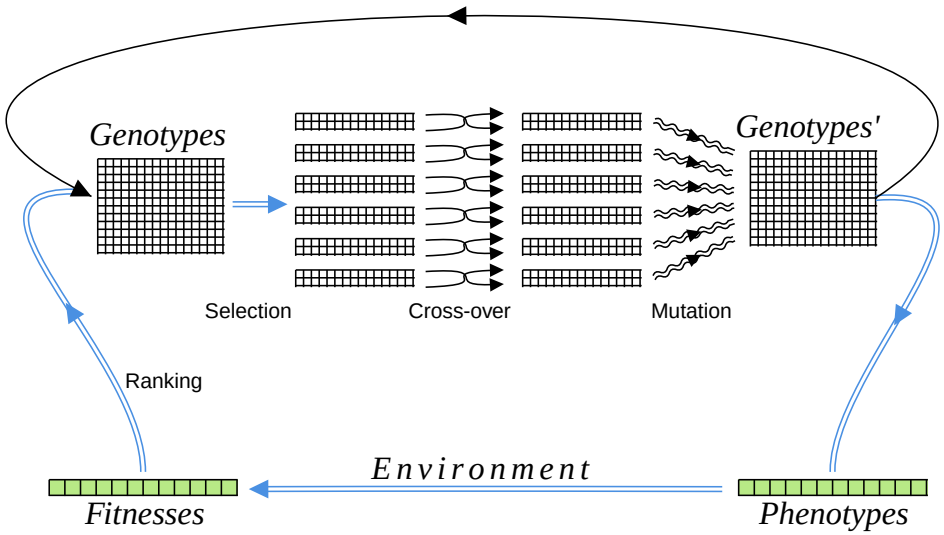

Figure 4.10: The classical GA is a directed graph with two loops. The initial population of genotypes (on the right) give phenotypes which are in turn used to calculate the fitnesses of the P individuals in the 'environment' which are then collected as a ranked population of parent genotypes (on the left). The fitness ranking of an individual determines the probability of it being selected to take part in a breeding pair. $P/2$ breeding pairs are formed in this manner, and then cross-over and mutation yield an entirely new generation, and the process is repeated.

ever, GAs might require tuning of various parameters, such as population size, mutation rate, and selection methods, to achieve optimal performance for a specific problem. It is worth mentioning that the procedure described

above can be thought of as the "vanilla" version of a GA, and many variations have been suggested (for a review of some of the improvements that can be made see Ref. [99]). However all implementations of GAs have in common these three elements. One crucial aspect to remember for the later GQAA discussion is that mutation is not just an improvement to the convergence, but is absolutely integral to the entire process because without it the system stagnates, as can be appreciated by optimising the mutation rate as in Ref. [90] and below.

4.4.2 Genetic Quantum Annealing

How might one incorporate some of the advantages of quantum annealers into a genetic algorithm? As is clear from the discussion in chapter 4, from a quantum computing perspective the difficult part of the GA to encode would be the problem itself and the fitness function, namely the environment. Therefore our hybrid algorithm rests on continuing to treat the environment classically.

The foundation of the approach is to redefine precisely what constitutes an 'individual': our definition is shown in Fig. 4.11. In effect it adds another layer to the classical individual of Fig. 4.9. Unlike the classical GA, the alleles in the genotype of an individual are *continuous*, and are comprised of a set of N of the linear couplings h_ℓ appearing in the spin Hamiltonian in Eq. (4.1), rather than a set of N discrete alleles. The crucial feature that the quantum annealer introduces is the ability to convert this continuous

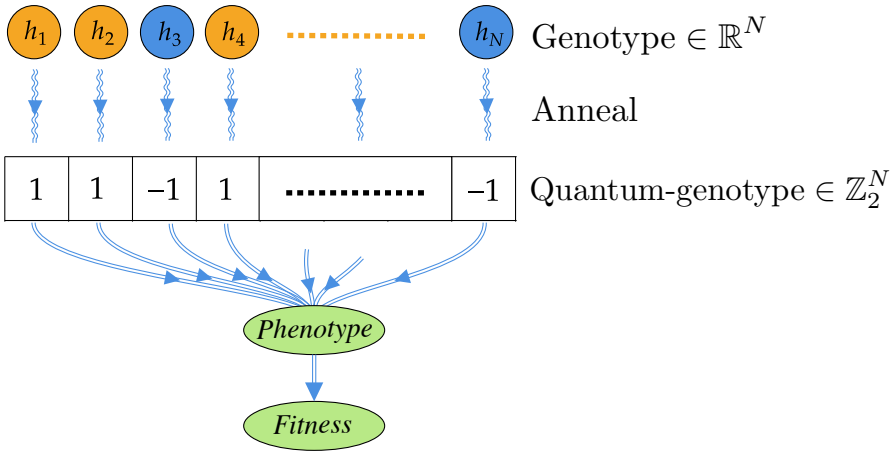

Figure 4.11: Representation of an individual member of the population in the GQAA, showing the relation between the genotype, quantum-genotype and phenotype. An individual corresponds to a chain of N entries in the Ising model on the annealer. The genotype is defined classically in $\mathbb{R}^N$ and corresponds to the real biasing linear couplings for the individual, with orange nodes biasing positively (i.e. they have negative h values) and blue biasing negatively. A quantum-genotype lives in $\mathbb{Z}_2^N$ and is the corresponding discrete set of eigenvalues that is read from the annealer, which is influenced by the genotype, but also by couplings to the neighbouring members of the population. The quantum-genotype takes fluctuating values, with fitter individuals having larger modulus $|h|$ and hence enforcing their biasing more strongly, resulting in a form of 'weighted mutation'. The phenotype is derived from the discrete quantum-genotype classically in the usual way.

genotype into a discrete genotype in a probabilistic way by performing a quantum read of the corresponding spin eigenvalues. The latter discrete genotype we shall refer to as a *quantum-genotype*, due to its ability to take discrete but fluctuating values. Note that it is the quantum-genotype which will determine the phenotype and hence the fitness of the individual. This is the main ingredient provided by the quantum annealer, and we argue that this separation of the genotype from its physical manifestation quantises the crucial biological feature that has to be incorporated into classical GAs with an artificial mutation stage, namely the fact that the genetic code for an individual does not absolutely determine its phenotype.

For later reference it is also of course possible to define the discrete genotype that the h_ℓ couplings would *like* to enforce in the spins, which we refer to as the *classical-genotype*, which is simply

$$\sigma_\ell^{\rm cl} \;=\; -\,\mathrm{sign}(h_\ell)\;. \tag{4.31}$$

Importantly, in the limit of zero quadratic couplings $J_{\ell m}$ on the annealer, and perfectly adiabatic annealing, the quantum-genotype is equal to the classical-genotype.

With this definition of an individual to hand, there is then a great deal of freedom in how one can configure them into a population on the annealer, and it is possible to go far beyond the classic framework in Fig. 4.10. The configuration that we adopt for the population is shown in Fig. 4.12.

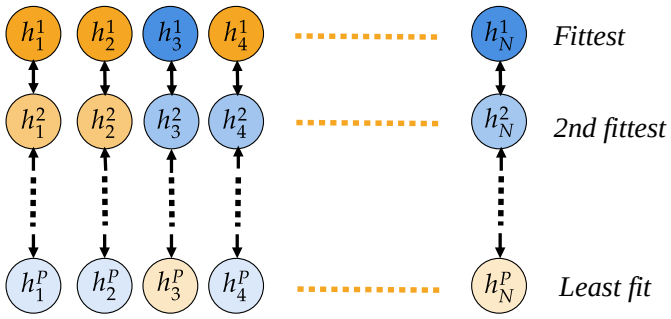

Figure 4.12: The arrangement of the population and the influence of fitness assignments before being selected for breeding. The genotype is stronger for the fitter individuals. Thus the quantum-genotype of the weaker individuals is influenced more by the couplings to the rest of the population (which are implemented vertically by allele). The Figure shows the naïve universal nearest-neighbour ferromagnetic configuration, in which the individuals with strong genotypes will more consistently enforce their corresponding quantum-genotypes, and will also impose them on neighbouring weaker members of the population, giving a form of 'directed mutation'.

There are two features that greatly enhance the classical GA. The first is that, being continuous, the genotype values do not need to have a universal weighting across the population, but they can be weighted by the fitness of the parent that gave rise to them. This weighting, which is shown in Fig. 4.12 as a stronger shading of the genotype nodes in the more highly ranked individuals, we will refer to as *nepotism*. For this study we will adapt a linear weighting for the couplings as follows:

$$|h_\ell| \;=\; \alpha_p \left(\frac{\alpha - 1}{P - 1}\, \ell + 1 \right) , \quad \ell = 0, ..., P-1 \,, \tag{4.32}$$

where α_p is another constant meta-parameter of the algorithm such that the bias of the fittest individual ($l = P-1$) is $\alpha \times \alpha_p$. The second feature is that corresponding alleles across individuals in the population can be coupled in the Ising model (with (anti)ferromagnetic (positive)negative $J_{\ell m}$ couplings in Eq. (4.1)). In other words, in contrast to a classical GA, the quadratic couplings in the quantum annealer allow the individuals to 'see' the rest of the population. This allows highly ranked individuals to influence the quantum-genotypes of other members of the population, a feature we refer to as *quantum-polyandry*. To avoid clutter Fig. 4.12 shows nearest-neighbour attractive (ferromagnetic) polyandry, but an important possibility to be discussed later is more connected quantum-polyandry, in which for example more members of a population can see the fittest individuals.

The framework for the entire algorithm is shown in Fig. 4.13. Like the

classical GA it is a two-loop directed graph, with the genetic material circulating in the top loop, while the feedback from the environment circulates in the bottom loop. The procedure begins as in the classical GA by randomly initialising the *discrete* quantum-genotypes in the population. The phenotypes and hence fitnesses for all the individuals are calculated, and the quantum-genotypes ranked accordingly. The biasing h_ℓ terms in Eq. (4.1) on the quantum annealer are then filled with couplings of the opposite signs, and with moduli that grow according to these fitnesses, with the expectation that fitter individuals will be able to enforce their corresponding quantum-genotype more strongly. In addition polyandric $J_{\ell m}$ couplings are filled on the annealer (and kept fixed throughout) and then selection and breeding can be carried out in exactly the same manner as in the classical GA. However for the GQAA this entails swapping the continuous coupling parameters in the rows of the h_ℓ and $J_{\ell m}$ matrices to form a new set of Ising model couplings. Finally this new Ising model is fed into the annealer to read off new sets of quantum-genotypes for the next generation. Note that if an individual is to breed several times then it may be preferable (and costs little) to avoid using the same set of quantum-genotypes twice, but to collect a pool of multiple reads of the quantum-genotypes.

One notable aspect of this configuration is that in nepotism the fitness weighting follows clusters of 'beneficial alleles' that may have conferred good fitness in the previous generation. From the viewpoint of Holland's original (and still somewhat controversial) schema theorem [106] (see Ref. [99] for

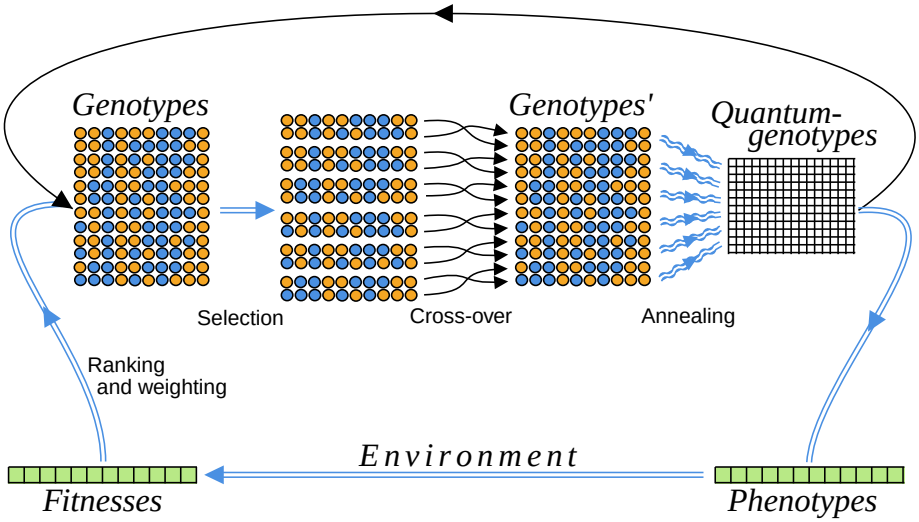

Figure 4.13: Like the classical GA in Fig. 4.10, the generic diagram for the GQAA has two loops. An initial population of discrete quantum-genotypes (on the right) is used to calculate the fitnesses of the P individuals in the 'environment'. These are in turn used to form a fitness-ranked population of parent genotypes (on the left) whose continuous allele values are weighted by the fitness. As in the classical GA the fitness ranking of an individual determines the probability of it being selected to take part in a breeding pair. $P/2$ breeding pairs are formed in this manner, and then cross-over (keeping the weightings attached to the alleles) yields a new intermediate set of continuous genotypes. Completing the loops, quantum annealing yields a new set of quantum-genotypes and the process repeats.

a summary of its various critiques), this can be thought of as a means of weighting powerful schema by the fitness of the individual from which they came.

Meanwhile, as should be now be clear, it is the generation of the quantum-genotype by annealing which is playing the role that mutation played in the classical GA. However in the configuration we are advocating here, both nepotism and quantum-polyandry work to direct the mutation towards configurations that confer fitness.

4.4.3 More on Quantum Polyandry

The configuration of the polyandric couplings can take many forms, and the universal nearest-neighbour ferromagnetic couplings shown in Fig. 4.12 are in fact not the optimal choice. Indeed this configuration leads to very rapid convergence and stagnation: in other words the fittest members of the population completely dominate the evolution very early. There are two modifications that can be made. One is to change the values of the couplings such that they can be either antiferromagnetic, or strengthened. In this work we will consider three values, namely ferromagnetic and antiferromagnetic couplings that are degenerate in modulus, and stronger ferromagnetic couplings. We shall denote the proportion of antiferromagnetic and enhanced couplings as ρ and ρ' respectively. Additionally, we will use the symbol κ to represent the strength of these latter couplings.

The second important modification is to allow more general topologies

among the polyandric $J_{\ell m}$ couplings. Although this modification comes at the cost of additional qubits (as it requires higher order couplings than those available in the quadratic Ising model, which have to be implemented using chain-locking), the advantage is that it allows more individuals of a population to be influenced by the fittest ones.

The motivation for these alternative configurations becomes clear when one considers also the possibility of antiferromagnetic couplings. One can imagine for example a stagnant situation where the fittest individuals are close to a solution modulo some minor flaw in the genotype. A set of antiferromagnetic couplings among the fittest subpopulation encourages some of its members to sacrifice their preferred quantum-genotype and explore minor modification. In this sense it is the GQAA equivalent of a *crowding penalty*. As such we expect the optimum proportion of antiferromagnetic couplings to be subdominant.

Fig. 4.14 is a example of such a non-trivial polyandric topology, which is in fact the configuration we use in this analysis. Differently from the topology shown in Fig. 4.12, in Fig. 4.14 the genes of the fittest individual are now attracting some of the genotypes of the weaker ones (thicker lines), instead of being coupled only to the second fittest creature as in Fig 4.12. The genes of the fittest individual are now attracting some of the genotypes of the weaker ones (thicker lines), instead of being coupled only to the second fittest creature as in Fig 4.12. Clearly there are a huge number of possible configurations, so we do not claim that this is the optimal one: it does

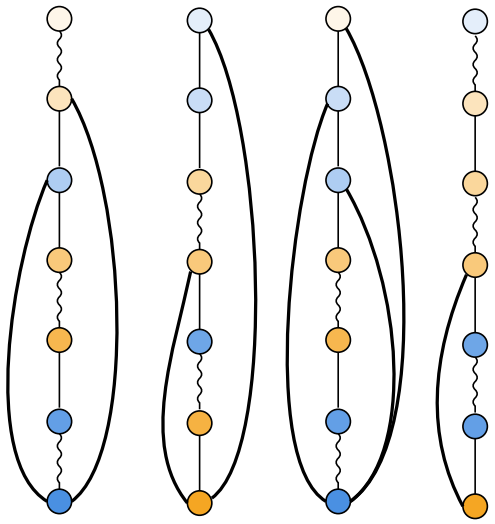

Figure 4.14: The polyandric 'islands' topology used for the analysis in this work. To illustrate we show a toy example with a population of 7 individuals with only 4 alleles each (going horizontally). Vertical nearest-neighbor couplings are included as in Fig. 4.12. Wavy lines refer to repulsive couplings, straight lines to attractive ones. In this case 10 out of 24 couplings are repulsive, thus $\rho \approx 0.42$. In addition polyandric couplings from the fittest individuals (at the bottom) link to the same alleles on weaker, randomly chosen, individuals. In this example we choose the total number of such couplings to be $\rho' = 0.25$ of the total number of alleles in the population. These enhanced couplings are indicated by thicker lines. The actual values of these parameters chosen for this study are shown in Table 5.2.

however perform better than the trivial nearest-neighbour topology.

4.4.4 Practicalities: moving away from the classical GA limit

Let now turn to an overview of the practical implementation. First an important remark regarding the efficiency of the implementation is that the topology of the couplings in the Ising model remain constant throughout the GQAA, and only the values of the couplings are changed. This is crucial because, as already mentioned, finding a new embedding for the Ising model is done through an embedding algorithm which is itself computationally intensive. Thus all updates on the annealer are done by simply adjusting the classical h and J couplings.

Next it is evident that the topologies in Fig. 4.10 and Fig. 4.13 are the same, and indeed there is a limit in which the GQAA becomes isomorphic to the classical GA. This limit is when nepotism and polyandry are turned off, by setting all the polyandric $J_{\ell m}$ couplings to zero and by dialing up s and making the fitness weighting universal, so that every individual just experiences the same level of mutation due to the quantum annealing stage. Thus the two parameters of polyandric coupling and fitness scaling are unique to the GQAA, while the parameter s plays the role of the overall mutation rate. The fact that we can go parametrically to the classical GA allows direct comparison between the two approaches.

Thus our approach will be to use the h and J couplings to move away from the classical GA limit, and this entails the use of a reverse anneal. The

initialisation of the reverse anneal is done with spins corresponding to the classical-genotype in Eq. (4.31). In the limit where the anneal parameter $s(t)$ is kept close to unity throughout the anneal, the spins do not change from their initialized values. By then turning on the quantum fluctuations but keeping the J couplings set to zero, we can introduce a mild mutation rate in the spins, and the algorithm is effectively operating as a classical GA. Then dialing down s and turning on J for the various topologies allows one to move away from the classical GA.

Some additional technical points: The annealer typically has an `auto_scale` parameter that automatically adjusts the h and J couplings to fill the physical range allowed on the annealer. This should be turned off to prevent the h couplings being automatically scaled to large values, which would result in the spins being locked to their initialized state.

In addition we implement *elitism* by replacing the least fit quantum-genotype with the best fit previous classical-genotype. We utilise the Pegasus annealer and find that a reverse anneal with $s(t)$ going to roughly 0.7, and a schedule with ramp-up and ramp-down times of 10μs and total anneal times of 120μs, can reproduce a mutation rate in the fittest individuals that is similar to that of the classical GA (which as we shall see is optimised at a few percent for the problems we shall consider). However it should be noted that the mutation rate in the fitter individuals is less than that in the rest of the population precisely because their larger couplings impose their classical-genotypes more forcefully. It is also worth noting that the mutation rate is

very sensitive to the minimum $s(t)$ value.

To complete the description of the practicalities, we collate all of the variables and parameters that need to be considered, and the values we preferred for this study, in Table 5.2.

Parameter	**Description**	**Value**
Topology	Polyandric $J_{\ell m}$ couplings	'Islands': Fig. 4.14
α	Learning rate, Eq. (4.30)	3
α_p	Nepotism, Eq. (4.32)	0.05
ρ	Proportion of antiferromagnetic	0.5
ρ'	Proportion of enhanced couplings	0.064 — 0.06
κ	Strength of enhanced couplings	$-\alpha \times \alpha_p$
s_q	Minimum anneal parameter	0.74,0.72 | 0.72,0.75,0.75
J_{ij}	Coupling strength	± 0.07 | ± 0.08

Table 4.9: Parameters, and the values used for this study. The two sets of values for ρ and ρ' correspond to the Diophantine problem on the left and function optimization on the right. The values of s_q on the left were used for the two consecutive $\lambda = 1$ and $\lambda = 20$ values used in Subsection 4.4.5, and on the right for the three Taxicab numbers (3,6,6), (3,7,7) and (3,8,8) in Subsection 4.4.6.

4.4.5 Results for optimising a 2D function

We now turn to the implementation of specific problems, and results. We should stress from the start that the goal of the exercise with the simple problems we shall look at is not to show that the GQAA can find results more quickly in real time: indeed the problems we will consider are so simple

that a classical GA can work exceedingly fast. By contrast the goal is to show that the GQAA can find solutions by making far fewer 'calls to the problem'. Minimising the number of times one has to evaluate the fitness of an individual is often the crucial efficiency factor in a GA when the problem to be solved is computationally intensive. Indeed, as mentioned in the introduction, the advantage of a GA is that it can operate on very complicated systems and this often means the majority of the effort is spent performing the computations required to find the fitnesses. It is precisely this advantage that the GQAA aims to enhance. In this sense the problems we will consider here should be considered as test problems. Thus the crucial parameter throughout will be the *call-count*, namely the number of individuals that have to be evaluated in total before a solution is found. We are also (in the spirit of optimisation of the mutation rate of the classical GA in Ref. [90]) looking for evidence that there is a preferred configuration of the nepotism and the polyandric couplings.

The first problem we shall consider is finding the global maximum of a complicated function. We will compare the GA and GQAA when perfoming the task of maximising the function

$$U_\lambda(x,y) \equiv \frac{1}{2}\,(x(1-x) + y(1-y)) + 12\cos(\lambda xy)\sin(2x+y)\,, \tag{4.33}$$

in the region $(-4,4)\times(-4,4)$ with various values of λ (increasing λ introduces

more local maxima making the function harder). For the fitness function we will just use the function itself.

We start with the easier case with $\lambda = 1$. According to Mathematica the function has a global maximum at $(x_{\max}, y_{\max}) \approx (0.68708, 0.170864)$ with $U_1(x_{\max}, y_{\max}) \approx 6.13506$. In order to compare the GA and the GQAA we use a fractional binary representation with 2 bits for the integer part and 10 for the fractional one and $P = 70$, and define $(x_{\rm sol}, y_{\rm sol})$ to be a solution if

$$U_1(x_{\rm sol}, y_{\rm sol}) \ > \ 6.13503\,. \tag{4.34}$$

In order to make the best use of the GA, we optimise the mutation rate following Ref. [90], as shown in Fig. 4.15. In Fig. 4.16a we plot the number of calls required to find the maximum of U_1 with the desired precision for both the GA and the GQAA. Fig. 4.16b shows the same information for the function with $\lambda = 20$. In that case the maximum is in $(x_{\max}, y_{\max}) \approx (0.488397, 0.642488)$ with $U_{20}(x_{\max}, y_{\max}) \approx 6.23257$. The lower bound that defines the solution is 6.23.

It is clear that the advantage of the GQAA is significant. Moreover it is crucial to bear in mind that the simplicity of the problem somewhat constrains the possibility for the GQAA to give dramatic improvement. This is because a problem for which the search space is somewhat limited, and which can for example be treated by gradient descent, is already unlikely to yield great advantage for the GA over conventional search techniques.

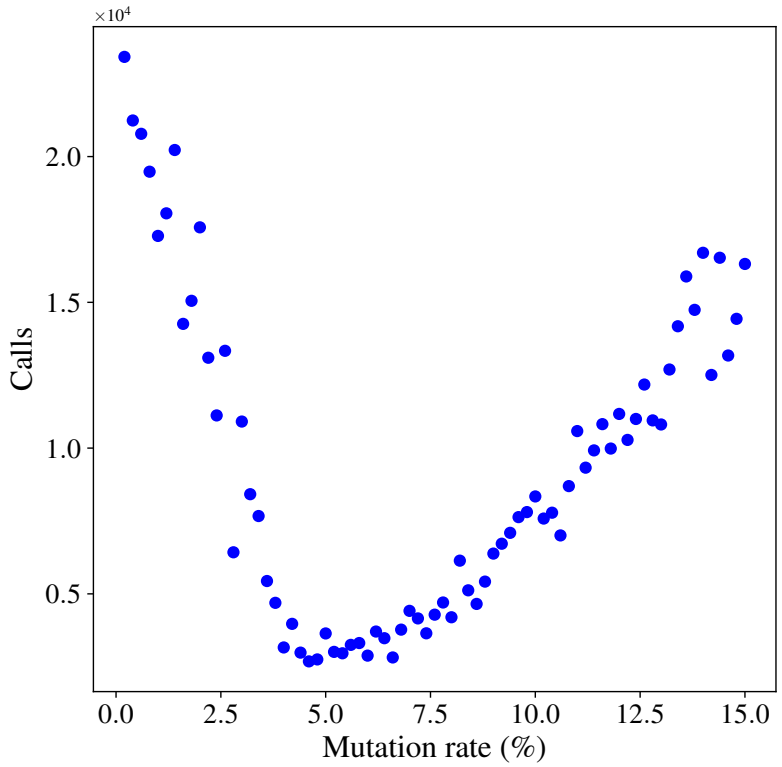

Figure 4.15: Number of calls required to find a solution for different mutation rates for the classical GA. For this specific problem the best mutation rate is around 5%.

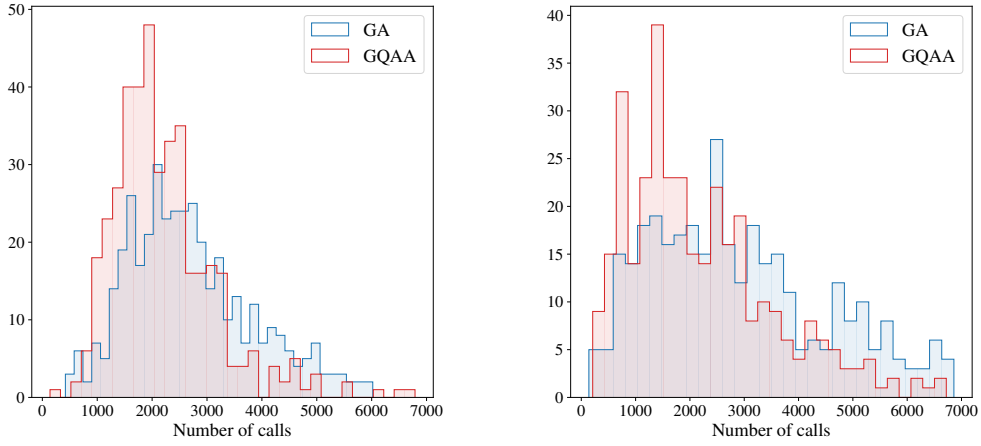

(a) $\lambda = 1$ (b) $\lambda = 20$

Figure 4.16: Number of calls required to find a solution with the demanded precision for finding the global maximum of the function in Eq. (4.33). For $\lambda = 1$ in Fig. 4.16a the average number of calls is: 2240 for GQAA and 2690 for GA (representing $\sim 18\%$ of improvement). Root-mean-square deviation (RMSD): 940.8 for GQAA and 1140.2 for GA. For the more complicated case with $\lambda = 20$ in Fig 4.16b the average number of calls is: 2186 for GQAA and 2883 for GA (representing $\sim 24\%$ of improvement). RMSD: 1331.6 for GQAA and 1620.2 for GA. In this second case, GA does not find any solution within the first 7000 calls in 17.3% of the cases. For GQAA this percentage reduces to 7.8%. In both cases the data are collected running 350 times for both GA and GQAA. The GQAA parameters are listed in Table 5.2. Performing the Kolmogorov-Smirnov test for both sets of data we conclude that the difference in the GA and GQAA distributions is statistically significant with a level of confidence of 99.9%.

4.4.6 Results for Diophantine problems

The second problem we shall consider is somewhat harder, namely the solution of simple Diophantine problems, of the kind that were discussed in Subsec. 4.2.2 also in the context of quantum annealers (but using direct Ising encoding of the problems). We shall adopt the same notation as before. Analogously to the previous part, here we will test our methods on the computationally intensive $(3, 6, 6)$, $(3, 7, 7)$, $(3, 8, 8)$ numbers.

In order to treat the problem on a GA or GQAA for the $(3, n, m)$ numbers, where $n, m \in \mathbb{N}^+$ we use the following fitness function:

$$\tilde{f} \;=\; -\left(\sum_{i=1}^{n} a_i^3 - \sum_{i=1}^{m} b_i^3\right)^2 + \mathit{constraints}\,, \tag{4.35}$$

where the constraints refer to an additional Kronecker-delta penalty if any of the a_i are equal to any of the b_i.

Optimising the mutation rate for the GA, as for the previous problem, we begin by displaying some specific examples of solution-finding for the (3,6,6) and (3,8,8) problems. Parameterising the integers with the obvious 5 digit binary encoding, we find the examples shown in Table 4.10. It is clear from these examples that the GQAA consistently outperforms the classical GA in finding solutions.

As the solutions to these problems are harder to find, we performed a systematic comparison by studying the progress of the maximum fitness in the population throughout the evolution. Figure 4.17 compares the progress

Call-count	Gen's	P	Solution
91650	1833	50	(1, 3, 3, 9, 13, 11 | 12, 8, 4, 6, 4, 12)
61320	876	70	(12, 29, 31, 4, 5, 6 | 9, 28, 23, 18, 25, 2)
9270	309	30	(27, 15, 27, 18, 10, 27 | 30, 16, 12, 31, 12, 17)
21390	713	30	(2, 2, 21, 27, 15, 15 | 30, 8, 3, 14, 11, 16)
25680	856	30	(7, 3, 31, 16, 24, 20 | 28, 18, 1, 8, 28, 18)
11610	387	30	(15, 26, 15, 15, 15, 22 | 19, 10, 2, 21, 27, 17)

(a) GA: (3,6,6)

Call-count	Gen's	P	Solution
2130	71	40	(13, 9, 8, 6, 8, 8 | 10, 2, 10, 11, 2, 11)
2680	67	40	(25, 9, 5, 10, 3, 9 | 7, 15, 21, 12, 11, 13)
8520	284	30	(18, 15, 29, 27, 23, 13 | 16, 26, 11, 30, 26, 4)
2220	74	30	(1, 23, 29, 18, 9, 13 | 24, 28, 10, 3, 20, 8)
3060	102	30	(21, 29, 19, 3, 11, 3 | 26, 13, 14, 9, 22, 20)
1170	39	30	(24, 26, 25, 3, 7, 11 | 22, 20, 20, 28, 5, 1)

(b) GA: (3,6,6)

Call-count	Gen's	P	Solution
25160	629	40	(22, 6, 2, 2, 19, 24, 4, 24 | 21, 13, 13, 5, 5, 12, 3, 31)
8280	207	40	(26, 6, 3, 13, 10, 19, 18, 26 | 17, 7, 5, 29, 16, 25, 4, 12)
21440	536	40	(2, 20, 23, 22, 15, 2, 22, 1 | 4, 3, 10, 29, 11, 5, 7, 26)
24640	616	40	(16, 16, 8, 21, 24, 31, 9, 21 | 30, 14, 19, 19, 29, 15, 7, 1)
30280	757	40	(21, 10, 15, 14, 19, 24, 22, 26 | 17, 2, 20, 7, 4, 6, 31, 28)
26800	670	40	(13, 21, 14, 17, 19, 27, 14, 15 | 12, 9, 26, 8, 2, 22, 28, 7)

(c) GA: (3,8,8)

Call-count	Gen's	P	Solution
6800	170	40	(25, 13, 21, 3, 25, 1, 25, 21 | 11, 24, 20, 30, 14, 14, 22, 11)
4440	111	40	(17, 29, 21, 14, 1, 19, 17, 1 | 26, 30, 7, 3, 11, 24, 12, 8)
3680	92	40	(24, 28, 8, 25, 20, 12, 6, 10 | 16, 23, 4, 26, 19, 16, 23, 18)
5280	132	40	(20, 30, 3, 18, 14, 12, 12, 30 | 25, 5, 2, 21, 19, 26, 29)
2720	68	40	(7, 28, 6, 4, 6, 28, 15, 29 | 19, 26, 21, 10, 9, 18, 25, 25)
3760	94	40	(17, 9, 16, 23, 4, 21, 17, 14 | 10, 5, 26, 7, 27, 3, 5, 2)

(d) GA: (3,8,8)

Table 4.10: Hands-on with the GQAA versus the classical GA for finding (3,6,6) and (3,8,8) Taxicab numbers for integers up to 32. Thus the search space is in principle $2^{60} \approx 10^{18}$ for the (3,6,6) problem, and $2^{80} \approx 10^{24}$ for the (3,8,8) problem. However the fact that the GA works with a rather small population indicates that the number of solutions in the search space is large. Nevertheless the efficiency of the GQAA is still consistently up to an order of magnitude better in terms of the call-count.

for the $(3, n, n)$ problems, where the maximum fitness has been averaged over 50 trials with $\beta = 5$ and $P = 30$, with the other GQAA parameters as given in Table. 5.2. As we can see from the figure, for the (3,6,6) problem, after 100 generation the fittest creature has, on average, fitness -759.1 in the GA case and -312.4 in the GQAA one. For the (3,7,7) case in Fig. 4.17b the fittest creature has, on average, fitness -1445.2 in the GA case and -108.3 in the GQAA one, while in for the (3,8,8) case in Fig. 4.17c the fittest creature has, on average, fitness -4383.3 in the GA case and -655.44 in the GQAA one. Again the performance appears to be roughly an order of magnitude better in terms of the maximum fitness for the GQAA versus the GA. It is notable that the GQAA appears to behave somewhat differently in order to achieve increasing fitness.

It evolves via a series of notably more dramatic jumps in improvement than the GA – for a particular choice of parameters the jumps in fitness in the GQAA persist (it is not a statistical artefact), whereas the GA appears to progress more smoothly but more slowly overall.

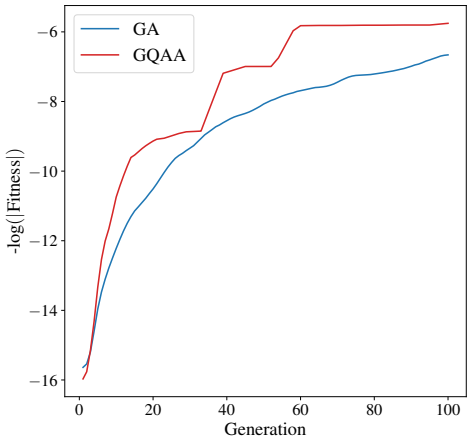

(a) Taxicab (3,6,6)

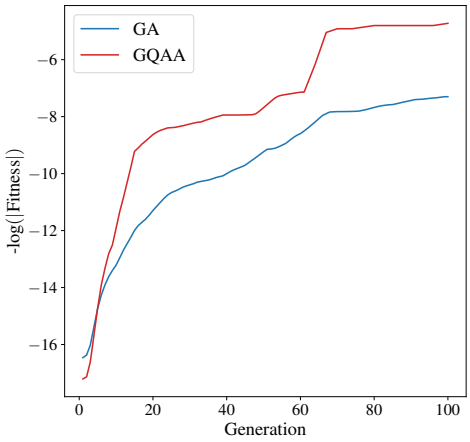

(b) Taxicab (3,7,7)

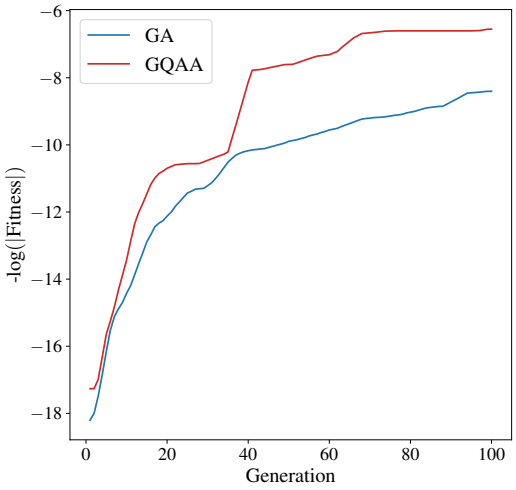

(c) Taxicab (3,8,8)

Figure 4.17: Averaged fitness of the fittest creature for both GA and GQAA throughout the first 100 generations for $(3, n, n)$ Taxicab problems.

Chapter 5

Quantum Annealing as a Tool in String Theory

5.1 String models and quantum annealers

Let us now move on to the direct applications of the tools we have developed in the previous chapter to string theory, which represents a natural framework for quantum annealing applications. The first half of this chapter is based on Ref. [5], where we investigated on how one can efficiently use these machines to search among $SO(10)$ models (see Ref. [107] for a review on these models). This is a direct application of the methods described in Sec. 4.2. The second half of the chapter is based on the results in Ref. [4], where GQAA — extensively described in Sec. 4.4 — has been applied in the context of heterotic line bundle models.

It is worth mentioning that both these applications are completely novel and represent the first time that a quantum annealer has been used in a string theory set-up.

5.2 Encoding $SO(10)$ string models

The general approach we use is a combined technique which embeds the string consistency conditions (*a.k.a.* the GSO conditions) themselves on the annealer, but which performs certain additional phenomenological checks (such as for example selecting only models with three generations) during a second step. In such an arrangement the quantum annealer is essentially providing a consistency filtering of models, which may then be classically tested against other constraints. We shall see that this approach significantly enhances the overall efficiency of the algorithm. It can successfully be used to search parameter spaces orders of magnitude more quickly than either a blind scan *or* more traditional classical heuristic methods such as genetic algorithms. The consistency conditions for these models amount to a set of generalized GSO (GGSO) projections determined by phases. The essential ingredients are described in Appendix B, to which we will continue to refer. The important aspect of these consistency conditions for the present study is that they can be written as a set of single qubit binary equations $f_A(\tau_i) = 0$, where $\tau_i \in \{0, 1\}$ map directly to the GGSO phases of 0 or π which determine the particular string model. The binary τ variables can in turn be mapped

to annealer spins as

$$\tau_i \;=\; \frac{1}{2}(1+\sigma_i)\;. \tag{5.1}$$

Thus these are arguably the string models that can most readily be encoded in an Ising spin model. As we are solving equations of purely single digit binaries we will use the names of the variables themselves to stand for the binary qubit value.

To get a broad idea of the form of the GGSO constraints, they partially consist of six (three for spinorial and three for vectorial representations) systems of four linear equations each, which can be synthesised in the following expression:

$$\Delta^I U_i^I \;=\; Y_i^I \mod 2\,, \qquad \text{with } I=1,2,3 \text{ and } i=s,v\,, \tag{5.2}$$

where each choice of (i, I) corresponds to a linear system of four equations (specifically $i = s, v$ refers to spinorial/vectorial representations and $I = 1, 2, 3$ refers to the three orbifold planes, respectively. See Appendix B for more details). The GGSO coefficients appear as components of the Y_i^I vectors (defined in Eqs. (B.12), (B.19)) and also as entries in the Δ^I matrices defined in Eqs. B.7, B.8, B.9. Being related to phases, these coefficients take values of 0 and 1. Finally, U_i^I is a vector of four elements which denote solutions of the (i, I) system, also with entries in $\{0, 1\}$. We shall refer to the set of the solutions of the system as Ξ_i^I: it can contain at most $2^4 = 16$ solutions due to the binary nature of the components of the U_i^I vectors.

Once Eq. (5.2) is satisfied, *i.e.*, once we have a consistent GGSO projection, we will as described in the introduction further demand that a viable model must have 3 generations by imposing the following constraint (in which $i \equiv s$) classically [108]:

$$N_F \;=\; \sum_{I=1}^{3} \sum_{p,q,r,s\in\Xi_s^I} X^{(I)}_{pqrs} \;=\; 3\,, \tag{5.3}$$

where $X^{(I)}_{pqrs} = \exp\Big(i\pi\chi^{(I)}_{pqrs}\Big)$ and $\chi^{(I)}_{pqrs}$ are defined in Eqs. (B.13), (B.14) and (B.15), for $I = 1, 2, 3$, respectively. We shall also require two additional properties: existence of at least one SM Higgs doublet and existence of a top Yukawa coupling. The first requirement corresponds to having at least one solution coming from one of the $\{(v, I),\, I = 1, 2, 3\}$ systems. The second requirement will be guaranteed by a particular choice of U_v^3 as we shall see in the following.

Having given an overview of the fundamental ingredients and phenomenological requirements that we will impose, let us now describe our method in detail. To encode the GGSO constraints we adopt a technique that is significantly different from those that have been used to analyse this specific class of models before, *e.g.* in Refs. [107–111]. Indeed the U_i^I parameters are typically scanned over along with the other variables corresponding to the GGSO phases. Here by contrast we first fix the values of U_s^I and U_v^I on the three orbifold planes which allows us to then search for suitable values of the GGSO coefficients. That is, following the discussion in Appendix B, we can

first without loss of generality set

$$U_s^1 = U_s^2 = U_v^3 = \begin{pmatrix} 0 \\ 0 \\ 0 \\ 0 \end{pmatrix} . \tag{5.4}$$

Note that we fix U_v^3 to zero, which guarantees the existence of a top Yukawa coupling as we shall see. However we are still free to fix the residual parameters in U_i^I. For this study it is convenient to compare the different methods by studying the models with

$$U_s^3 = \begin{pmatrix} 0 \\ 1 \\ 0 \\ 0 \end{pmatrix} , \; U_v^1 = \begin{pmatrix} 1 \\ 0 \\ 0 \\ 0 \end{pmatrix} , \; U_v^2 = \begin{pmatrix} 1 \\ 1 \\ 1 \\ 1 \end{pmatrix} . \tag{5.5}$$

Of course in a full treatment one would scan through the $2^{12} \approx 4000$ possible choices of U_s^3, U_v^1, U_v^2. Having fixed these parameters, the remainder of the GGSO constraints may be solved by quantum annealing. That is we are required to encode and solve the following equations on the quantum

annealer:

$$\begin{cases} \Delta^3 U_s^3 \;=\; Y_s^3 \\ \Delta^1 U_v^1 \;=\; Y_v^1 \\ \Delta^2 U_v^2 \;=\; Y_v^2 \\ \chi^{(3)}_{pqrs} \;=\; 0 \end{cases} \qquad \text{mod } 2\,, \tag{5.6}$$

where all the quantities involved can be expressed in terms of the GGSO coefficients following the definitions in Appendix B. Comparing Eqs. (5.6) with Eq. (5.2), one may wonder why spinorial projectors appear only on the third plane along with the corresponding chirality constraint. A similar question applies to the vectorial projectors, which are only present on the first and second plane. Indeed, it is straightforward to show that the choice in Eq. (5.4) (see Appendix B for details) trivialises the corresponding constraints on the first and second planes for spinorials as well as those on the third plane for vectorials. In a similar fashion, the chirality constraints on the first and second planes are satisfied by the conventions adopted in Eq. (B.34).

The first three lines in Eq. (5.6) correspond to four linear equations, yielding a total of 13 equations with 27 unknown GGSO coefficients. Thus, we take the corresponding problem Hamiltonian to be effectively a "loss-function" for this set of equations, which is to say that we take it to be the sum of the squares of the 13 equations with additional integer parameters

$K_{i=1,\ldots,13}$ to absorb the modulo 2 operation,

$$\begin{aligned} H \;=\; & \sum_{i=1}^{4} \left(\Delta^3_{ij} U^3_{s,j} - Y^3_{s,i} - 2K_i\right)^2 \;+\; \sum_{i=1}^{4} (\Delta^1_{ij} U^1_{v,j} - Y^1_{v,i} - 2K_{4+i})^2 \\ & + \sum_{i=1}^{4} (\Delta^2_{ij} U^2_{v,j} - Y^2_{v,j} - 2K_{8+i})^2 \;+\; \left(\chi^{(3)}_{pqrs} - 2K_{13}\right)^2 \,, \end{aligned} \tag{5.7}$$

where the sum over j in each square is to be understood. The auxiliary variables $K_{i=1,\ldots,13}$ are encoded using binary representations and take values in $[-3, 4]$, while Δ and Y are binary variables in $\{0, 1\}$, which are straightforwardly encoded in annealer spins via Eq. (5.1). This means that even for this restricted choice of U^I_i the parameter space is $2^{28} \approx 10^8$.

Once models have been acquired from this quantum annealing stage, they as mentioned need to be post-filtered classically to satisfy our additional phenomenological requirements. As discussed these conditions include the imposition of three generations, and the requirement of at least one Higgs doublet. However as explained in Appendix B the third constraint, namely the existence of a top Yukawa coupling, is already ensured by our choice of U^3_ν and by Eqs. (B.32) and (B.33) and is therefore already encoded in Eq. (5.7). Thus, from on now on we need focus only on the first two conditions.

Let us start by analysing the 3 generations constraint. As already mentioned, the chirality on the first and on the second planes is set to one thanks to the conventions adopted in Eq. (B.34). Therefore, the only chirality that needs to be checked is that on the third plane, which translates into the

following equation (also without loss of generality):

$$\sum_{p,q,r,s\in\Xi_s^3} X^{(3)}_{pqrs} \;=\; \sum_{p,q,r,s\in\Xi_s^3} e^{i\pi\chi^{(3)}_{pqrs}} \;=\; 1\,. \tag{5.8}$$

As the reader may have already noticed, to ensure the desired number of generations we must sum over *all* the spinorial solutions on the third plane. However, it may happen that the proposed solution U_s^3 in Eq. (5.5) is not unique. In other words, since we are not imposing any constraint on the number of solutions, nothing prevents the system representing the spinorial projectors on the third plane from having solutions in addition to that already designated in Eq. (5.5). Indeed, the Hamiltonian in Eq. (5.7) does not contain a term that enforces the uniqueness of that solution: it simply guarantees that U_s^3 is a solution. Therefore, in order to ensure the fulfillment of the generations constraint, we post-process all the candidate models proposed by the annealer and discard those that have additional solutions besides the one that we have already assigned. Similar arguments hold for the number of vectorials, however in this case the constraints are less severe as we only require there to be at least one Higgs doublet, that is we require at least one solution coming from one of the planes.

5.2.1 Results and performance comparison with other search methods

As in the previous analysis, we use the D-Wave's `Advantage_system4.1`. To assess the different methods we first note that a comprehensive scan of this system is possible, and this was performed for comparison: this took about 48 hours on a DELL PowerEdge R630 workstation with 32 GB of memory which resulted in a total number of 1024 models, *i.e.*, the search space of the set of models we have described contains one viable SM-like model in 10^5. The second method we considered was simulated annealing optimised with a linear β-schedule. We also for comparison implemented the same system in a genetic algorithm (see Sec. 4.4 for more details on genetic algorithms). The genetic algorithm (GA) was implemented with a fitness function defined linearly by the ranking, and optimised to find the best values for the mutation rate and for the learning rate (*i.e.*, the number of times breeding occurs for the fittest individual compared to the least fit): these were found to be 3% and 4, respectively.

To compare these four methods, we examined the rate at which each finds acceptable models in terms of machine-time. Apart from quantum annealing, all the other algorithms were run on standard computers. The results are collected in Fig. 5.1 where we plot number of found SM-like theories against machine-time. The definition of machine-time on quantum annealers is complicated by the fact that currently they are shared resources, and need to

handle the influx of traffic and requests from multiple users simultaneously. This can lead to bottlenecks, resulting in longer wait times of a few seconds for accessing the machine or retrieving spin values after an anneal run. Since these are external factors (and even depend on the traffic on the machine) we have excluded them from our definition of quantum annealing machine-time. Indeed, these factors are the main obstruction preventing the reproduction of the saturation plot in Fig. 5.1. Hence the dashed quantum annealer lines are built upon the simulated annealing data by extrapolating comparative early performance. Specifically, the grey dashed line represents a projection of the quantum annealer performance, including the time required to perform the classical checks.

As we can see from Fig. 5.1, both quantum and simulated annealing are far more efficient than random scans and genetic algorithms (red and green solid lines, respectively). Modulo the above caveats, in this case we estimate that the quantum annealing method is 1.3 times faster even than simulated annealing. The orange dashed line is an estimate of a hypothetical pure quantum annealing implementation, in which we assume that *all* of the additional classical checks are instead also encoded on the annealer (using methods that we discuss below), with no additional classical post-processing being required. This would result in a 4.125 times better performance than simulated annealing. The number of independent GGSO coefficients is 28, yielding to a search space of $2^{28} \sim 10^8$ possible models. The superiority of the methods using annealers is clearly evident in this case, surpassing the

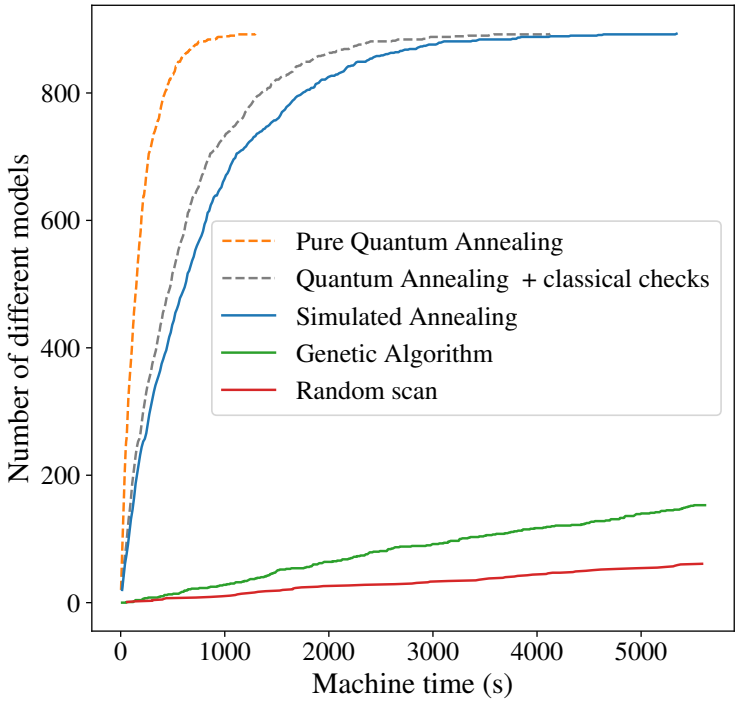

Figure 5.1: Comparison of the machine-time efficiency of various techniques for finding viable models. The methods analysed are: random scans, genetic algorithms, simulated annealing and quantum annealing. For the first three methods "machine-time" is equivalent to CPU-time. In the latter case it implies time on the annealer.

other techniques. The total number of models found using simulated annealing is 894 in approximately 6000s *vs* 153 and 61 models found using a genetic algorithm and a random scan, respectively. For the quantum annealer each anneal run had 2000 reads and used auxiliary variables $K_i \in [-3, 4]$. The

dashed lines both indicate quantum annealing and are projections based on the simulated annealing data. In these two cases the machine-time does not take into account the dead-time required due to bottlenecks in exchanging information with the annealer (which incurs a delay of order a second, and which could be removed if a portion of the machine were dedicated to the search). The machine time is computed based on the anneal schedule time only, which is fixed to $160\,\mu s$. The grey line takes also into account the time required to do all the classical checks on the models found by the annealer. The orange line is an estimation of the performance of a quantum annealer supposing that all the classical checks are also encoded in the annealer Hamiltonian.

Overall then, in this study annealing methods appear to surpass other techniques in terms of performance, efficacy. They outshine alternative approaches and show superior outcomes. Quantitatively, the initial model discovery rate (*i.e.*, within the first $1000s$) is one model in 0.66 seconds for simulated annealing, compared to one models in 33 seconds for the genetic algorithm and one in 100 seconds for the random scan. Using quantum annealing, the rate increases to one model in 0.50 seconds when model checks are performed classically (the grey line in Fig. 5.1) and to one model in 0.16 seconds for a hypothetical purely quantum annealing implementation (orange dashed line). However one caveat we should add for completeness is that the search in this study may be somewhat disadvantageous for the GA as the number of SM-like models in the search space is relatively dense: as

discussed in Ref. [90] a GA becomes more effective when the search is very difficult, say one model in 10^6 or more. The future challenge then is to compare quantum annealers and GAs when they are both confronted by much harder problems such as those discussed in Refs. [4, 99].

5.2.2 Towards pure QA model building

In Fig. 5.1 we included a line for hypothetical purely quantum annealing in which no classical post-processing would need to be done. In this section we briefly consider how such a complete implementation might be achieved. This discussion will illustrate the potential and also the complexity of performing pure quantum computing analyses.

The first hurdle for a complete quantum implementation of the models under discussion is the fact that the only spin Hamiltonians that can currently be considered are quadratic Ising models, as already explained in the previous sections. Let us suppose for this discussion that this will remain the case for the foreseeable future. For example if we do not fix the values of U_s^3, U_v^1, U_v^2 in advance but allow all the U parameters to be set by the quantum annealing (in which case we are searching the larger space of size 10^{12}) we are then obliged to encode the squares of Eqs. (5.5) in the Hamiltonian, which would be quartic in the spins. However, applying the reduction procedure described in Subsec. 4.2.1 we can easily quadratise the Hamiltonian with the price of adding auxilliary spins. Thus, in principle, all the remaining degrees of freedom may be put on to the annealer with the GGSO constraints being

entirely enforced by the Hamiltonian, at the expense of using an additional ancillary qubit for every term in the Hamiltonian that requires reducing.

There remains the problem of incorporating phenomenological counting constraints. That is, suppose that the annealer with this larger system has found a solution to Eqs. (5.6) having thereby determined a set of U's and Δ's. We are required to include something in the Hamiltonian which will now implement the three generations check in Eq. (5.3) which previously we did classically. This requires the introduction of "counting" qubits and it can be achieved as follows.

We are required to impose Eq. (5.3) which boils down to imposing $\#(\chi = \text{even}) = 3 + \#(\chi = \text{odd})$, or in other words

$$\sum_{I=1}^{3} \sum_{p,q,r,s \in \Xi_s^I} \left(2\,\overline{\chi}_{pqrs} - 1\right) \;=\; -\,3\;, \tag{5.9}$$

where $\overline{\chi} \equiv \chi \mod(2)$. Note that the quantity on the left is actually just given by the sum of the σ qubits corresponding to the binary $\overline{\chi}$ variable. This is sufficient to ensure that even if we have cancelling positive and negative chiralities the net number of generations is 3.

In these equations the χ_{pqrs} are functions of the p, q, r, s as in Eqs. (B.13), (B.14), (B.15), so they are also polynomial objects in spins. However each χ can be mapped to a single ancillary binary qubit $\overline{\chi}$ by adding the terms

$$H \;\supset\; (\chi + 2K_\chi - \overline{\chi})^2 \tag{5.10}$$

for every χ, where here $\overline{\chi}$ is another ancillary binary qubit and K_χ is as before a binary encoded integer, $K_\chi \in \mathbb{Z}$. Thus $\overline{\chi} = \chi$ is enforced at the minimum. Of course given that the χ_{pqrs} in Eqs. (B.13),(B.14),(B.15) are not linear in spins, Eq. (5.10) will also require reduction. Finally to impose the three generation constraint in Eq. (5.9) we then add to the quadratic Hamiltonian the term

$$H \supset \left(\sum_{I=1}^{3} \sum_{p,q,r,s \in \Xi_s^I} \left(2\overline{\chi}_{pqrs} - 1 \right) + 3 \right)^2 \tag{5.11}$$

which is quadratic and therefore requires no further reduction.

In principle therefore all the consistency conditions may be straightforwardly implemented on the annealer in this fashion. Currently the limiting factor is the size of the architecture and the relatively large number of ancillary qubits that would be generated by this method. Therefore one might also contemplate an alternative approach which is to implement annealing on a quantum gate computer. In such an approach the Hamiltonian is "Trotterized" in order to evolve the system in small time-steps on a universal gate quantum computer [112]. Thus in principle spin Hamiltonians of high order are allowed and no reduction would be required in order to implement all the consistency conditions. Currently no such system of large enough physical size is available to encode the system under discussion, and unfortunately one cannot simulate more than approximately 30 qubits. However this approach would be a promising avenue to explore once universal gate machines

of sufficient size become available.

5.3 GQAA on heterotic line bundle models

Having used quantum annealers to directly build and search for SM-like string models, we turn now to another application of quantum annealing in the string context. In particular we shall discuss how Genetic Quantum Annealing can be employed as a tool to search for viable string models.

One of the most promising route which could conduct to a SM-like model from string theory is the $E_8 \times E_8$ heterotic string compactified on smooth Calabi-Yau threefolds with holomorphic vector bundles. In this context, the geometrical data describing the 6-dimensional compactification space consists of a Calabi-Yau threefold X and a holomorphic bundle V on X, needed to break the $E_8 \times E_8$ gauge symmetry to the Standard Model gauge group or to one of its grand unification embeddings. The set of topologically distinct pairs (X, V) that can serve as compactification data is virtually unbounded, however, there are strong hints that physically viable models can only be found within a finite, though extremely large, subset [113, 114].

In the following we shall apply both GA and GQAA to a class of compactifications where V is a sum of line bundles. In this case, two of the major technical difficulties, checking slope-stability of the bundle and checking the low-energy spectrum, become manageable. Stability checks are relatively straightforward due to the split nature of the bundle, while computations of

the spectrum are made virtually instantaneous by the aforementioned discovery of line bundle cohomology formulae [115, 116]. As a result, deciding the physical viability of a heterotic line bundle sum model at the level of the particle spectrum (three families of quarks and leptons, the presence of a Higgs field and the absence of any exotic matter charged under the Standard Model gauge group) can be accomplished within a fraction of a second, something that has never been possible before. By comparison, traditional constructions in the literature have taken several years of laborious work to achieve a comparable level of analysis.

5.3.1 Preliminaries on heterotic line bundle models

Let us now briefly discuss more concretely the details of the string models we shall treat. Throughout the following, V will be a rank-5 line bundle sum $V = \oplus_{a=1}^{5} L_a$ over a Calabi-Yau threefold X, so that the resulting model has $SU(5) \times S(U(1)^5)$ symmetry. The notation $L_a = \mathcal{O}_X(k_a)$ indicates a line bundle with first Chern class $c_1(L_a) = k_a^i J_i$, where k_a^i are the components of the integer vectors $k_a \in \mathbb{Z}^h$ and $(J_1, \ldots, J_h)$ is a suitably chosen basis of $H^2(X, \mathbb{Z})$, with dimension $h = h^{1,1}(X)$. The five integer vectors $(k_1, \ldots, k_5)$ uniquely specify the line bundle sum V. The manifold X will be assumed to admit a free action of a non-trivial discrete group Γ, such that the quotient manifold X/Γ has a non-trivial fundamental group (in fact, isomorphic to Γ). Given such a group action, there are, in general, several ways to break $SU(5)$ to the SM group using an appropriate discrete Wilson line on X/Γ.

Fixing X, the aim will be to identify the line bundle sums V that satisfy the following constraints:

(C1) E_8 **embedding** $c_1(V) = \sum_{a=1}^{5} k_a \stackrel{!}{=} 0$.

In order to guarantee that the structure group of V is $S(U(1))^5$ and not smaller, no proper subsets of line bundles in V are allowed to have a vanishing first Chern class.

(C2) Anomaly cancellation

$$c_{2,i}(V) = -\frac{1}{2} d_{ijk} \sum_{a=1}^{5} k_a^j k_a^k \stackrel{!}{\leq} c_{2,i}(TX) \ ,$$

$\forall i = 1, \ldots, h$, where d_{ijk} denote the triple intersection numbers and $c_2(TX)$ the second Chern class of the tangent bundle of X, relative to the basis $(J_1, \ldots, J_h)$.

(C3) Supersymmetry/poly-stability There exists a non-trivial common solution t^i to the vanishing slopes

$$\mu(L_a) = d_{ijk} k_a^i t^j t^k \stackrel{!}{=} 0 \text{ for } a = 1, \ldots, 5$$

such that $J = t^i J_i$ is in the interior of the Kähler cone, which in our examples corresponds to $t^i > 0$. Solving the slope-zero equations is computationally expensive and this check is replaced by the weaker condition that each of the five matrices $M_a = (d_{ijk} k_a^i)$ has at least one positive and one negative entry. Moreover, the same should hold for

every linear combination $v^a M_a$. In practice, considering all the vectors v^a with integer entries between -2 and 2 provides a strong enough check.

(C4) Spectrum: cohomology dimensions must satisfy

10-multiplets: $h^1(X,V) = 3|\Gamma|$

no $\overline{\mathbf{10}}$-multiplets: $h^1(X,V) = 0$

$\overline{\mathbf{5}}$-multiplets: $h^1(X,\wedge^2 V) = 3|\Gamma| + n_h$, $n_h > 0$

Higgs: $h^2(X,\wedge^2 V) = n_h$

Here $|\Gamma|$ is the order of the discrete group Γ and n_h represents the number of Higgs doublet pairs. In the absence of a cohomology formula, (C4) can be replaced by the weaker constraint (C4').

(C4') Chiral spectrum $\chi(X,V) = \chi(X,\wedge^2 V) = 3|\Gamma|$

(C5) Equivariance Require that V descends to a bundle on X/Γ. For symmetries acting trivially on the basis $(J_1,\ldots,J_h)$ we require that the Euler characteristic of every (maximal) partial sum $\oplus_{a_i} L_{a_i}$ in V consisting of line bundles with identical first Chern classes, is divisible by $|\Gamma|$. For symmetries with a non-trivial action on the basis $(J_1,\ldots,J_h)$, V must admit a partition into partial sums that are invariant under the induced action of Γ on $(J_1,\ldots,J_h)$ and, moreover, the Euler characteristic of each partial sum must be divisible by $|\Gamma|$.

The GA scans discussed below have been carried out on four different Calabi-Yau threefolds realised as complete intersections in products of projective

spaces. Using the standard notation for configuration matrices, with superscript indices on X indicating the Hodge numbers $(h^{1,1}(X), h^{1,2}(X))$ and a subscript index indicating the position in the CICY list [117], these four manifolds are generic members of the following deformation families:

$$X^{(4,68)}_{7862} = \begin{matrix}\mathbb{P}^1\\ \mathbb{P}^1\\ \mathbb{P}^1\\ \mathbb{P}^1\end{matrix}\begin{bmatrix}2\\2\\2\\2\end{bmatrix}, \quad X^{(5,45)}_{7447} = \begin{matrix}\mathbb{P}^1\\ \mathbb{P}^1\\ \mathbb{P}^1\\ \mathbb{P}^1\\ \mathbb{P}^1\end{matrix}\begin{bmatrix}1&1\\1&1\\1&1\\1&1\\1&1\end{bmatrix}$$

$$X^{(6,30)}_{5302} = \begin{matrix}\mathbb{P}^1\\ \mathbb{P}^1\\ \mathbb{P}^1\\ \mathbb{P}^1\\ \mathbb{P}^1\\ \mathbb{P}^1\end{matrix}\begin{bmatrix}0&1&1\\0&1&1\\1&1&0\\1&1&0\\1&0&1\\1&0&1\end{bmatrix}, \quad X^{(7,27)}_{4071} = \begin{matrix}\mathbb{P}^1\\ \mathbb{P}^2\\ \mathbb{P}^1\\ \mathbb{P}^1\\ \mathbb{P}^1\\ \mathbb{P}^2\\ \mathbb{P}^3\end{matrix}\begin{bmatrix}1&1&0&0&0&0&0&0\\0&1&1&0&0&0&1&0\\0&0&1&0&0&1&0&0\\0&0&0&0&2&0&0&0\\0&0&0&1&1&0&0&0\\1&0&0&0&0&1&0&1\\0&0&0&1&1&0&1&1\end{bmatrix} \tag{5.12}$$

All four embeddings are favourable, in the sense that a basis $(J_1, \ldots J_h)$ of $H^2(X, \mathbb{Z})$ can be obtained by pulling back to X the Kähler classes of the h projective factors. Line bundle cohomology formulae on the manifolds X_{7862} and X_{7447}, used to implement the constraints (C4) in the GA searches, are presented in Appendix B in Ref. [4]. For the manifolds X_{5302} and X_{4071} cohomology formulae are not yet available and we have used the weaker spectrum constraint (C4'). The first three manifolds admit symmetries of orders 2 and 4 which leave the basis $(J_1, \ldots J_h)$ invariant, while X_{4071}, admits a free action by $\mathbb{Z}_2$ which maps $(J_1, J_2, J_3, J_4, J_5, J_6, J_7) \mapsto (J_1, J_6, J_3, J_4, J_5, J_2, J_7)$.

5.3.2 The Genetic Algorithm and Quantum Annealing

Fixing the manifold X, a sum of five line bundles V is specified by $4h$ integers $(k_a^i)_{a=1,\ldots 4}^{i=1,\ldots,h}$, where the condition (C1) is used to fix the fifth line bundle in terms of the first four. There are no a priori bounds on these $4h$ integers. However, our previous experience from systematic scans [11, 113] indicates that only a relatively small range is relevant, as bundles involving larger integers either violate the anomaly cancellation condition or fail to match the required Euler characteristic. We choose this range as $k_a^i \in \{-2^n+1, \ldots, 2^n\}$, so that every integer can be encoded by $n+1$ bits without redundancy, and a complete model is described by a bit list of length $N_{\text{bits}} = 4h(n+1)$. In practice, we take $n = 3$ for the first three manifolds and $n = 2$ for the manifold X_{4071}.

The classic GA algorithm begins by forming a random population of N_{pop} individuals, with details on the fitness functions f presented in Appendix A in Ref. [5]. The population is then evolved via the three main evolutionary ingredients: selection, breeding and mutation. We use a selection method based on fitness-ranking, which means that individuals are selected for breeding with a probability that increases linearly with their ranking, such that the probability for the fittest individual to be selected is a multiple α of the probability for the least fit one. Typically, α is chosen in the range $2 \leq \alpha \leq 5$. The breeding of the $N_{\text{pop}}/2$ pairs that are selected in this manner is implemented by cutting and splicing each pair at a number of matching random points. We implemented a single point cross-over, in which a cut is made at

a single random point and the 'tails' swapped. As an additional feature, our implementation includes *elitism*, which means that the fittest individual in every generation is copied to the next generation without modification.

The genetic quantum annealing algorithm (GQAA) described in Ref. [2] makes a further step by realising the genotype of individuals in a quantum mechanical way, that is, as quantum reads on a system of spins on a quantum annealer. This approach uses quantum annealing to enhance the GA but maintaining the same topology for the algorithm. We shall discuss results with GA and GQAA in order.

5.3.3 Results with GA

We have implemented the classic genetic algorithm and the line bundle environment (performing the binary encoding and the computation of the fitness function) in C, and the code is available here [118, 119]. We performed 7 different searches, as summarised in Table 5.1. Each search was divided into a large number of genetic episodes, with every episode containing 300 generations of 300 individuals each. The mutation rate was set to 0.5%, and the selection probability factor to $\alpha = 3$.

The manifolds X_{7862}, X_{7447} and X_{5302}

Systematic and comprehensive scans on these manifolds have been previously carried out in Ref. [113]. On the manifold X_{5302} a search using reinforcement

Table 5.1: Summary of results for the 7 GA searches. The table compares the number of models found here (GA) with numbers found in previous comprehensive searches (Scan) for manifolds with $h < 7$, both as actual numbers and as percentages. For the first three manifolds these numbers refer to the models that pass a sufficient criterion for poly-stability, performed after the GA search. The last column indicates the fraction of the environment explored in the GA search.

Manifold	h	$\lvert\Gamma\rvert$	Range	GA	Scan	Found	Explored
7862	4	2	[-7,8]	5	5	100%	10^{-10}
7862	4	4	[-7,8]	30	31	97%	10^{-10}
7447	5	2	[-7,8]	38	38	100%	10^{-14}
7447	5	4	[-7,8]	139	154	90%	10^{-14}
5302	6	2	[-7,8]	403	442	93%	10^{-19}
5302	6	4	[-7,8]	722	897	80%	10^{-19}
4071	7	2	[-3,4]	11,937	N/A	N/A	10^{-14}

learning was carried out in Ref. [97]. Our purpose here is to gauge the GA performance as a heuristic method of search. The results are surprising. For the manifold X_{7862} with $h^{1,1}(X) = 4$, the environment contains $\sim 10^{19}$ line bundle sums[1]. All $\mathbb{Z}_2$-models and 97% of the $\mathbb{Z}_4$-models were found after visiting a fraction of 10^{-10} of this environment. For the manifold X_{7447} with $h^{1,1}(X) = 5$, the size of the environment is $\sim 10^{24}$. All $\mathbb{Z}_2$-models and 90% of

[1]The comprehensive scan of Ref. [113] on environments of this size was only possible due to the split nature of the bundle, which implied that vast regions of the solution space could be discarded by imposing constraints on individual line bundles, pairs of line bundles etc. The present GA search does not make use of such simplifications.

the $\mathbb{Z}_4$-models were found after visiting an even smaller fraction of 10^{-14} of the environment. Most impressively, for the manifold X_{5302} with $h^{1,1}(X) = 6$ the environment contains $\sim 10^{29}$ bundles and after visiting only a tiny fraction of 10^{-19} of it, 93% of the $\mathbb{Z}_2$-models and 80% of the $\mathbb{Z}_4$-models were found.

In Fig. 5.2 we present the saturation curve for the number of inequivalent $\mathbb{Z}_4$-models found in the GA search on X_{7447} as a function of the number of states visited. Similar saturation curves were also obtained in the other cases. An important common feature of these saturation curves, relevant for evaluating the performance of the GA, is that the initial rate of finding new viable models is of order 1 (inequivalent) models per 100 episodes. This implies that, although the size of the environment increases by several orders of magnitude with every additional Kähler parameter, while the number of viable models is expected to increase only by an order of magnitude, the initial rate at which GA identifies these is independent of the number of Kähler parameters.

The computational time required for a genetic episode is $O(10)\,s$ on a standard desktop and displays a linear increment with the number of Kähler parameters ($\sim 23\,\mathrm{s}$ for X_{5302}, compared to $\sim 17.5\,\mathrm{s}$ for X_{7447} and $\sim 12\,\mathrm{s}$ for X_{7862}). This means that each of the searches mentioned above finished within a few hours on a cluster of 100 CPUs.

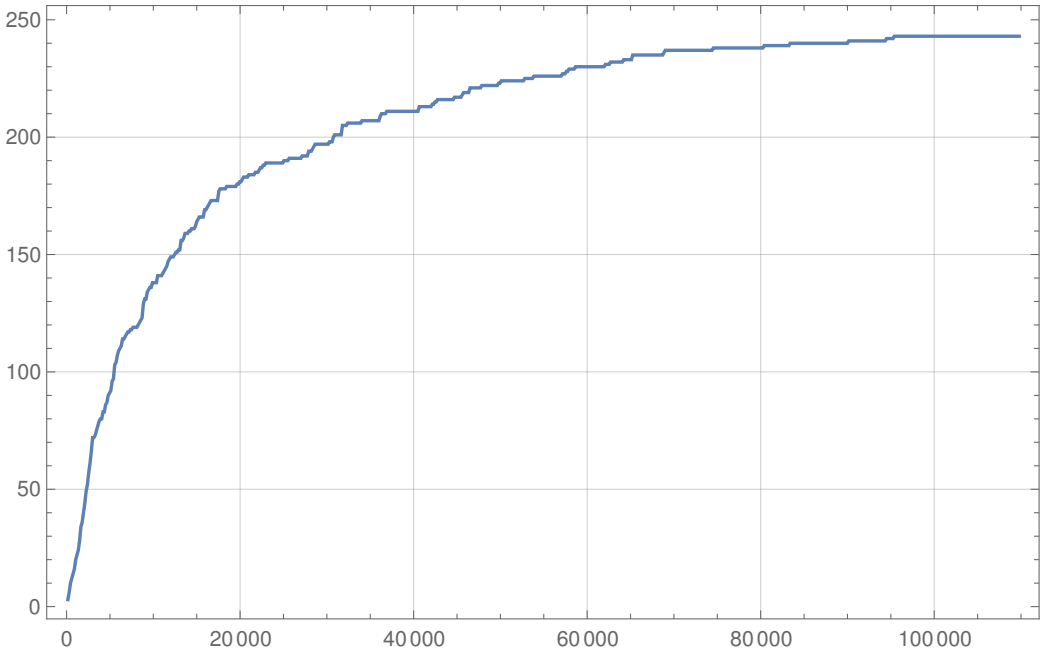

Figure 5.2: Saturation plot for the GA search on X_{7447} with $|\Gamma| = 4$ and $h^{1,1}(X_{7447}) = 5$. The horizontal axis represents the number of genetic episodes, in each episode a number of 90,000 states being visited. The vertical axis corresponds to the number of inequivalent models found in the search satisfying the necessary criterion (C3) for poly-stability. The computational time for a genetic episode is $O(10)$ seconds on a standard machine.

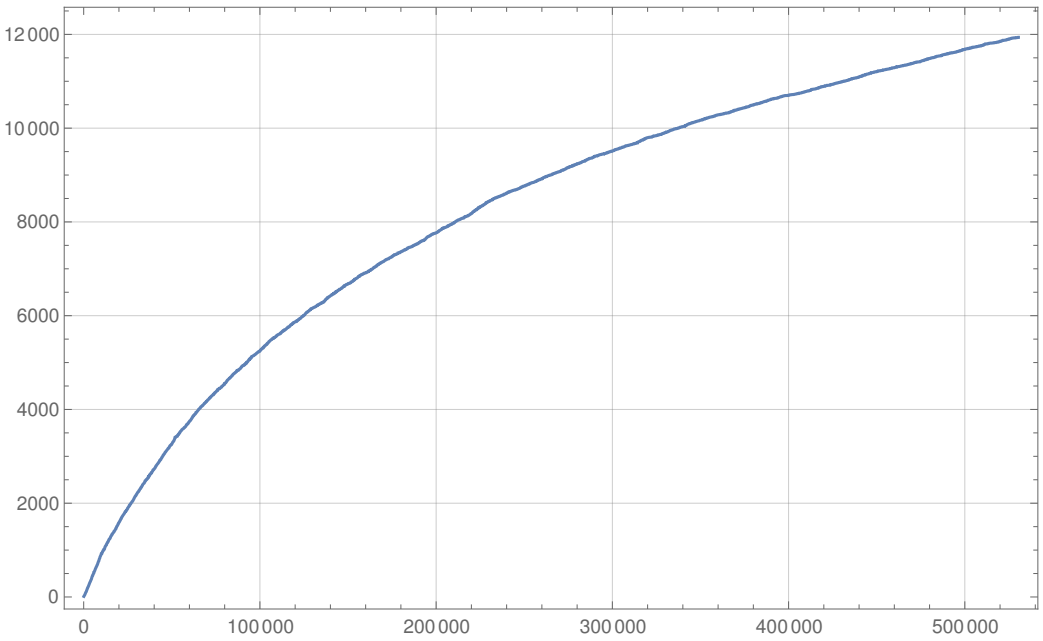

Figure 5.3: Saturation plot for the GA search on X_{4071} with $|\Gamma| = 2$ and $h^{1,1}(X_{4071}) = 7$. The horizontal axis represents the number of genetic episodes, each episode containing a number of 90,000 visited states. The vertical axis corresponds to the number of inequivalent models found in the search, satisfying the necessary criterion (C3) for poly-stability. The computational time for a genetic episode is $O(1)$ minute on a standard machine.

The manifold X_{4071}

The manifold X_{4071} pushes the search for realistic string models of particle physics into a new realm of larger Picard numbers, with much more involved bundle equivariance checks.

The saturation curve for the number of inequivalent models found on X_{4071} as a function of the number of states visited is shown in Fig. 5.3. The plot indicates that after 500,000 genetic episodes saturation has not been reached. However, by doubling the computational time a good degree of saturation would likely be achieved.

Due to the more involved equivariance checks, the computational time required for a single genetic episode was slightly longer than for the previous manifolds and averaged at around 1 minute.

5.3.4 Results with GQAA

Let us now compare the potential performance of the GQAA on X_{7447} and X_{5302}, with the results obtained using the classical GA. For quantum annealing, we used again D-Wave's `Advantage_system4.1` and *Pegasus* structure. As such machines are still in development it is not possible at the time of writing to reproduce analogous plots to the saturation plots in Figures 5.2 and 5.3 for GQAA. (Indeed, considering only the available space on the annealer, a GQAA reproduction of Fig. 5.2 with the same population and the same range for the integers k_a^i would already require 24000 qubits, which is far beyond

the available number of qubits on the D-Wave's Advantage_system4.1.)

Given these practical constraints, comparing the GQAA with the GA then requires careful consideration. For example one might consider resorting to smaller problems, such as a saturation plot on X_{7862} with $k_a^i \in [-2, 1]$ using a smaller population. However such a problem is then already somewhat trivial for both algorithms to solve since there are a high number of perfect models in the search space. In other words the classical GA already finds a solution in every other genetic episode (by comparison with the saturation plot of the 7447 model in Fig. 5.2 where it finds a perfect model roughly once in every 100 genetic episodes), so there is little room for the GQAA to show advantage over the classical GA (although we should add that both algorithms are still orders of magnitude better than a random search).

Therefore to ensure that we are analysing a problem that is *hard for the traditional GA*, we can instead compare the early improvement in the best fitnesses for the much more difficult cases, and with higher k_a^i. We show this in Figures 5.4 and 5.5, which compare the fitness evolution for the two algorithms on X_{7447} and X_{5302}, respectively. After optimising all the GA parameters and choosing a suitable set of GQAA parameters (which can be found in Table 5.2), we determined the fitness of the fittest individual for the first 100 generations for both GA and GQAA, averaged over 20 runs.

By this measure we can indeed see evidence that the GQAA has advantage over the classical GA. We note that the GQAA best fitness grows faster throughout the generations than that of the classical GA. Indeed, after 100

generations, the GQAA best fitness is, on average, $\sim 52\%$ better than GA in the first case and $\sim 26\%$ in the second case, respectively. We also note a much smoother behaviour of the fitness improvement in the GQAA. For example, the stall in fitness improvement for the classical GA on the X_{7447} manifold is reproducible and remains after many more runs have been performed. Thus, it appears that, depending on the manifold in question, the GA can encounter blocks in the fitness improvement that the GQAA is able to circumvent.

Parameter	**Description**	**Value**
Topology	Polyandric $J_{\ell m}$ couplings	'Islands'
α	Selection probability factor	4.0 — 1.16
α_p	Nepotism	0.05 — 0.6
ρ	Proportion of antiferromagnetic	0.5
ρ'	Proportion of enhanced couplings	6.4%
κ	Strength of enhanced couplings	$-\alpha \times \alpha_p$
s_q	Minimum anneal parameter	0.75 — 0.2
J_{ij}	Coupling strength	$\pm 0.08 \pm 0.15$

Table 5.2: GQAA parameters and related values. For definitions, see Sec. 4.4. Two entries in the "Value" column refer to X_{7447} and X_{5302}, respectively. A single entry refers to both manifolds.

This partly explains why the improvement on the classical GA in the first case (Fig. 5.4) is twice that in the second case (Fig. 5.5): 52% and 26%, respectively. However, we should also note in this respect that besides being intrinsically dependent on the characteristics of the problem (manifold structure, range of the variables, *etc.*), the efficacy of the GQAA depends strongly on the choice of GQAA parameters in Table 5.2. Thus while for the

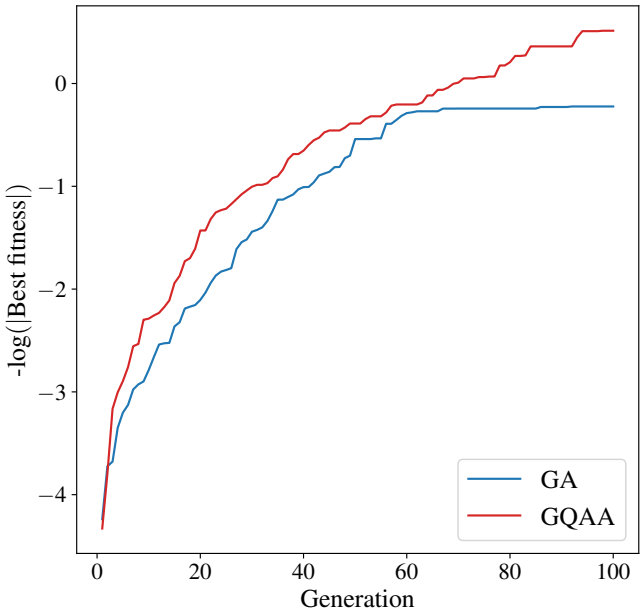

Figure 5.4: Fitness of the fittest individual for both GA and GQAA for the first 100 generations on X_{7447} with $|\Gamma| = 4$. The optimal value of the GA mutation rate is 0.5% and the range for the integers k_a^i is chosen to be $[-4, 3]$. N_{pop} was set to 50 for both GA and GQAA. The fitness was averaged over 20 runs. All the other parameters related to the GQAA part are specified in Table 5.2.

GA it is possible to optimise meta-parameters such as mutation rate, this becomes too time-consuming an operation for the GQAA due among other things to the much larger number of meta-parameters (the values of all the couplings for example). Thus we consider Figures 5.4 and 5.5 to be evidence of advantage even before a full optimisation has been performed. From these

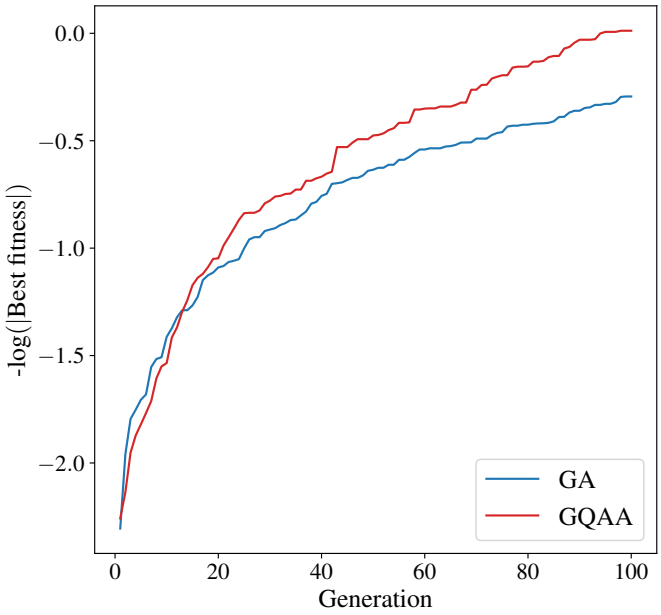

Figure 5.5: Fitness of the fittest individual for both GA and GQAA for the first 100 generations on X_{5302} with $|\Gamma| = 2$. The optimal value of the GA mutation rate is 1% and the line bundle integers are chosen in the range $k_a^i \in [-7, 8]$. N_{pop} was set to 35 for both GA and GQAA. The fitness was averaged over 20 runs. All the other parameters related to the GQAA part are specified in Table 5.2.

results, it seems reasonable to believe that once the technological limitations have been overcome, a GQAA saturation plot on the manifold X_{7447} would require roughly half of the genetic episodes required by the classical GA (Fig. 5.2) to reach saturation or possibly even less once a full optimisation becomes possible.

Finally it is worth mentioning a salient fact which is that one might suppose that the quantum annealing step could be replaced with classical simulated annealing, but this does not appear to offer similar improvement. Surprisingly, in all our studies there seemed to be a significant difference in behaviour such that quantum annealing appears to be crucial to the technique.

Chapter 6

Conclusions

In the first part of this thesis we have developed a general framework for analysing the running of gauge couplings within closed string theories. Unlike previous discussions in the literature, our calculation fully incorporates the underlying modular invariance of the string and includes the contributions from the infinite towers of string states which are ultimately responsible for many of the properties for which string theory is famous, including its enhanced degree of finiteness and UV/IR mixing.

In general, this formalism — which builds upon the Rankin-Selberg technique [29, 30] but which also includes additional critical features such as an identification between worldsheet parameters and an effective spacetime energy scale μ — gives rise to an "on-shell" EFT description in which the final results are expressed in terms of supertraces over the physical string states, and in which these quantities exhibit an EFT-like "running" as a function

of the scale μ. We found that results have a particular modular structure which causes them to depend on supertraces over *off-shell* string states as well. Indeed, as explained in chapter 3, the entwinement induced by the modular completion of the helicity operator needed for calculating the gauge couplings has "deformed" the notion of physicality for the string states, allowing states which are not level-matched to nevertheless act as physical states which contribute to the physical supertraces describing the values of physical string amplitudes. We have also seen that although our results yield the expected logarithmic running of the gauge couplings within certain energy scales, they also yield a number of intrinsically stringy behaviors that transcend what might be expected within an effective field theory approach.

With this framework at hand we moved on to the second part of this work in which we have developed techniques aiming to improve our current computational capabilities in solving problem related to the string landscape. In particular, we have employed quantum annealing to construct string models, focusing on their efficiency and effectiveness in the model discovery process. By comparing quantum annealing with other established methods such as simulated annealing, random scans, and genetic algorithms, we have gained valuable insights into the possible advantages of using quantum annealers for this purpose.

We should add that annealers are possibly most advantageous when the search space consists of relatively dense regions of SM-like models (in this study one model in 10^5), a situation in which for example genetic algorithms

do not usually lead to significant improvement with respect to alternative methods such as random scans. By contrast, genetic algorithms are known to excel in scenarios with more challenging searches, where the exploration of extremely large solution spaces is required. Therefore, it would be interesting in future investigations to compare these methods in more difficult problem domains in order to provide a comprehensive assessment of their respective strengths and weaknesses.

Furthermore, a novel hybrid approach which combines quantum annealing and genetic algorithms has been developed. We have presented the GQAA to implement genetic algorithms on quantum annealers, which takes advantage of the quantum properties of the annealers to significantly improve performance over a classical GA.

There are two novel aspects of the GQAA with respect to the classical GA. The first is that the genotype of each individual is encoded as a continuous set of annealer couplings and not as a discrete set. This then yields via the annealer the discrete 'quantum-genotypes' from which the individuals are actually to be built. Thus there are several ways in which the genotype couplings can be chosen to influence their offspring. For example the fitness of previous generations can be encoded in the couplings so as to enforce good schema in the next generation (adopting Holland's viewpoint) – so-called *nepotism*. In a classical GA such enhancement can only come at the expense of large portions of the population carrying the same schema. The second novel feature that is incorporated into the GQAA is so-called

polyandry. That is the Ising couplings on the quantum annealer can be turned on (with various topologies and couplings) so that the entire population can be influenced by the fittest individuals. In the bench-marking examples we found that the GQAA performed up to roughly an order of magnitude better, in terms of the number of individuals that had to be constructed before a solution of some simple test problems was found. Moving on to the string theory context, the analysis becomes more involved. We have applied this method to search for SM-like heterotic line bundle models, which represents one of the most viable way to connect string theory to particle physics. The results give valuable insights on how this technique could probably overcome classical genetic algorithms in the near future. Although we are not able to provide a full comparison of the two techniques, we have gained valuable insights on the possibility that GQAA will be more effective than classical GA as a search tool for viable heterotic line bundle models. The main obstacles which prevent to fully compare the two techniques are due to technical obstructions, mostly related to delays in exchanging information with the actual quantum annealer. Being shared resources, annealers have to handle the traffic generated by multiple requests coming from different users. As a consequence, delays in reading off the values of the spins at the end of each anneal run occur very frequently. However, comparing the best fitness evolution throughout the first 100 generations reveals how the GQAA has a remarkable advantage over classical GA. In both manifolds we have analysed, we note that the GQAA best fitness grows faster throughout

generations compared to classical GA. It is worth noting that this improvement was found with rather generic choices of the GQAA parameters, and a full optimisation of the method was not carried out in this study (due to time constraints on the annealer). It would be naturally very interesting to perform a full study to determine the optimum set-up for performance.

As a final remark, it would be certainly worthwhile to deepen the development of the framework we have illustrated in chapter 3 until the point in which one can use it to extract universal constraints which ultimately serve as effective filters in the realm of these new search methods developed in the second part. This will certainly open a new rich and florid avenue for further studies.

Appendix A

Evaluation of Regularised Amplitudes

In the following appendix we shall evaluate integrals of the following form

$$\begin{aligned} I_\ell(\rho, a) &= \langle \tau_2^\ell \, \mathbb{X}_\ell \, \widehat{\mathcal{G}}_\rho(\tau, a) \rangle \\ &= \int_{\mathcal{F}} \frac{d^2\tau}{\tau_2^2} \, \tau_2^{\ell-1} \sum_{m,n} (-1)^F \, (\mathbb{X}_l)_{mn} \, \overline{q}^m q^n \, \widehat{\mathcal{G}}_\rho(\tau, a) \,, \end{aligned} \tag{A.1}$$

where the operator $\mathbb{X}_\ell$ is defined as $\mathbb{X}_\ell \equiv \mathbb{A} + \overline{E}_2 \mathbb{B}$ with $\mathbb{A}$, $\mathbb{B}$ some insertions. The regulator $\widehat{\mathcal{G}}_\rho(\tau, a)$ is defined as in Eq. (3.25). To evaluate the integral above we shall use the results in Appendix A of Ref. [21] and generalise them for insertions that depend on the normalised weight-two anti-holomorphic Eisenstein function $\overline{E}_2$, as in this case and in the case of gauge couplings.

To start, we first observe that the form of the regulator function $\widehat{\mathcal{G}}_\rho(a, \tau)$

in Eq. (3.25) allows us to reduce the calculation of I_ℓ to a calculation of the "reduced" amplitude

$$\begin{aligned} P(a) &= \left\langle \tau_2^\ell \; \mathbb{X}_\ell \; Z_{\rm circ}(a,\tau) \right\rangle \equiv P_{\mathbb{A}}(a) + P_{\mathbb{B}}(a) \\ &= \left\langle \tau_2^\ell \; \mathbb{A} \; Z_{\rm circ}(a,\tau) \right\rangle + \left\langle \tau_2^\ell \; \mathbb{B} \; \overline{E}_2 \; Z_{\rm circ}(a,\tau) \right\rangle \end{aligned} \tag{A.2}$$

where $Z_{\rm circ}(a,\tau)$ is the circle-compactification function in Eq. (3.26). Indeed, once we have evaluated $P(a)$, it follows from Eq. (3.25) that we can then easily evaluate I_ℓ through the relation

$$I_\ell(\rho,a) = \frac{a^2}{1+\rho a^2}\frac{\rho}{\rho-1}\frac{\partial}{\partial a}\Big[P(\rho a) - P(a)\Big] \,. \tag{A.3}$$

Following the unfolding procedure described in detail in Ref. [21], it is straightforward to compute the first term in the second line of Eq. (A.2). Limiting the cases to $\ell = 1, 2$ (which are the values of our interests) one arrives at the following expressions of $P(a)$ in term of supertraces

$$\begin{aligned} \ell = 1: \qquad P_{\mathbb{A}}(a) &= \operatorname*{Str}_{M=0} \mathbb{A}\left[f_1(a) + f_2(a)\right] + \operatorname*{Str}_{M>0} \mathbb{A}\left[f_2(a) + f_4(M,a)\right] , \\ \ell = 2: \qquad P_{\mathbb{A}}(a) &= \operatorname*{Str}_{M=0} \mathbb{A}\left[f_3(a)\right] + \operatorname*{Str}_{M>0} \mathbb{A}\left[f_5(M,a)\right] . \end{aligned} \tag{A.4}$$

where

$$f_1(a) \;=\; \frac{\pi a}{3}\,, \qquad\qquad f_2(a) \;=\; \frac{\pi}{3a}\,, \qquad\qquad f_3(a) \;=\; -\frac{2}{a}\log\,a\;,$$

$$f_4(M,a) \;=\; \frac{2}{\pi}\sum_{r=1}^{\infty}\left(\frac{M}{r\mathcal{M}}\right)K_1\left(\frac{rM}{a\mathcal{M}}\right)\,, \quad f_5(M,a) \;=\; \frac{4}{a}\sum_{r=1}^{\infty}K_0\left(\frac{rM}{a\mathcal{M}}\right)\,. \tag{A.5}$$

Here $\mathcal{M} = M_s/(2\pi)$ is the reduced string scale and $K_\nu(z)$ denotes the modified Bessel function of the second kind. Most importantly, our supertrace 'Str' notation indicates a statistics-weighted trace over the spectrum of only physical string states [27]:

$$\mathrm{Str}\,A \;\equiv\; \lim_{y\to 0}\sum_{\text{states }i}(-1)^{F_i}\,A_i\,e^{-y\alpha' M_i^2} \tag{A.6}$$

with the index i labelling the different physical states in the spectrum.

Thus we see from Eq. (A.4) that the first term in the second line of Eq. (A.2) can ultimately be expressed in terms of combinations of supertraces of the form $\mathrm{Str}\left[\mathbb{A}f(M)\right]$ with functions $f(M)$. We further note that the functions f_1 through f_3 are wholly independent of any aspect of the spectrum of the string theory under study, and thus these functions can be taken outside their respective supertraces. By contrast, the functions f_4 and f_5 depend not only on the regulator parameter a but also on the mass M of the contributing state. Such functions are thus intrinsically part of the supertrace

and cannot be factored out.

The $\overline{E}_2$ dependent term in the second line of Eq. (A.2) requires a similar treatment, with the only difference coming from an extra τ dependence in the Eisenstein function. As we shall see, this require additional care in performing the τ_1 integral. Using similar notations and procedures of Ref. [21] define the τ_1 integral as

$$g_{\mathbb{X}_\ell,\mathbb{B}}(\tau_2) \;\equiv\; \int_{-1/2}^{1/2} d\tau_1 \; \tau_2^{\ell-1} \; \sum_{m,n} (-1)^F \; \overline{E}_2 \; \mathbb{B}_{mn} \; \overline{q}^m q^n \,. \tag{A.7}$$

Using the Fourier expansion of E_2 in Eq. (3.13) we compute

$$\begin{aligned}
& g_{\mathbb{X}_\ell,B}(\tau_2) \;= \\
& \int_{-1/2}^{1/2} d\tau_1 \tau_2^{\ell-1} \; \sum_{m,n} (-1)^F \; \mathbb{B}_{mn} \; e^{2i\pi\tau_1(n-m)} e^{-2\pi\tau_2(m+n)} \; \Big(1 - 24 \sum_{k=1}^{\infty} \sigma(k) \overline{q}^k\Big) \\
&= \; \tau_2^{\ell-1} \; \sum_m \mathbb{B}_{mm} \, e^{-\pi\alpha'\tau_2 M^2} \\
&\qquad - 24 \int_{-1/2}^{1/2} d\tau_1 \tau_2^{\ell-1} \; \sum_{m,n} \sum_{k=1}^{\infty} (-1)^F \sigma(k) \; \mathbb{B}_{mn} \; e^{2i\pi\tau_1(n-m-k)} e^{-2\pi\tau_2(m+n+k)} \\
&= \; \tau_2^{\ell-1} \left\{ \sum_m \mathbb{B}_{mm} \, e^{-\pi\alpha'\tau_2 M^2} - 24 \; \sum_{k=1}^{\infty} \sigma(k) \; \sum_n (-1)^F \; \mathbb{B}_{n-k,n} \; e^{-\pi\alpha'\pi\tau_2 M_L^2} \right\}
\end{aligned} \tag{A.8}$$

where we have defined $M_L^2 \equiv \frac{\alpha'}{4} n$, the spacetime mass of the left excitation of the string. Analogously the spacetime mass of the right excitation is defined as $M_R^2 \equiv \frac{\alpha'}{4} m$ such that the total spacetime mass, given in the first line of

Eq. (2.30), is $M^2 = \frac{1}{2}(M_L^2 + M_R^2) = 2/\alpha'(m+n)$, where m and n can be expressed in terms of number operators (see below Eq. (2.37)).

The primary distinction from the previous computation, which lacks the E_2 insertion, lies in the second term in the last line of Eq. (A.8). This term accounts for the contribution exclusively from non-level-matched states, weighted by their individual spacetime left mass. The evident left-right asymmetry in the above expression is a consequence of the purely anti-holomorphic insertion of $\overline{E}_2$, leading to a shift solely in the left sector. We refer to this phenomenon as *entwinement*, which is further discussed in the main text. The computation now follows a similar pattern as described in Ref. [21], with the sole distinction being the inclusion of an extra term that accounts for the contribution of unphysical states. To this purpose we define a shifted supertrace, which we shall call *E-entwined supertrace* Str_E, as follows

$$\mathrm{Str}_E\, X \;\equiv\; \sum_{r=0}^{\infty} \chi_r\, \mathrm{Str}^{(r)} X \tag{A.9}$$

where

$$\chi_n \;=\; \begin{cases} 1 & n = 0 \\ -24\sigma(n) & n > 0\ , \end{cases} \tag{A.10}$$

and having slightly simplified the notation by writing $E_2(\tau) = \sum_{n=0}^{\infty} \chi_n q^n$. Finally, in Eq. (A.9) we have also defined an analogous *shifted supertrace* as

the sum over the states that lie along the $r^{\rm th}$ *shifted* diagonal:

$$\mathrm{Str}^{(r)} X \;\equiv\; \lim_{\tau_2\to 0} \sum_p a_{p-r,p}\, X_{p-r,p}\, e^{-\pi\alpha' M_L^2 \tau_2} \tag{A.11}$$

where $\alpha' M_L^2 = 4p$ and where the p-sum, as always, is over all of the states in the spectrum of the string model under consideration. As usual, $a_{p-r,n}$ is the net (bosonic minus fermionic) number of string states with right- and left-moving worldsheet energies $(p-r,n)$ in the string spectrum. Note that for $r=0$, level-matching implies that $M_L = M_R = M$. We thus find that the $r=0$ shifted supertrace is nothing but our ordinary supertrace:

$$\mathrm{Str}^{(r=0)} X \;=\; \mathrm{Str}\, X \;. \tag{A.12}$$

As illustrated in Fig. A.1, the shifted supertraces with $r>0$ may thus be considered to be the generalisations of the ordinary supertrace to off-shell states — *i.e.*, states that lie along non-principal diagonals. As noted above, the p-sums along non-principal diagonals typically begin with non-zero values of p, so that $p-r$ continues to exceed the right-moving vacuum energy Δ of the string model under consideration (with $\Delta = -1/2$ for the heterotic string). However, this restriction merely characterizes the existing states in the theory. No states are excluded by these observations, and indeed these sums continue to tally all of the (off-shell) states that exist in the theory. As such, this entwined supertrace $\mathrm{Str}_E X$ not only tallies both the physi-

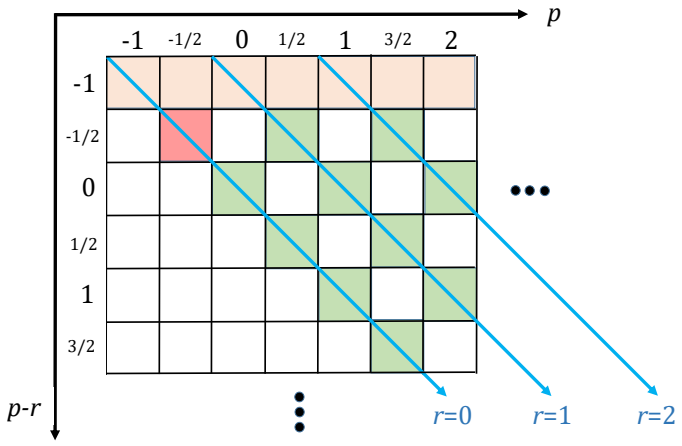

Figure A.1: String states arranged as a matrix according to their right-moving (vertical) and left-moving (horizontal) worldsheet energies $(m, n) \equiv (p-r, p)$, respectively. The states with $r = 0$ lie along the principal diagonal, while the states with $r = 1, 2, ...$ lie along successive shifted diagonals. The requirement $r \geq 0$ selects only those string states along or above the principal diagonal, and the $\tau \to \tau + 1$ invariance of the partition function ensures that only those "squares" shaded in green with $m - n \in \mathbb{Z}$ can be populated. The pink square is necessarily empty in any tachyon-free theory, and the row shaded in orange is excluded for heterotic strings because such strings have right-moving worldsheet energies $\geq -1/2$. In drawing this figure we have assumed that states populate only integer or half-integer mass levels, but in general the spectrum of states can be far denser and may even approach a continuum in (m, n) [or equivalently in p] for exceedingly large or small compactification radii.

cal and the unphysical string states, but also organizes the latter naturally according to how non-level-matched they are. In this way the E-entwined supertraces elegantly capture the string-theoretic nature of our full string spectrum, where the $\overline{E}_2$ function determines the χ_r coefficients and thereby determines the precise nature of the entwinement (motivating us to refer to this as an E_2-entwinement, or E-entwinement for short).

With this tools at hand, it is not difficult to generalise the previous results for non-entwined amplitudes to the case in which the insertion takes the form $\mathbb{B} \cdot \overline{E}_2$ with $\mathbb{B} \neq 0$. Indeed, tracing through the derivations explained in Ref. [21], we find that in such cases we can simply replace

$$\mathrm{Str}\left[\mathbb{B}\, f(M)\right] \;\longrightarrow\; \mathrm{Str}_E\left[\mathbb{B}\, f(M_L)\right], \tag{A.13}$$

within Eq. (A.3). This illustrates the power of the entwined-supertrace formalism we have developed. Moreover, when restricting to massive states [*i.e.*, states whose contributions to $g(\tau_2)$ have an exponential τ_2-dependent suppression], we have

$$\mathop{\mathrm{Str}}_{M>0}\left[\mathbb{B}\, f(M)\right] \;\longrightarrow\; \mathop{\mathrm{Str}_E}_{M_L>0}\left[\mathbb{B}\, f(M_L)\right], \tag{A.14}$$

The critical point here is that the restriction to massive states for $\mathbb{X}$ becomes a restriction to states with positive *left*-moving mass M_L for the E-entwined supertrace. This makes sense since the exponential suppression within $g(\tau_2)$ for the entwined supertrace depends on M_L^2 rather than M^2. By contrast,

when restricting to *massless* states [*i.e.*, states that contribute to $g(\tau_2)$ without exponential suppression], the $f(M)$ function becomes a constant which can be pulled outside the trace. We can then push this one step further and write

$$\operatorname*{Str}_{M=0} \mathbb{B} \;\longrightarrow\; \operatorname*{Str}_{E\,M_L=0} \mathbb{B} \;=\; \operatorname*{Str}_{M=0} \mathbb{B}\;. \tag{A.15}$$

The top line is of course analogous to what occurs in Eq. (A.14), but the additional step — the passage to the second line — follows from the fact that states with $M_L = 0$ have $p = 0$, but for heterotic strings this in turn implies that we can only have $r = 0$ (in the definition of Str_E in Eq. (A.9)), since any greater value of r would result in a right-moving worldsheet energy less than $-1/2$.

As before, we limit the cases to $\ell = 1, 2$ and apply the prescriptions in Eqs. (A.13),(A.14),(A.15). We thus arrive at

$$\begin{aligned}
\ell \;=\; 1: \qquad P_{\mathbb{B}}(a) \;&=\; \operatorname*{Str}_{M=0} \mathbb{B}\left[f_1(a) + f_2(a)\right] \;+\; \operatorname*{Str}_{E\,M_L>0} \mathbb{B}\left[f_2(a) + f_4(M_L, a)\right]\;, \\
\ell \;=\; 2: \qquad P_{\mathbb{B}}(a) \;&=\; \operatorname*{Str}_{M=0} \mathbb{B}\left[f_3(a)\right] \;+\; \operatorname*{Str}_{E\,M_L>0} \mathbb{B}\left[f_5(M_L, a)\right]\;,
\end{aligned} \tag{A.16}$$

for the amplitude with the $\overline{E}_2$ insertion in Eq. (A.2).

Thus far we have computed the two reduced amplitudes in Eq. (A.2). The last step to get the full amplitude in Eq. (A.1) is given in Eq. (A.3). Using the results in Eqs. (A.4), (A.16) in conjunction with Eq. (A.3) we can then trivially evaluate our full desired amplitude I_ℓ for the running of the

gauge couplings. Indeed, we see from Eq. (A.3) that we can turn $P(a)$ into I_ℓ simply by replacing each term within $P(a)$ according to the schematic substitution $\mathrm{Str}[\mathbb{X}f_i(a)] \to \mathrm{Str}[\mathbb{X}\phi_i(\mu)]$ where the operators $\mathbb{X}$ (can be either $\mathbb{A}$ or $\mathbb{B}$) are unchanged and where the new functions $\phi_i(\mu)$ for each $f_i(a)$ are given by

$$\phi_i(\mu) \equiv \frac{1}{1+\rho a^2}\,\frac{\rho}{\rho-1}\,a^2\frac{\partial}{\partial a}\Big[f_i(\rho a) - f_i(a)\Big] \tag{A.17}$$

where we first evaluate the right side of Eq. (A.17) as a function of ρ and a, and then identify $\mu^2 \equiv \rho a^2 M_s^2$ with $\rho = 2$ chosen as a benchmark value. Indeed, given the f_i-functions in Eq. (A.5), we find

$$\begin{aligned}
\phi_1(\mu) &= \frac{\pi}{3}\,\frac{\mu^2/M_s^2}{1+\mu^2/M_s^2}\\
\phi_2(\mu) &= \frac{\pi}{3}\,\frac{1}{1+\mu^2/M_s^2}\\
\phi_3(\mu) &= \frac{2}{1+\mu^2/M_s^2}\,\log\left(\frac{2\sqrt{2}eM_s}{\mu}\right)\\
\phi_4(M,\mu) &= \frac{1}{1+\mu^2/M_s^2}\,\frac{1}{\pi}\left(\frac{M}{\mathcal{M}}\right)^2\Big[\mathcal{K}_0^{(0,1)}(z)+\mathcal{K}_2^{(0,1)}(z)\Big]\\
\phi_5(M,\mu) &= \frac{2}{1+\mu^2/M_s^2}\,\Big[\mathcal{K}_1^{(1,2)}(z) - 2\mathcal{K}_0^{(0,1)}(z)\Big]
\end{aligned} \tag{A.18}$$

where $z \equiv 2\sqrt{2}\pi M/\mu$ and where we have defined the Bessel-function combi-

nations [21]

$$\mathcal{K}_{\nu}^{(n,p)}(z) \equiv \sum_{r=1}^{\infty} (rz)^n \Big[K_\nu(rz/\rho) - \rho^p K_\nu(rz) \Big] . \tag{A.19}$$

Note that $\phi_1(\mu) + \phi_2(\mu) = \pi/3$.

This completes the list of tools we need to evaluate the integrals of the form in Eq. (A.2) for $l = 1, 2$. This procedure is easily generalisable for higher values of ℓ.

Appendix B

Construction of $SO(10)$ models

In this appendix we focus on heterotic string models defined in the free fermionic formulation using the basis $b = \{\beta_1, \ldots, \beta_{12}\}$, where [107]

$$
\begin{aligned}
\beta_1 &= \mathbb{1} = \{\psi^\mu, x^{1,\ldots,6}, y^{1,\ldots,6}, \omega^{1,\ldots,6}; \bar{y}^{1,\ldots,6}, \bar{\omega}^{1,\ldots,6}, \bar{\psi}^{1,\ldots,5}, \bar{\eta}^{1,2,3}, \bar{\phi}^{1,\ldots,4}, \bar{\phi}^{5,\ldots,8}\}\,, \\
\beta_2 &= S = \{\psi^\mu, x^{1,\ldots,6}\}\,, \\
\beta_{2+i} &= e_i = \{y^i\omega^i; \bar{y}^i, \bar{\omega}^i\}\,, i = 1, \ldots, 6\,, \\
\beta_9 &= b_1 = \{x^{34}, x^{56}, y^{3,4}, y^{5,6}; \bar{y}^{3,4}, \bar{y}^{5,6}, \bar{\psi}^{1,\ldots,5}, \bar{\eta}^1\}\,, \\
\beta_{10} &= b_2 = \{x^{12}, x^{56}, y^{1,2}, y^{5,6}; \bar{y}^{1,2}, \bar{y}^{5,6}, \bar{\psi}^{1,\ldots,5}, \bar{\eta}^2\}\,, \\
\beta_{11} &= z_1 = \{\bar{\phi}^{1,2,3,4}\}\,, \\
\beta_{12} &= z_2 = \{\bar{\phi}^{5,6,7,8}\}\,,
\end{aligned}
\tag{B.1}
$$

and a set of phases $c\binom{\beta_1}{\beta_1} = \pm 1, c\binom{\beta_i}{\beta_j} = \pm 1, i > j = 1, \ldots, 6$. The basis vectors β_i describe the parallel transportation properties of the fermionic coordinates

along the world-sheet torus while the phases link to generalised GSO projections (GGSO). Following the standard notation, included fermions are periodic, while all rest are anti-periodic. For $c\binom{S}{e_i} = c\binom{s}{z_a} = -1, i = 1, \ldots, 6, a = 1, 2$ and generic choice of the remaining GGSO phases, the above basis describes a $\mathcal{N} = 1$ supersymmetric model possessing $SO(10)\times U(1)^3\times SO(8)^2$ gauge symmetry. $SO(10)$ spinorials arise from the sectors

$$\mathcal{S}^I_{\vec{P}^I_s} = S + b_I + \vec{P}^I_s\cdot\vec{E}\,, \quad I = 1, 2, 3\,, \tag{B.2}$$

where

$$\begin{aligned} P^1_s &= (0, 0, p^1_s, q^1_s, r^1_s, s^1_s)\,, \\ P^2_s &= (p^2_s, q^2_s, 0, 0, r^2_s, s^2_s)\,, \\ P^3_s &= (p^3_s, q^3_s, r^3_s, s^3_s, 0, 0)\,, \\ \vec{E} &= (e_1, e_2, e_3, e_4, e_5, e_6)\,. \end{aligned} \tag{B.3}$$

Here, $b^3 = b^1 + b^2 + x$ with $x = \mathbb{1} + S + \sum_{i=1}^{6} e_i + \sum_{a=1}^{2} z_a$. Similarly, $SO(10)$ vectorials come from the sectors

$$\mathcal{V}^I_{\vec{P}^I_v} = S + b_I + x + \vec{P}^I_v\cdot\vec{E}\,, \quad I = 1, 2, 3\,, \tag{B.4}$$

where

$$P_v^1 = (0, 0, p_v^1, q_v^1, r_v^1, s_v^1)\,,$$
$$P_s^2 = (p_v^2, q_v^2, 0, 0, r_v^2, s_v^2)\,,$$
$$P_v^3 = (p_v^3, q_v^3, r_v^3, s_v^3, 0, 0)\,. \tag{B.5}$$

Since the basis vector have trivial overlaps, *i.e.*, $e_i \cap \mathcal{S}^1_{\vec{P}_s^1} = \emptyset, i = 1, 2$, $e_i \cap \mathcal{S}^2_{\vec{P}_s^1} = \emptyset, i = 3, 4$, $e_i \cap \mathcal{S}^3_{\vec{P}_s^1} = \emptyset, i = 5, 6$ and $z_a \cap \mathcal{S}^I_{\vec{P}_s^1} = \emptyset, a = 1, 2$, $I = 1, 2, 3$ the spinorial projectors can be recast in the form

$$\Delta^I U_s^I = Y_s^I\ ,\ I = 1, 2, 3\,, \tag{B.6}$$

where

$$\Delta^1 = \begin{pmatrix} (e_1|e_3) & (e_1|e_4) & (e_1|e_5) & (e_1|e_6) \\ (e_2|e_3) & (e_2|e_4) & (e_2|e_5) & (e_2|e_6) \\ (z_1|e_3) & (z_1|e_4) & (z_1|e_5) & (z_1|e_6) \\ (z_2|e_3) & (z_2|e_4) & (z_2|e_5) & (z_2|e_6) \end{pmatrix}, \tag{B.7}$$

$$\Delta^2 = \begin{pmatrix} (e_3|e_1) & (e_3|e_2) & (e_3|e_5) & (e_3|e_6) \\ (e_4|e_1) & (e_4|e_2) & (e_4|e_5) & (e_4|e_6) \\ (z_1|e_1) & (z_1|e_2) & (z_1|e_5) & (z_1|e_6) \\ (z_2|e_1) & (z_2|e_2) & (z_2|e_5) & (z_2|e_6) \end{pmatrix}, \tag{B.8}$$

$$\Delta^3 = \begin{pmatrix} (e_5|e_1) & (e_5|e_2) & (e_5|e_3) & (e_5|e_4) \\ (e_6|e_1) & (e_6|e_2) & (e_6|e_3) & (e_6|e_4) \\ (z_1|e_1) & (z_1|e_2) & (z_1|e_3) & (z_1|e_4) \\ (z_2|e_1) & (z_2|e_2) & (z_2|e_3) & (z_2|e_4) \end{pmatrix} , \tag{B.9}$$

where we have employed the following notation

$$c \begin{bmatrix} \alpha \\ \beta \end{bmatrix} = \mathrm{e}^{\mathrm{i}\pi(\alpha|\beta)} . \tag{B.10}$$

Moreover

$$U_s^1 = \begin{pmatrix} p_s^1 \\ q_s^1 \\ r_s^1 \\ s_s^1 \end{pmatrix} , \; U_s^2 = \begin{pmatrix} p_s^2 \\ q_s^2 \\ r_s^2 \\ s_s^2 \end{pmatrix} , \; U_s^3 = \begin{pmatrix} p_s^3 \\ q_s^3 \\ r_s^3 \\ s_s^3 \end{pmatrix} \tag{B.11}$$

and

$$Y_s^1 = \begin{pmatrix} (e_1|b_1) \\ (e_2|b_1) \\ (z_1|b_1) \\ (z_2|b_1) \end{pmatrix} , Y_s^2 = \begin{pmatrix} (e_3|b_2) \\ (e_4|b_2) \\ (z_1|b_2) \\ (z_2|b_2) \end{pmatrix} , Y_s^3 = \begin{pmatrix} (e_5|b_3) \\ (e_6|b_3) \\ (z_1|b_3) \\ (z_2|b_3) \end{pmatrix} . \tag{B.12}$$

For the surviving spinorials we calculate chiralities using the formulae [108], $\mathrm{B}X^{(I)}_{pqrs} = \exp\Big(i\pi\chi^{(I)}_{pqrs}\Big)$, with

$$\begin{aligned}
\chi^{(1)}_{pqrs} &= \alpha_0 + (1-r)(e_5|b_1) + (1-s)(e_6|b_1) + p(e_3|b_2) + q(e_4|b_2) + r(e_5|b_2) \\
&\quad + s(e_6|b_2) + p(1-r)(e_3|e_5) + p(1-s)(e_3|e_6) + q(1-r)(e_4|e_5) \\
&\quad + q(1-s)(e_4|e_6) + (r+s)(e_5|e_6)\,, \qquad \text{(B.13)} \\
\chi^{(2)}_{pqrs} &= \alpha_0 + (1-r)(e_5|b_2) + (1-s)(e_6|b_2) + p(e_1|b_1) + q(e_2|b_1) + r(e_5|b_1) \\
&\quad + s(e_6|b_1) + p(1-r)(e_1|e_5) + q(1-r)(e_2|e_5) + p(1-s)(e_1|e_6) \\
&\quad + q(1-s)(e_2|e_6) + (r+s)(e_5|e_6)\,, \qquad \text{(B.14)} \\
\chi^{(3)}_{pqrs} &= \alpha_0 + (1-p)(e_1|b_1) + (1-q)(e_2|b_1) + (1-r)(e_3|b_2) + (1-s)(e_4|b_2) \\
&\quad + (1-r)(1-p)(e_1|e_3) + (1-r)(1-q)(e_2|e_3) + (1-s)(1-p)(e_1|e_4) \\
&\quad + (1-s)(1-q)(e_2|e_4) + (1-r)\left[(e_3|e_5) + (e_3|e_6)\right] \\
&\quad + (1-s)\left[(e_4|e_5) + (e_4|e_6)\right] + (1-r)\left[(e_3|z_1) + (e_3|z_2)\right] \\
&\quad + (1-s)\left[(e_4|z_1) + (e_4|z_2)\right] + (e_5|b_1) + (e_6|b_1) + (z_1|b_1) + (z_2|b_1)\,, \\
&\qquad \text{(B.15)}
\end{aligned}$$

where we can set $\alpha_0 = 0$ as it depends on conventions

$$e^{i\pi\alpha_0} = -\mathrm{ch}(\psi^\mu) c \begin{bmatrix} \mathbb{1} \\ S \end{bmatrix} c \begin{bmatrix} S \\ b_1 \end{bmatrix} c \begin{bmatrix} S \\ b_2 \end{bmatrix} c \begin{bmatrix} b_1 \\ b_2 \end{bmatrix}\,. \qquad \text{(B.16)}$$

Similarly, vectorial projectors can be recast in the form

$$\Delta^I U_v^I = Y_v^I \ , \ I = 1, 2, 3 \, , \tag{B.17}$$

where

$$U_v^1 = \begin{pmatrix} p_v^1 \\ q_v^1 \\ r_v^1 \\ s_v^1 \end{pmatrix} \ , \ U_v^2 = \begin{pmatrix} p_v^2 \\ q_v^2 \\ r_v^2 \\ s_v^2 \end{pmatrix} \ , \ U_v^3 = \begin{pmatrix} p_v^3 \\ q_v^3 \\ r_v^3 \\ s_v^3 \end{pmatrix} \ , \tag{B.18}$$

and

$$Y_v^1 = \begin{pmatrix} (e_1|b_1^x) \\ (e_2|b_1^x) \\ (z_1|b_1^x) \\ (z_2|b_1^x) \end{pmatrix} , \ Y_v^2 = \begin{pmatrix} (e_3|b_2^x) \\ (e_4|b_2^x) \\ (z_1|b_2^x) \\ (z_2|b_2^x) \end{pmatrix} , \ Y_v^3 = \begin{pmatrix} (e_5|b_3^x) \\ (e_6|b_3^x) \\ (z_1|b_3^x) \\ (z_2|b_3^x) \end{pmatrix} , \tag{B.19}$$

with $b_i^x = b_i + x$. The GGSO associated coefficients in $Y_s^3, Y_v^I, i = 1, 2, 3$ can be reduced as follows

$$(e_i|b_3) = (e_i|b_1) + (e_3|b_2) + (e_i|x) \tag{B.20}$$

$$(z_a|b_3) = (z_a|b_1) + (z_a|b_2) + (z_a|x) \tag{B.21}$$

$$(e_i|b_I + x) = (e_i|b_I) + (e_i|x)\,, I = 1, 2 \tag{B.22}$$

$$(z_a|b_I + x) = (z_a|b_I) + (z_a|x)\,, I = 1, 2 \tag{B.23}$$

$$(e_i|b_3 + x) = (e_i|b_1) + (e_i|b_2)\,, \tag{B.24}$$

$$(z_a|b_3 + x) = (z_a|b_1) + (z_a|b_2)\,, \tag{B.25}$$

with

$$(e_i|x) = \sum_{\substack{j=1 \\ j\neq i}}^{6} (e_i|e_j) + (e_i|z_1) + (e_i|z_2)\,, \tag{B.26}$$

$$(z_a|x) = 1 + \sum_{j=1}^{6} (z_a|e_j) + (z_1|z_2)\,. \tag{B.27}$$

Moreover,

$$(e_i|e_j) = (e_j|e_i)\ ,\ (e_i|z_a) = (z_a|e_i)\ , \tag{B.28}$$

$$(z_1|z_2) = (z_2|z_1)\ ,\ (e_i|b_k) = (b_k|e_i)\,. \tag{B.29}$$

For a given set of spin structure coefficients $c\begin{bmatrix}\beta_i \\ \beta_j\end{bmatrix}$ the solutions $U_s^I, U_v^I, I = 1, 2, 3$ of (B.6), (B.17) determine the number of surviving spinorials/vectorials.

Without loss of generality, we can assume that one spinorial comes from the $S + b_1$ sector, that is we have a solution with $p_s^1 = q_s^1 = r_s^1 = s_s^1 = 0$. This amounts to setting

$$(e_1|b_1) = (e_2|b_1) = (z_1|b_1) = (z_2|b_1) = 0 \tag{B.30}$$

as dictated by the relevant equation of (B.6), i.e $\Delta^1 U_s^1 = Y_s^1$. Furthermore, we can also assume that the second spinorial arises from $S + b_2$, i.e. that $p_s^2 = q_s^2 = r_s^2 = s_s^2 = 0$ is a solution of $\Delta^2 U_s^2 = Y_s^2$, which then implies

$$(e_3|b_2) = (e_4|b_2) = (z_1|b_2) = (z_2|b_2) = 0\,. \tag{B.31}$$

The existence of a coupling of the form $\mathbf{16} \times \mathbf{16} \times \mathbf{10}$ at the trilinear effective superpotential (top mass Yukawa coupling) requires at least one vectorial coming from $S + b_1 + b_2 + x$, that is Eq. (B.17) has a solution with $p_v^3 = q_v^3 = r_v^3 = s_v^3 = 0$ [120]. Consequently, we also set

$$(e_5|b_1) = (e_5|b_2)\ ,\ (e_6|b_1) = (e_6|b_2)\ , \tag{B.32}$$

$$(z_1|b_1) = (z_1|b_2)\ ,\ (z_2|b_1) = (z_2|b_2)\,. \tag{B.33}$$

Finally additional constraints come from adjusting spinorial chiralities, in order to satisfy the chirality constraints on the first and second plane – i.e. to solve the equivalent of Eq. (5.8) for Eqs. (B.13) and (B.14). These

conditions are

$$(e_5|b_1) = (e_6|b_1)\ ,\ (e_5|b_2) = (e_6|b_2)\,. \tag{B.34}$$

Bibliography

[1] S. A. Abel and L. A. Nutricati, "Ising Machines for Diophantine Problems in Physics," Fortsch. Phys. **70** no. 11, (2022) 2200114, [arXiv:2206.09956 [hep-th]].

[2] S. Abel, L. A. Nutricati, and M. Spannowsky, "A Genetic Quantum Annealing Algorithm," [arXiv:2209.07455 [quant-ph]].

[3] S. Abel, K. R. Dienes, and L. A. Nutricati, "Running of gauge couplings in string theory," Phys. Rev. D **107** no. 12, (2023) 126019, [arXiv:2303.08534 [hep-th]].

[4] S. Abel, A. Constantin, T. R. Harvey, A. Lukas, and L. A. Nutricati, "Decoding Nature with Nature's Tools: Heterotic Line Bundle Models of Particle Physics with Genetic Algorithms and Quantum Annealing," [arXiv:2306.03147 [hep-th]].

[5] S. A. Abel, L. A. Nutricati, and J. Rizos, "String Model Building on Quantum Annealers," Fortsch. Phys. (6, 2023) .

[6] S. Abel, K. R. Dienes, and L. A. Nutricati, "Non-Renormalization Theorems Without Supersymmetry," [to appear].

[7] S. Abel, K. R. Dienes, and L. A. Nutricati, "Probing the Off-Shell Structure of String Theory: Off-Shell Misaligned Supersymmetry and Off-Shell Supertraces," [to appear].

[8] M. R. Douglas, "The Statistics of string / M theory vacua," JHEP **05** (2003) 046, [arXiv:hep-th/0303194].

[9] S. Ashok and M. R. Douglas, "Counting flux vacua," JHEP **01** (2004) 060, [arXiv:hep-th/0307049 [hep-th]].

[10] W. Taylor and Y.-N. Wang, "The F-theory geometry with most flux vacua," JHEP **12** (2015) 164, [arXiv:1511.03209 [hep-th]].

[11] A. Constantin, Y.-H. He, and A. Lukas, "Counting String Theory Standard Models," Phys. Lett. B **792** (2019) 258–262, [arXiv:1810.00444 [hep-th]].

[12] M. B. Green, J. H. Schwarz, and E. Witten, *SUPERSTRING THEORY. VOL. 1: INTRODUCTION*. Cambridge Monographs on Mathematical Physics. 7, 1988.

[13] J. Polchinski, *String theory. Vol. 1: An introduction to the bosonic string*. Cambridge Monographs on Mathematical Physics. Cambridge University Press, 12, 2007.

[14] R. Blumenhagen, D. Lüst, and S. Theisen, *Basic concepts of string theory*. Theoretical and Mathematical Physics. Springer, Heidelberg, Germany, 2013.

[15] E. Kiritsis, *String theory in a nutshell*. Princeton University Press, USA, 2019.

[16] F. Gliozzi, J. Scherk, and D. I. Olive, "Supergravity and the Spinor Dual Model," Phys. Lett. B **65** (1976) 282–286.

[17] N. Seiberg and E. Witten, "Spin Structures in String Theory," Nucl. Phys. B **276** (1986) 272.

[18] L. J. Dixon and J. A. Harvey, "String Theories in Ten-Dimensions Without Space-Time Supersymmetry," Nucl. Phys. B **274** (1986) 93–105.

[19] L. Alvarez-Gaume, P. H. Ginsparg, G. W. Moore, and C. Vafa, "An O(16) x O(16) Heterotic String," Phys. Lett. B **171** (1986) 155–162.

[20] D. J. Gross, J. A. Harvey, E. J. Martinec, and R. Rohm, "The Heterotic String," Phys. Rev. Lett. **54** (1985) 502–505.

[21] S. Abel and K. R. Dienes, "Calculating the Higgs mass in string theory," Phys. Rev. D **104** no. 12, (2021) 126032, [arXiv:2106.04622 [hep-th]].

[22] V. S. Kaplunovsky, "One Loop Threshold Effects in String Unification," Nucl. Phys. B **307** (1988) 145–156, [arXiv:hep-th/9205070, hep-th/9205068]. [Erratum: Nucl.Phys.B 382, 436–438 (1992)].

[23] L. J. Dixon, V. Kaplunovsky, and J. Louis, "Moduli dependence of string loop corrections to gauge coupling constants," Nucl. Phys. B **355** (1991) 649–688.

[24] E. Kiritsis and C. Kounnas, "Infrared regularization of superstring theory and the one loop calculation of coupling constants," Nucl. Phys. B **442** (1995) 472–493, [arXiv:hep-th/9501020].

[25] E. Kiritsis, C. Kounnas, P. M. Petropoulos, and J. Rizos, "Universality properties of N=2 and N=1 heterotic threshold corrections," Nucl. Phys. B **483** (1997) 141–171, [arXiv:hep-th/9608034].

[26] E. Kiritsis, C. Kounnas, P. M. Petropoulos, and J. Rizos, "String threshold corrections in models with spontaneously broken supersymmetry," Nucl. Phys. B **540** (1999) 87–148, [arXiv:hep-th/9807067].

[27] K. R. Dienes, M. Moshe, and R. C. Myers, "String theory, misaligned supersymmetry, and the supertrace constraints," Phys. Rev. Lett. **74** (1995) 4767–4770, [arXiv:hep-th/9503055 [hep-th]].

[28] K. R. Dienes, "Modular invariance, finiteness, and misaligned supersymmetry: New constraints on the numbers of physical string states," Nucl. Phys. **B429** (1994) 533–588, [arXiv:hep-th/9402006 [hep-th]].

[29] R. Rankin, "Contributions to the theory of ramanujan's function $\tau(n)$ and similar arithmetical functions, i." Proc. Cambridge Phil. Soc. **35** (07, 1939) 351–356.

[30] R. Rankin, "Contributions to the theory of ramanujan's function $\tau(n)$ and similar arithmetical functions, ii." Proc. Cambridge Phil. Soc. **35** (07, 1939) 357–372.

[31] A. Selberg, "Bemerkungen über eine dirichletsche reihe, die mit der theorie der modulformen nahe verbunden ist," Arch. Math. Naturvid. **43** (1940) 47–50.

[32] R. B. Paris, "The evaluation of single Bessel function sums," Math. Eterna **8** (2018) 71–82.

[33] K. R. Dienes and A. E. Faraggi, "Making ends meet: String unification and low-energy data," Phys. Rev. Lett. **75** (1995) 2646–2649, [arXiv:hep-th/9505018].

[34] K. R. Dienes and A. E. Faraggi, "Gauge coupling unification in realistic free fermionic string models," Nucl. Phys. B **457** (1995) 409–483, [arXiv:hep-th/9505046].

[35] K. R. Dienes, A. E. Faraggi, and J. March-Russell, "String unification, higher level gauge symmetries, and exotic hypercharge normalizations," Nucl. Phys. B **467** (1996) 44–99, [arXiv:hep-th/9510223].

[36] K. R. Dienes, "String theory and the path to unification: A Review of recent developments," Phys. Rept. **287** (1997) 447–525, [arXiv:hep-th/9602045].

[37] K. R. Dienes, E. Dudas, and T. Gherghetta, "Extra space-time dimensions and unification," Phys. Lett. **B436** (1998) 55–65, [arXiv:hep-ph/9803466 [hep-ph]].

[38] K. R. Dienes, E. Dudas, and T. Gherghetta, "Grand unification at intermediate mass scales through extra dimensions," Nucl. Phys. **B537** (1999) 47–108, [arXiv:hep-ph/9806292 [hep-ph]].

[39] T. Lanting, "The D-Wave 2000Q Processor," 2017. presented at AQC 2017.

[40] G. 't Hooft, "Naturalness, chiral symmetry, and spontaneous chiral symmetry breaking," NATO Sci. Ser. B **59** (1980) 135–157.

[41] N. S. Dattani and N. Bryans, "Quantum factorization of 56153 with only 4 qubits," arXiv preprint (2014) .

[42] R. Tanburn, E. Okada, and N. Dattani, "Reducing multi-qubit interactions in adiabatic quantum computation without adding

auxiliary qubits. part 1: The "deduc-reduc" method and its application to quantum factorization of numbers," 2015.

[43] S. Jiang, K. A. Britt, A. J. McCaskey, T. S. Humble, and S. Kais, "Quantum annealing for prime factorization," 2018.

[44] W. Peng, B. Wang, F. Hu, Y. Wang, X. Fang, X. Chen, and C. Wang, "Factoring larger integers with fewer qubits via quantum annealing with optimized parameters," SCIENCE CHINA Physics, Mechanics & Astronomy **62** no. 6, (2019) 1–8.

[45] R. H. Warren, "Factoring on a quantum annealing computer," Quantum Information & Computation **19** no. 3-4, (2019) 252–261.

[46] B. Wang, F. Hu, H. Yao, and C. Wang, "Prime factorization algorithm based on parameter optimization of Ising model," Scientific reports **10** no. 1, (2020) 1–10.

[47] C. C. Chang, A. Gambhir, T. S. Humble, and S. Sota, "Quantum annealing for systems of polynomial equations," Scientific Reports **9** no. 1, (Jul, 2019) .

[48] T. H. Chang, T. C. Lux, and S. S. Tipirneni, "Least-squares solutions to polynomial systems of equations with quantum annealing," Quantum Information Processing **18** no. 12, (2019) 1–17.

[49] I. G. Rosenberg, "Reduction of bivalent maximization to the quadratic case." Cahiers du Centre d'Etudes de Recherche Operationnelle **17** (1975) 71–74.

[50] N. Dattani, "Quadratization in discrete optimization and quantum mechanics," 2019.

[51] P. Hauke, H. G. Katzgraber, W. Lechner, H. Nishimori, and W. D. Oliver, "Perspectives of quantum annealing: methods and implementations," Reports on Progress in Physics **83** no. 5, (May, 2020) 054401.

[52] S. Abel, J. C. Criado, and M. Spannowsky, "Completely Quantum Neural Networks," [arXiv:2202.11727 [quant-ph]].

[53] R. Babbush, B. O'Gorman, and A. Aspuru-Guzik, "Resource efficient gadgets for compiling adiabatic quantum optimization problems," Annalen der Physik **525** no. 10-11, (Sep, 2013) 877–888.

[54] E. Boros and P. L. Hammer, "Pseudo-Boolean optimization," Discrete Applied Mathematics **123** no. 1-3, (2002) 155–225.

[55] V. Chvatal, "A greedy heuristic for the set-covering problem," Mathematics of operations research **4** no. 3, (1979) 233–235.

[56] R. K. Guy, "Sums of like powers. euler's conjecture, §D1 in unsolved problems in number theory," 1994.

[57] J.-C. Meyrignac, "Computing minimal equal sums of like powers.".

[58] Eulernet, "http://euler.free.fr/database.txt.".

[59] E. W. Weisstein, "Diophantine equation–nth powers (replace "n" by the power): From mathworld–a wolfram web resource.".

[60] T. Piezas, "A collection of algebraic identities.".

[61] C. Boyer, "New Upper Bounds for Taxicab and Cabtaxi Numbers.".

[62] P. Langacker, "The physics of heavy Z' gauge bosons," Rev. Mod. Phys. **81** (Aug, 2009) 1199–1228.

[63] P. Z. *et al.* (Particle Data Group), "Review of Particle Physics," Progress of Theoretical and Experimental Physics **2020** no. 8, (08, 2020) , [https://academic.oup.com/ptep/article-pdf/2020/8/083C01/34673722/ptaa104.pdf]. 083C01.

[64] T. Appelquist, B. A. Dobrescu, and A. R. Hopper, "Nonexotic neutral gauge bosons," Phys. Rev. D **68** (Aug, 2003) 035012.

[65] P. Batra, B. A. Dobrescu, and D. Spivak, "Anomaly-free sets of fermions," J. Math. Phys. **47** (2006) 082301, [arXiv:hep-ph/0510181].

[66] J.-Y. Liu, Y. Tang, and Y.-L. Wu, "Searching for Z' Gauge Boson in an Anomaly-Free U(1)$'$ Gauge Family Model," J. Phys. G **39** (2012) 055003, [arXiv:1108.5012 [hep-ph]].

[67] A. Ismail, W.-Y. Keung, K.-H. Tsao, and J. Unwin, "Axial vector Z' and anomaly cancellation," Nucl. Phys. B **918** (2017) 220–244, [arXiv:1609.02188 [hep-ph]].

[68] B. C. Allanach, J. Davighi, and S. Melville, "An Anomaly-free Atlas: charting the space of flavour-dependent gauged $U(1)$ extensions of the Standard Model," JHEP **02** (2019) 082, [arXiv:1812.04602 [hep-ph]]. [Erratum: JHEP 08, 064 (2019)].

[69] Y. Tang and Y.-L. Wu, "Flavor non-universal gauge interactions and anomalies in B-meson decays," Chin. Phys. C **42** no. 3, (2018) 033104, [arXiv:1705.05643 [hep-ph]]. [Erratum: Chin.Phys.C 44, 069101 (2020)].

[70] J. Ellis, M. Fairbairn, and P. Tunney, "Anomaly-free models for flavour anomalies," The European Physical Journal C **78** no. 3, (2018) 1–9.

[71] B. C. Allanach, B. Gripaios, and J. Tooby-Smith, "Solving local anomaly equations in gauge-rank extensions of the Standard Model," Phys. Rev. D **101** no. 7, (2020) 075015, [arXiv:1912.10022 [hep-th]].

[72] D. B. Costa, B. A. Dobrescu, and P. J. Fox, "General solution to the $U(1)$ anomaly equations," Phys. Rev. Lett. **123** (Oct, 2019) 151601.

[73] A. Smolkovič, M. Tammaro, and J. Zupan, "Anomaly free Froggatt-Nielsen models of flavor," Journal of High Energy Physics **2019** no. 10, (2019) 1–50.

[74] B. C. Allanach, B. Gripaios, and J. Tooby-Smith, "Geometric General Solution to the $U(1)$ Anomaly Equations," JHEP **05** (2020) 065, [arXiv:1912.04804 [hep-th]].

[75] D. B. Costa, "Anomaly-free $U(1)^m$ extensions of the Standard Model," Phys. Rev. D **102** (Dec, 2020) 115006.

[76] B. C. Allanach, B. Gripaios, and J. Tooby-Smith, "Anomaly cancellation with an extra gauge boson," Phys. Rev. Lett. **125** no. 16, (2020) 161601, [arXiv:2006.03588 [hep-th]].

[77] B. C. Allanach, B. Gripaios, and J. Tooby-Smith, "Semisimple extensions of the Standard Model gauge algebra," Phys. Rev. D **104** no. 3, (2021) 035035, [arXiv:2104.14555 [hep-th]].

[78] D. A. Sofge, "Prospective algorithms for quantum evolutionary computation," CoRR **abs/0804.1133** (2008) , [0804.1133].

[79] R. Lahoz-Beltra, "Quantum genetic algorithms for computer scientists," Computers **5** no. 4, (2016) .

[80] R. Ibarrondo, G. Gatti, and M. Sanz, "Quantum vs classical genetic algorithms: A numerical comparison shows faster convergence," in

2022 IEEE Symposium Series on Computational Intelligence. 7, 2022. [arXiv:2207.09251 [quant-ph]].

[81] N. Chancellor, "Modernizing quantum annealing ii: genetic algorithms with the inference primitive formalism," Natural Computing (2022) .

[82] N. Chancellor, "Modernizing Quantum Annealing II: Genetic algorithms with the Inference Primitive Formalism," [arXiv:1609.05875 [quant-ph]].

[83] G. E. Coxson, C. R. Hill, and J. C. Russo, "Adiabatic quantum computing for finding low-peak-sidelobe codes," 2014 IEEE High Performance Extreme Computing Conference (HPEC) (2014) 1–6.

[84] J. King, M. Mohseni, W. Bernoudy, A. Fréchette, H. Sadeghi, S. V. Isakov, H. Neven, and M. H. Amin, "Quantum-Assisted Genetic Algorithm," arXiv e-prints (June, 2019) , [arXiv:1907.00707 [quant-ph]].

[85] D. V. Dollen, S. Yarkoni, D. Weimer, F. Neukart, and T. Bäck, "Quantum-enhanced selection operators for evolutionary algorithms," Proceedings of the Genetic and Evolutionary Computation Conference Companion (2022) .

[86] A. Yamaguchi and H. Nakajima, "Landau gauge fixing supported by genetic algorithm," Nucl. Phys. Proc. Suppl. **83** (2000) 840–842, [arXiv:hep-lat/9909064 [hep-lat]].

[87] B. C. Allanach, D. Grellscheid, and F. Quevedo, "Genetic algorithms and experimental discrimination of SUSY models," JHEP **07** (2004) 069, [arXiv:hep-ph/0406277 [hep-ph]].

[88] Y. Akrami, P. Scott, J. Edsjo, J. Conrad, and L. Bergstrom, "A Profile Likelihood Analysis of the Constrained MSSM with Genetic Algorithms," JHEP **04** (2010) 057, [arXiv:0910.3950 [hep-ph]].

[89] J. Blåbäck, U. Danielsson, and G. Dibitetto, "Fully stable dS vacua from generalised fluxes," JHEP **08** (2013) 054, [arXiv:1301.7073 [hep-th]].

[90] S. Abel and J. Rizos, "Genetic Algorithms and the Search for Viable String Vacua," JHEP **08** (2014) 010, [arXiv:1404.7359 [hep-th]].

[91] F. Ruehle, "Evolving neural networks with genetic algorithms to study the String Landscape," JHEP **08** (2017) 038, [arXiv:1706.07024 [hep-th]].

[92] S. Abel, D. G. Cerdeño, and S. Robles, "The Power of Genetic Algorithms: what remains of the pMSSM?," [arXiv:1805.03615 [hep-ph]].

[93] A. Cole, A. Schachner, and G. Shiu, "Searching the Landscape of Flux Vacua with Genetic Algorithms," JHEP **11** (2019) 045, [arXiv:1907.10072 [hep-th]].

[94] S. AbdusSalam, S. Abel, M. Cicoli, F. Quevedo, and P. Shukla, "A systematic approach to Kähler moduli stabilisation," JHEP **08** no. 08, (2020) 047, [arXiv:2005.11329 [hep-th]].

[95] F. Ruehle, "Data science applications to string theory," Phys. Rept. **839** (2020) 1–117.

[96] I. Bena, J. Blåbäck, M. Graña, and S. Lüst, "The tadpole problem," JHEP **11** (2021) 223, [arXiv:2010.10519 [hep-th]].

[97] M. Larfors and R. Schneider, "Explore and Exploit with Heterotic Line Bundle Models," Fortsch. Phys. **68** no. 5, (2020) 2000034, [arXiv:2003.04817 [hep-th]].

[98] I. Bena, J. Blåbäck, M. Graña, and S. Lüst, "Algorithmically Solving the Tadpole Problem," Adv. Appl. Clifford Algebras **32** no. 1, (2022) 7, [arXiv:2103.03250 [hep-th]].

[99] S. Abel, A. Constantin, T. R. Harvey, and A. Lukas, "Evolving Heterotic Gauge Backgrounds: Genetic Algorithms versus Reinforcement Learning," Fortsch. Phys. **70** no. 5, (2022) 2200034, [arXiv:2110.14029 [hep-th]].

[100] S. Abel, A. Constantin, T. R. Harvey, and A. Lukas, "String Model Building, Reinforcement Learning and Genetic Algorithms," in *Nankai Symposium on Mathematical Dialogues: In celebration of S.S.Chern's 110th anniversary*. 11, 2021. [arXiv:2111.07333 [hep-th]].

[101] A. Cole, S. Krippendorf, A. Schachner, and G. Shiu, "Probing the Structure of String Theory Vacua with Genetic Algorithms and Reinforcement Learning," in *35th Conference on Neural Information Processing Systems*. 11, 2021. [arXiv:2111.11466 [hep-th]].

[102] G. J. Loges and G. Shiu, "Breeding Realistic D-Brane Models," Fortsch. Phys. **70** no. 5, (2022) 2200038, [arXiv:2112.08391 [hep-th]].

[103] S. Abel, N. Chancellor, and M. Spannowsky, "Quantum Computing for Quantum Tunnelling," [arXiv:2003.07374 [hep-ph]].

[104] S. Abel and M. Spannowsky, "Observing the fate of the false vacuum with a quantum laboratory," P. R. X. Quantum. **2** (2021) 010349, [arXiv:2006.06003 [hep-th]].

[105] S. Abel, A. Blance, and M. Spannowsky, "Quantum Optimisation of Complex Systems with a Quantum Annealer," [arXiv:2105.13945 [quant-ph]].

[106] J. Holland, *Adaptation in Natural and Artificial Systems*. The MIT Press reprinted, 1992.

[107] A. E. Faraggi, C. Kounnas, S. E. M. Nooij, and J. Rizos, "Towards the classification of $Z_2 \times Z_2$ fermionic models," in *2nd String Phenomenology 2003*, pp. 143–151. 11, 2003. [arXiv:hep-th/0311058].

[108] A. E. Faraggi, C. Kounnas, S. E. M. Nooij, and J. Rizos, "Classification of the chiral $Z_2 \times Z_2$ fermionic models in the heterotic superstring," Nucl. Phys. B **695** (2004) 41–72, [arXiv:hep-th/0403058].

[109] A. E. Faraggi, C. Kounnas, and J. Rizos, "Chiral family classification of fermionic $Z_2 \times Z_2$ heterotic orbifold models," Phys. Lett. B **648** (2007) 84–89, [arXiv:hep-th/0606144].

[110] A. E. Faraggi, C. Kounnas, and J. Rizos, "Spinor-Vector Duality in fermionic $Z_2 \times Z_2$ heterotic orbifold models," Nucl. Phys. B **774** (2007) 208–231, [arXiv:hep-th/0611251].

[111] A. E. Faraggi, C. Kounnas, and J. Rizos, "Spinor-vector duality in N=2 heterotic string vacua," Nucl. Phys. B **799** (2008) 19–33, [arXiv:0712.0747 [hep-th]].

[112] S. Efthymiou, S. Ramos-Calderer, C. Bravo-Prieto, A. Pérez-Salinas, D. García-Martín, A. Garcia-Saez, J. I. Latorre, and S. Carrazza, "Qibo: a framework for quantum simulation with hardware acceleration," Quantum Science and Technology **7** no. 1, (Dec, 2021) 015018.

[113] L. B. Anderson, A. Constantin, J. Gray, A. Lukas, and E. Palti, "A Comprehensive Scan for Heterotic SU(5) GUT models," JHEP **01** (2014) 047, [arXiv:1307.4787 [hep-th]].

[114] E. I. Buchbinder, A. Constantin, and A. Lukas, "The Moduli Space of Heterotic Line Bundle Models: a Case Study for the Tetra-Quadric," JHEP **03** (2014) 025, [arXiv:1311.1941 [hep-th]].

[115] A. Constantin and A. Lukas, "Formulae for Line Bundle Cohomology on Calabi-Yau Threefolds," Fortsch. Phys. **67** no. 12, (2019) 1900084, [arXiv:1808.09992 [hep-th]].

[116] C. R. Brodie, A. Constantin, and A. Lukas, "Flops, Gromov-Witten Invariants and Symmetries of Line Bundle Cohomology on Calabi-Yau Three-folds," [arXiv:2010.06597 [hep-th]].

[117] P. Candelas, A. Dale, C. Lutken, and R. Schimmrigk, "Complete Intersection Calabi-Yau Manifolds," Nucl. Phys. B **298** (1988) 493.

[118] S. Abel, A. Constantin, T. R. Harvey, A. Lukas, and L. A. Nutricati, "A realisation of genetic algorithms in c," tech. rep., April, 2023.

[119] S. Abel, A. Constantin, T. R. Harvey, A. Lukas, and L. A. Nutricati, "An environment for heterotic line bundle models, realised in c," tech. rep., April, 2023.

[120] J. Rizos, "Top quark mass coupling and classification of weakly-coupled heterotic superstring vacua," Eur. Phys. J. C **74** no. 6, (2014) 2905, [arXiv:1404.0819 [hep-ph]].